Republic of Iraq
Ministry of Higher Education and Scientific Research
University of Babylon
College of Science for Women
Department of Laser Physics and its Application

Random Laser Emission at (Visible-NIR) Wavelengths in Different Active Media

A Thesis
Submitted to the Council of the College of Sciences for Women,
University of Babylon
In Partial Fulfillment of the Requirements for the Degree of
Doctor of Philosophy in Laser Physics and its Applications

By

Mohammed Salah Rahoomi

B. Sc. Physics 2009
M. Sc. Physics 2018

Supervised by

Prof. Ph.D. Jassim Mohammed Jassim

2023 A.D **1444 A.H**

بِسْمِ ٱللَّهِ ٱلرَّحْمَٰنِ ٱلرَّحِيمِ

قَالُواْ سُبْحَٰنَكَ لَا عِلْمَ لَنَآ إِلَّا مَا عَلَّمْتَنَآ ۖ إِنَّكَ أَنتَ ٱلْعَلِيمُ ٱلْحَكِيمُ

صَدَقَ اللّٰهُ العَظيم

البقرة (الآية-32)

Supervisor Certification

I certify that this thesis entitled (**Random Laser Emission at (Visible-NIR) Wavelengths in Different Active Media**) was prepared by **Mohammed Salah Rahoomi** under my supervision at laser physics department, college of sciences for women, university of Babylon as a partial fulfillment of the requirements for the degree of Doctor of Philosophy in Laser Physics and its Applications.

Signature:

Name: **Dr. Jassim Mohammed Jassim**

Title: Professor

Address :Dept. of laser physics, College of sciences for women, University of Babylon

Date: / /2023

In view of the available recommendations, I forward this thesis for debate by the examination committee.

Signature:

Name: **Asst. Prof. Dr. Jinan Ali Abd**

Title: Head of the department

Address: Dept. of laser physics, College of sciences for women, University of Babylon.

Date: / /2023

Examination Committee Certification

We certify that after reading this thesis, entitled: **"*Random Laser Emission at (Visible- NIR) Wavelengths in Different Active Media*"**, and as committee, examined the student **"Mohammed Salah Rahoomi Saleh"** its contents and that in our opinion it meets the standards of a thesis for the Degree of Philosophy of Doctorate in Laser Physics and its Application.

Signature:
Name: **Dr. Fareed Faris Rasheed**
Title: Professor

Date: / / 2023
(Chairman)

Signature:

Name: **Dr. Wajehaa Abd Al-Daim**
Title: Professor

Date: / / 2023
(Member)

Signature:
Name: **Dr. Qussay Mohammed Salman**
Title: Assistant Professor

Date: / /2023
(Member)

Signature:
Name: **Dr. Samira Adnan Mahdi**
Title: Assistant Professor

Date: / / 2023
(Member)

Signature:
Name: **Dr. Mohammed Hamza Khudair**
Title: Assistant Professor

Date: / / 2023
(Member)

Signature:
Name: **Dr. Jassim Mohammed Jassim**
Title: Professor

Date: / / 2023
(Member/Supervisor)

Approved by the Dean of College
Signature:
Name: **Dr. Abeer Fauzi Al-Rubaye**
Title: Professor
Address: Dean of the College of Science for Women.
Date: / / 2023

Dedication

To ..

My mother, God save her

And My father's soul

Acknowledgments

Above all, praise be to Allah, the Lord of all worlds, for who Iam. May Allah's Blessings and Peace be upon the most honored of Messengers, our prophet Muhammad and his pure immediate family.

Then, I would like to extend my thanks and gratitude to my supervisor **Prof. Dr. Jassim Mohammed Jassim** for his valuable contribution, continuous help, encouragement, and his continuous advice and his guidance throughout this work.

Thanks are due to the Department of Laser Physics and its Applications.

Special thanks to **Alshuhada Foundation** for all the best.

All thanks and gratitude are due to the **Minstry of Oil** for giving me a chance join Ph.D program.

Special thanks to **Prof.Dr.Ayad Alkaim**, my thesis supervisor, for his scientific advice and help.

Also, I would like to thank my brothers & bests friend's **Eng.Mostafa Salah**, **Eng.Ahmed albadry** and **Haider Sarmad** who shared all the times of happiness & sadness with me.

My thanks and appreciation are due to **Dr. Mohammed Hashim** and **Dr. Ameer Montader**, for their unlimited support throughout the research period.

Special thanks to my friends **Arshad Al Dulaimy**, **Bashar miseer, Hani A. Jawad**, **Zaid Al Shawka** and **Ahmed Jawad**, for their unlimited support.

My thanks are due to **Dr. Saddam Flayeh Haddawi**, **Dr**. **Raheem Abdallah Ejbarah** and **Dr. Ahmed Bager** for their support & advice.

Thanks and appreciation are due to my colleagues and brothers in the Ph.D. course, for the academic year **2019/2020**, wishing them success.

Abstract

This study aims to prepare random laser emission media within the wavelengths range from the **Vis** to **NIR**. The active medium of the random laser that was prepared to produce such wavelengths consists of a laser dye dissolved in a suitable solvent and nanoparticles. The laser dyes in such system (**Rhodamine -640**, **Methylene blue MB** and **LDS 821**) were used in methanol as solvent. The nanoparticles that were used as scattering centers are (**magnetic Fe_3O_4 iron oxide, silver Ag nanowires and Au nanorods**). Nanoparticles of different types and morphology were prepared using **Chemical methods**. The absorption and spectral fluorescence properties of dyes dissolved in methanol at different concentrations were studied. Also, the preparation of random laser media composed of dyes with addition of nanoparticles was studied in different concentrations of dye and nanoparticles. It was found that the concentration of dyes and the type of nanoparticles with a specific morphology have a significant effects on the spectra of dyes by increasing the absorption and emission spectrum with specific considerations. Also, the wavelengths shift to the longer wavelengths (**red shift**) and to shorter wavelengths (**blue shift**) was proportional to the concentration of both the dye and nanoparticles. The effect of the dynamic properties of dispersed magnetic nanofluids (Fe_3O_4) at different concentrations on the Gaussian laser beam passing through them has been studied. The results showed that both the magnitude of the external magnetic field and the response time have a clear effect on the re-spreading and distribution of nanoparticles (NPs), forming a layer of chains of different sizes. Moreover, controlling the length of the scattering mean free path where its value changes from (160- 30) μm. The possibility of using an external magnetic field on a mixture (active medium to random

laser) of Rhodamine-640 doped with Fe_3O_4 nanoparticles in methanol on random laser output parameters have been tested. The results showed the possibility of controlling the emission to longer wavelength (redshift) of up to (6) nm and a spectral bandwidth of less than (15) nm by changing the threshold energy to reach less than (3.5) mJ and by applying an external magnetic field between (0-125)G. The energy transfer factors for a mixture of two dyes, Rhodamine-640 as donor, methylene blue as acceptor, dissolved in methanol were also calculated and included the critical transfer distance, half quenching concentration, and transfer efficiency. It was found that the transfer efficiency reaches 85% at the concentration of dye (Methylene blue = 1×10^{-3} M). The addition of silver Ag nanowires to the mixture of the two dyes was then studied in order to prepare an effective medium for the random laser, two wavelengths of (600 and 700) nm were produced from this laser. As for the random laser with a medium composed of a mixture of LDS 821 dye dissolved in methanol with the addition of a certain concentration of gold nanorods of two different diameters (6.3 and 7.3) nm with a same lengths. The results showed a rapid change from incoherent to coherent lasing, by the system come to be exhibit distinct characteristics through several discrete peaks appear in the emission spectrum with a number of up to (10) and a spectral bandwidth of less than (1 nm). This is caused by the effect of both Plasmon resonance and the diameter of the gold nanorods. The field emission scanning electron microscope (FESEM), scanning electron microscopy (TEM) and X-ray diffraction (XRD) were used to study the morphological and structural characteristics of the nanoparticles.

Table of Contents

LIST OF SYMBOLS

Symbol	Description	Unit
σ_{SR}	Scattering cross section for Rayleigh approximation	cm^2
λ_0	Wavelength of incident photon	m
r	Particle radius	m
n_p	Refractive index of nanoparticle	---
n_m	Refractive index of surrounding medium	---
α_n	Scattering coefficient	---
l_t	Transport mean free path	m
$k = 2\pi/\lambda$	Wave vector	m^{-1}
l_G	Generation length	m
l_P	Mean path length	m
γ	Spatial coherence	---
n	Average photon number	---
l_g	Gain length	
l_s	Scattering mean free path	m
ρ	Particle density	cm^{-3}
σ_s	Scattering cross section	cm^2
W	Full width at half maximum of backscattering cone	---
θ	Scattering angle	---
l_{amp}	Amplification length	m
n_g	The density of gain molecules	cm^{-3}
σ_e	Emission cross section	cm^2
$\Delta\lambda$	FWHM	nm
C	Light velocity	m/s
τ	The lifetime of the upper level of random laser	s
V_{cr}	Critical volume	m^2
l_{cr}	Critical penetration depth	m
φ	Excitation spot beam diameter	m
σ_a	Absorption cross section	cm^2
l	Cuvette thickness	mm
I_0	Incident intensity through pure solvent without gain or scatterers	---
I	transmitted intensity through pure solvent with gain and scatterers	---
NF	Narrowing Factor	---
E_{th}	Threshold of pumping energy	Joule
h	Plank's constant	J.s

ν_p	Frequency of pumping photon	Hz
g_{th}	Gain coefficient	m^{-1}
G	The gain	---
A_{21}	spontaneous emission rate	s^{-1}
μ	Electric dipole moment	C.m
ϵ_0	Vacuum permittivity	F/m
M_w	Molecular weight	g/mol.
a.u.	Arbitrary unit	---
l_a	Absorption length	m
Q	Quality factor	---
λ_{peak}	Wavelength of peak emission	nm
τ_r	Residence time of photon inside random medium	s

LIST OF ABBREVIATION

Abbreviations	Description
NPs	Nanoparticles
FWHM	Full width at half maximum
l_s	Scattering mean free path
P_{th}	Pumping threshold
λ	wavelength
PI	Peak intensity
ITO	Indium tin oxide
ZnO	Zinc oxide
TiO_2	Titanium dioxide
Rh640	Rhodamine 640
Al_2O_3	Aluminum oxide
FRET	Fluorescence resonance energy transfer
R_0	Critical radius
NTs	Nanotubes
NRs	Nanorods
PDMS	Polydimethylsiloxane
SiO_2	Silicon dioxide
MB	Methylene blue dye
PS	Polystyrene
FDTD	Finite-difference time-domain
TMM	Transfer matrix method
ASE	Amplified spontaneous emission
SPR	Surface plasmon resonance
Ag	Silver
Au	Gold
0D	Zero dimension
1D	One dimension
2D	Two dimension

FESEM	Field emission scanning electron microscopy
TEM	Transmission electron microscopy
XRD	X-ray diffraction
PVP	Polyvinylpyrrolidone
$AgNO_3$	Silver nitrate
NaOH	Sodium hydroxide
CBS	Coherent backscattering
CW	Continuous laser
EF	Enhancement factor
CTAB	Cetylrimethylammonium Bromide
$NaBH_4$	Sodium Borohydrate
$C_6H_8O_5$	Ascorbic acid salt
$HAuCl_3.4H_2O$	Chloroauric acid
SNPs	Super magnetic nanoparticles
HC_1	First critical magnetic field
HC_2	Second critical magnetic field

LIST OF TABLES

LIST OF FIGURES

Chapter One

Introduction

Background & Motivation

1.1 Introduction

A laser has mainly three basic components: a pumping source, material with an optical gain induced via stimulated emission, and an optical cavity for trapping the light partially. As a well-known phenomenon, multiple scattering takes place in nearly all optical materials with opaque nature. Thus, it is frequently seen in daily life and determines the appearance of a wide range of objects, including clouds, powders, paints, and even human tissues [1]. When the light ray penetrates these materials, it is randomly scattered numerous times before exiting again, being similar to the random propagation by the Brownian motion of particles suspended in a liquid medium. Fundamentally speaking, the parameters involved in this process are as follows: the mean free path and the diffusion constant. Although the occurrence of scattering in disordered optical materials is known to be complex, it is completely of a coherent mode. The visualization of interference in the multiple scattered light can be clearly realized in laser speckles [2]. The difference between the multiple scattering and light diffusion is that the latter corresponds to a simplified picture of multiple scattering with no interference effects.

It is worth noting that, in addition to the natural materials, the multiple scattering arising from the randomness is intrinsically present in photonic materials such as photonic crystals, being aimed to be utilized in optical devices. In the case of photonic materials, structural artifacts lead to multiple scattering, which is considered an unwanted phenomenon. It is difficult to prevent the formation of these artifacts, thereby presenting a major industrial challenge [3].

As a result, one can employ multiple scattering to introduce improved functionalities and performances in an entirely novel point of view on disorder in photonic materials , it is so-called random laser.

From a theoretical aspect, Letokhov discussed the light diffusion with gain in the 1960s. By suspending microparticles in laser dye, a different strategy was taken into consideration by Lawandy et al. [4] in order to achieve multiple scattering with gain. Accordingly, as an advantage, it is possible to change the amount of scattering by varying the particle concentration. The other advantage is that the material is a suspension or a fluid [5].

In fact, the residence time of photon and efficiency of light amplification are enhanced by the multiple scattering in the medium. Under these conditions, the addition of reflectors is not needed for trapping light as the scattering centers can trap it in the disordered medium [6].

Random lasers are classified into two types: incoherent (non-resonant) and coherent (resonant), depending on the feedback mechanism. In the incoherent feedback type, scattering increases the paths of light and the feedback is provided by an increase in the photon lifetime of the system. This is characterized by the appearance of a single narrow emission peak (i.e., FWHM in the order of 10’s of nm) and determined by the diffusive nature of light. In the coherent feedback type, interference effects appear evidently where the photon returns to its first position, thus forming a closed path characterized by multiple sub-nm width peaks [7].

Basically, a laser is an optical structure that can satisfy the following criteria: (i) randomness and amplification via stimulated emission multiply

scatter the light, and (ii) the multiple scattering forms a threshold, above which the total gain exceeds the total loss. In this case, a broad range of the scattering mean free paths (l_s) is considered for multiple scattering systems with gain. While no lower bound is found for l_s, an upper bound is approximately the system size. Otherwise, the sample would be transparent.

Interestingly, the phenomenon of random laser has been observed in semiconductors powders, laser crystals, polymer thin films with and without scatterers, organic materials, and biological tissues. Research interests in the field of random lasers demonstrate lasing action in dye solution containing dispersed nanoparticles (NPs) [8]. Despite the numerous theoretical and experimental studies in the field of random lasers, finding an agreement between them remains a major challenge for researchers in this field [9].

Experimental studies conducted on the random laser have proven the importance of choosing nanomaterials that can act as scattering centers due to their significant impact on the performance of this type of laser [10]. Thereby, in this work, a great deal of emphasis will be placed on the experimental aspect, where the effect of selecting nanomaterials in terms of type, shape, concentration, and size, and the extent of the impact of each parameter will be studied on the properties of the random laser in order to achieve the appropriate medium for this system. These parameters will be discussed in terms of their effect on the intensity of emission spectrum, lasing threshold, FWHM, the appearance of spikes and their number as well as their impact on other factors such as scattering mean free path (l_s) transport mean free path (l_t), gain length (l_g), etc., being influential quantities for realizing the physics of a random laser.

In addition to studying the influence of some other factors on the random laser output, two classes of effects will be investigated as follows: (i) the external effect involving the application of magnetic field, and (ii) the internal effect represented by energy transfer mechanism. Also, the transition from non-coherent random laser to the coherent random laser will be discussed by increasing the concentration of scattering centers for the same nanomaterials (in terms of type, shape, and size). Therefore, the two types of random laser will be discussed, and the difference between them will be clarified. Then, the focus will be on the coherent random laser.

1.2 Laser Dyes

Laser dyes consisting of organic compounds can emit in the visible to infrared (IR) range when they are relaxed radiatively following the optical excitation. In 1966, Sorokin and Lankard were the ones who first discovered the laser dye phthalocyanine [11]. In this regard, they used a giant pulsed ruby laser together with a resonator, producing a powerful laser beam at the wavelength of 755.5 nm. Nevertheless, this laser is rarely utilized today. Currently, the performance of circulating liquid lasers has been optimized by a wide variety of luminescent dyes. The practical applications of these dyes have also been improved by rigidizing them in a polymer host, thus directing studies towards this emerging technology for solid state dye lasers [12].

1.3 Literature Survey

The working principles, characteristics, applications, and outputs of random lasers with different media have been extensively studied by several research groups. These studies will be presented in some detail, especially those related to the present work.

In 2010, C. S. Wang et al. employed the fluorescence resonance energy transfer (FRET) technology to enhance random laser action. They prepared ZnO nanorods (NRs) decorated by TiO_2 NPs for their work as these two substances had comparable band gap energies. A Q-switched laser (266 nm, 3–5 ns pulse, 10 Hz) was used to excite the ZnO/TiO_2 nanocomposites optically. A significant improvement was observed in the random laser action of TiO_2-decorated ZnO NRs compared to that of bare ZnO NRs. This was attributed to an increase in the scattering of light, arising from the presence of a rough surface after the decoration [13].

In 2011, Liling Yang et al. studied the effect of dye concentration and NP concentration on random laser behavior in a rhodamine 6G (R6G) dye dissolved in ethylene glycol solution containing Al NPs as scatterers. The dye concentration varied from 0.02 to 0.0 8M, whereas the concentration of Al NPs changed from 0.0015 to 0.009 M. Moreover, the pumping energy varied from 0.05 to 3.6 mJ. When the pumping energy was 0.05 mJ, the emission spectrum had broadband fluorescence, By increasing pumping energy to 0.6 mJ, spikes began to appear accompanied by a decrease in the value of FWHM. By exceeding the pumping above the lasing threshold, the emission intensity continued to increase, whereas the FWHM value was found be constant. It was also observed that when the concentration of dye

increased to 0.008 M and that of Al NPs was fixed at 0.0015 M, the number of spikes increased with pumping energy compared to the initial state when the dye concentration was 0.002 M. Alternatively, the influence of different Al NP concentrations on the emission spectrum at a constant dye concentration of 0.005 M was studied. The maximum of the emission peak as a function of the pump energy, low lasing threshold, and narrowed FWHM were observed with increasing the Al NP concentration [14].

In 2012, Firdaus et al. improved ZnO random laser characteristics by adding organic dye to a suspension containing ZnO nanopowder. The lasing emission intensity and threshold power of the ZnO/dye random laser clearly depended on the dye molecule concentration (donor). The optimum dye concentration was reported to be 1.2×10^{-5} M, leading to an increase and a decrease in the lasing emission intensity and threshold power, respectively. The Förster-type radiationless-RET occurring from the dye-molecule (acting as a donor) to ZnO nanopowder (as an acceptor) was able to explain the improved lasing performance. In continuance, the performance of ZnO/dye random lasers was further enhanced by selecting appropriate dye molecules. In turn, this led to spectral overlap taking place between the dye-donor luminescence and ZnO acceptor, which was the main criterion to have energy transfer [15].

In 2013, Bhupesh Kumar et al. fabricated different morphologies of TiO_2 nanomaterials such as NPs, NRs and nanotubes (NTs). They employed them as scattering centers in the dye solution in order to investigate their effect on the random laser performance. Depending on the morphological characteristics, it was possible to vary the lasing threshold, FWHM, and emission intensity. In this regard, the peak emission was

observed to occur at ~ 591, 587, and 590 nm for NPs, NRs, and NTs, respectively. The lasing threshold in the dye solution was ~1.0, 1.28, and 1.83 MW/cm^2 for NPs, NRs, and NTs respectively. Meanwhile, the corresponding FWHMs were ~ 4.2, 6.1, and 8.0 nm [16].

In 2014, Tianrui Zhai et al. fabricated a tunable random laser based on a waveguide plasmonic gain channel. This was achieved by adding Ag nanowires (NWs) to rhodamine 6G organic dye doped with polydimethylsiloxane (PDMS), followed by depositing them onto a silicone rubber slab. Owing to considerable overlap of the plasmon resonance peak (relating to Ag NWs) with both the photoluminescence spectrum and pump wavelength, a low threshold was obtained while also tuning properties of the random laser. Furthermore, the emission spectrum wavelength was tuned from 565 to 558 nm by increasing the stretching amount from 0 to 6 mm. The tunability can be justified by considering the blue shift and plasmon resonance narrowing of Ag NWs as determined by their uniform length distribution and reorientation after stretching [17].

Also, in 2014, Zhaona Wang employed Ag NWs (120 nm in diameter and dozens of micrometers in length) as scattering source at a constant particle density of $\rho = 7.31 \times 10^7 \mathrm{cm}^{-3}$. Different concentrations of Rhodamine 6G (R6G) dye ($1.1 \times 10^{-4}, 2 \times 10^{-3}, 10.44 \times 10^{-3}, 18.79 \times 10^{-3}$ M) were dissolved in methanol in order to study the transition from incoherent to coherent emission. By comparing between results of the four dye concentrations pumped with different power intensities, it was found that the dye concentration not only determined the emission peak position but also affected the feedback mechanism in random systems (having the same concentration of scatterer). This was attributed to the fact that the

gain length decreased with increasing the concentration of the dye. In addition, the scattering mean free path remained unchanged [18].

In 2015, Johannes Ziegler et al. reported that gold nanostars (NSs) could outperform nanogold materials with conventional morphologies (e.g., spherical NPs and anisotropic NRs) when they acted as scattering centers in random lasers composed of R6G-doped polymer thin films. The NSs provided broadband plasmon resonances that overlapped with the emission spectrum of R6G. Furthermore, highly enhanced electric fields were observed to be strongly localized at their tips with spiky morphology. The experimental results showed that the NS-based random laser was capable of operating at a threshold lasing of 0.9 mJ/cm^2, demonstrating multiple lasing modes with FWHM of 0.2 nm or even below [19].

Also, in 2015, Brojabasi et al. studied magneto-optical transmission in ferrofluids consisting of different Fe_3O_4 NP sizes. The average diameters of Fe_3O_4 NPs were reported to be 15, 30 and 46 nm, respectively. Initially, the external field was absent, observing only a bright circular spot on the screen. The external field was then applied to the ferrofluids. By increasing the intensity of the external field, a straight-line scattering pattern with spotty parts was seen as justified by the aggregation process. In fact, this process was induced by the external field.

It was also found that the intensity of the transmitted light was enhanced in the initial state, followed by reaching a maximum value. Beyond this value, the transmitted intensity was inversely reduced as a function of field intensity, reaching a minimum value. Interestingly, decreasing the average diameters of the NPs in the ferrofluids increased both the critical field intensities to higher values. The authors attributed the observed phenomena

to the formation of particle chains and column structures in the aggregation process. In other words, at a constant concentration, ferrofluids with smaller sizes of NPs required stronger field intensities to form chains of particles [20].

Also, in 2015, Ye et al. used the Fe_3O_4@SiO_2 core–shell NPs as scatters in Rhodamine B solutions. The average diameter of the NPs was 200 nm, whereas the thickness of SiO_2 shell was 50 nm. The pump source employed was the second harmonic of a Nd:YAG laser (532nm, 10 ns, 10 Hz). The first threshold was found to be at 100 μJ/pulse in the absence of a magnetic field. Additionally, well-separated sharp spikes with linewidth smaller than 0.2 nm appeared around 590 nm, indicating the occurrence of coherent random lasing. Nevertheless, threshold energy was reported to be 120 μJ/pulse in the presence of a magnetic field. It was because most of the NPs in the solution were effectively separated from the pump region under the application of the magnetic field. It was revealed that Fe_3O_4@SiO_2 doped dye solution possessed a magnetically controllable feature. Also, the sharp spikes disappeared when the diameter of Fe_3O_4 NPs was relatively large (about 100 nm), whereas the laser peaks existed when the diameter of Fe_3O_4 was relatively small (about 12 nm). Accordingly, that kind of random laser had potential applications in the fabrication of magnetic sensors and integrated optical devices [21].

In 2015, Ismail et al. studied the effect of fluorescence resonance energy transfer on the emission spectra and threshold of Rh6G/methylene blue/titania random lasers to get the laser emission peak at 700 nm. They used different dye ratio from Rh6G/MB mixture (1:1, 2:1 and 3:1). The concentration of Rh6G is (1×10^{-3} M), of methylene blue is (5×10^{-4} M) and

of titania is (1×1011 cm^{-3}). They found that for a dye concentration ratio of 1:1, a narrow emission peak (12 nm) appears at ~560 nm as the Rh6G dominates and the energy is not effectively transferred from Rh6G to MB dye. The emission spectrum at ~560 nm substantially reduces for 2:1 dye concentration ratio as the energy transfer to the acceptor provides sufficient optical gain. Adding more Rh6G increases the emission spectrum at ~560 nm and broadens the emission linewidth at ~700 nm due to excessive pump absorption. Also, they observed a lasing threshold at ~25 mJ/cm^2 for MB emission at 700 nm was dominante at a 2:1 dye concentration ratio, upon further Rh6G concentration increase to 3:1, the lasing threshold of MB emission increases again (~50 mJ/cm2) while the lasing threshold of rhodamine 6G emission occurs at 15 mJ/cm2. This is due to the competition of gain and loss between these two dyes for high levels of pump excitation [22].

In 2016, Li Long, et al. investigated the selection of appropriate nanomaterial to obtain the best properties of a random laser, while also evaluating the effect of localized SPR on the output of this laser. To compare between performances of the random laser, they selected metal Ag NPs and dielectric silicon dioxide (SiO_2) NPs as scatterers separately doped with dye. The authors noted that the lasing threshold reached 0.09 mJ without NPs, and 0.012 mJ with SiO_2 NPs, and 0.003 mJ with Ag NPs. It was also observed that, above the lasing threshold, while the emission intensity increased sharply, the FWHM of the emission spectrum decreased rapidly [23].

In 2016, Dawes et al. employed FRET in order to increase the wavelength range of emission. They used FRET between dye molecules

and studied the influence of different gain scattering media in random lasers. The authors evidenced that the incorporation of Au NPs instead of dielectric Al_2O_3 NPs can lead to an increase in the emission intensity as well as an enhancement in the efficiency of random lasing properties. A trade-off occurred between the enhancement in the random laser performance (arising from the localized SPR field effects) and a decrease in the laser performance (induced by fluorescence quenching of Au NPs) [24].

In 2017, Shuya Ning et al. analyzed the effect of the size of the nanomaterial on the properties of the random laser. Different sizes of Ag NPs were prepared using a seed-mediated growth method together with citrate reduction of silver nitrate ($AgNO_3$) with $NaBH_4$ as a strong reducing agent. The diameters of prepared Ag NPs were 20, 40, 60, 80, and 100 nm. The device structure was glass/Ag film (50 nm)/SiO_2 (10 nm)/Ag NPs/LiF (5 nm)/PS:BMT-TPD. For the sake of comparison, the gain medium was deposited on glass and employed as the reference (Glass/LiF (5 nm)/PS:BMT-TPD). For Ag NPs with a diameter smaller than 40 nm, the enhanced localized electric field was responsible for an increase in the lasing performance. By increasing the Ag NP diameter in the hybrid structure above 40 nm, the lasing performance improved due to an increase in the localized electric field and scattering. For Ag NPs with a diameter larger than 80 nm, the competition between the scattering effect and the enhanced localized electric field was the deciding factor in the enhanced laser performance. The best results for the random laser properties were achieved due to both the enhanced localized electric field and the scattering effect [25].

Also, in 2017, Tsai et al. designed and fabricated magnetically controllable random lasers (MCRLs). Under a prescribed magnetic field (0, 1066, and 2008 Gauss), they used a random medium composed of stilbene 420 laser dye as gain medium and mixture of TiO_2 and Fe_3O_4 NPs as scatters. The wavelength excitation was a Q-switched Nd:YAG laser (266 nm, 3–5 ns pulse duration, 10 Hz). The Fe_3O_4 NPs possessed magnetic controllability due to their susceptibility with good responsivity and durability for the magnetic field. They found at zero magnetic field, the slope of spontaneous emission intensity was relatively small. With increasing the magnetic field, two thresholds were observed, reaching 12.4 and 25.4 mJ cm^{-2} [26].

In 2018, Jiajia Yinl et al.. studied the effect of the size of NPs on random laser systems. They prepared three samples: S_1, containing R6G with Au NRs (diameter: 40±2 nm, and length: 68±2 nm), S_2: R6G with Au NRs (diameter: 40±2 nm, and length: 84±2 nm), and S_3: R6G with Au NRs (diameter: 40±2 nm, and length: 96±2 nm). The concentrations of Au and R6G were fixed. The experimental results showed that the medium of maximum length provided a lower lasing threshold. In this way, when the pump energy reached its threshold value, several distinct narrow laser spikes appeared in the emission spectra, having FWHM of less than 1 nm [27].

Also, in 2018, Moura André et al. developed a near-IR (NIR) random laser. This was emitted by silica-gel single beads with nanoporous structure and infiltrated with Rh640 dye. By changing Rh640 dye concentration and the light pathway inside the nanoporous beads, several parameters such as the excitation pulse energy threshold, central wavelength and minimum

bandwidth were considerably affected. To prepare the samples, silica-gel beads with millimeter range dimensions were infiltrated by ethanol solutions containing Rh640 with different concentrations in the range between 10^{-5}–10^{-2} M. RL emissions in the range between ≈670 –720 nm were obtained, arising from reabsorption/reemission processes by Rh640 molecules and their aggregates. On the other hand, multiple scattering of light was induced by the nanoporous silica-gel structure of the beads [28].

In 2019, Wan Zakiah et al. demonstrated that the properties of random lasers in terms of the emission intensity, FWHM, and lasing threshold were significantly influenced by the concentration of the nanomaterial. They observed that there was only amplified spontaneous emission in the absence of scatterers. By adding TiO_2 NPs to the system, intensity of the emission spectrum began to increase and became narrow with the decay of the background fluorescence. Six different concentrations of TiO_2 NPs (ranging from 1×10^{9} to 2×10^{11} cm^{-3}) were used, leading to a reduction in the lasing threshold from 23 to 11 mJ/cm^2. Also, the emission peak shifted to a shorter wavelength (indicating a blue shift) when increasing the NP concentration [29].

In 2019, Zhi Ren et al. were able to fabricate a wavelength-tunable random laser. The film consisted of R6G, PVP and Au NRs using a silicon rubber slab as a substrate. The silicon slab used provided excellent mechanical stretching properties. When the stretching amount increased from 0 to 12 mm, the central wavelength of the laser emission shifted towards shorter wavelengths (from 592 to 585 nm), being indicative of a blue shift. Also, the presence of Au NPs induced SPR, which greatly increased the light absorbed by the dye molecules. Accordingly, the

fluorescence of the dye molecules was considerably enhanced, giving rise to a decrease in the random laser threshold to about 9.8 mJ/cm^2. Furthermore, around the threshold value, the FWHM decreased from 40 to 3 nm. [30].

Also, in 2019, Dai et al. fabricated a magnetically tunable random laser. In this case, polymer dispersed liquid crystal (PDLC) in the capillary was achieved by means of doping magnetic NPs at varied pump energies. They used 532 nm laser pulses (10 ns &10 Hz) focused on the samples with a cylindrical lens (f=20 cm). The external magnetic field was applied by a cylindrical magnet. The intensity of the magnetic field was tuned by varying the distance between the magnet and the capillary. Experimental results showed the lasing threshold was enhanced with increasing doping concentration (0, 0.01, 0.02, and 0.03 wt%) of the NPs. The respective thresholds were 9.5, 11.5, 12.3, and 18.5 μJ. As well, this effect was due to the larger absorption of NPs with a higher concentration. By increasing the applied external magnetic field, the blue-shift of emission spectra was observed following an increase in the NP concentration [31].

In 2020, Gummaluri et al. succeeded in preparing a random laser system using Au nano-urchins acting as scatterers. These nanomaterials were distributed in polymer films doped with rhodamine 6G dye. The authors compared this system with another one with the same specifications, except that the scatterer was Au nanospheres instead of Au nano-urchins. To evaluate lasing performance, finite-difference time-domain simulation was used, taking into account the following three aspects: the local field enhancement, absorption cross-section, and scattering cross-section. The field intensity magnitude for nano-urchins was observed to be 2 times higher than that of nanospheres. At the pump wavelength, the authors

monitored a higher scattering cross-section and a low absorption cross-section for nano-urchins compared to those for nanospheres. This, in turn, indicated that materials with nano-urchin structure can be better scatterer candidates than spheres with isotropic structure when it comes to enhanced random lasing performance [32].

Also, in 2020, Peng and Deng. fabricated a composite nanostructure of Ag-TiO_2 by a solution-reduction method and mixed into a DCM-gain medium to investigate its role in random lasing. They showed that the RL device based on this nanostructure has a threshold of 3.01 μJ/pulse, which was lower than those achieved using TiO2 NPs or a mixture of TiO2 and Ag NPs. The threshold of the Ag-TiO_2-composite-based laser system was reduced by 91.9 percent compared to that with TiO_2 NPs, or 70.7 percent compared to that with the mixture. They demonstrated that the prepared hybrid nanostructure could significantly reduce the threshold and improve random lasing due to its broader LSPR band, which could adequately cover both the absorption and emission spectra of dyes and the enhancement of new nanostructures [33].

In 2021, Ejbarah et al. used a silver nanowire random laser (different sizes and concentrations)-based random lasers with a fixed concentration of laser dye rhodamine B pumped by a nanosecond pulsed laser. They indicated that the sizes and concentrations of scattering centers greatly affect the optical amplification mechanism, thresholds, narrowing the emission intensity. They used three sizes of Ag nanowires (length ≤ 50 microns, diameter 50 nm, 100 nm, and 200 nm) at concentrations (particle density 9×10^{17} cm^{-3}, 6×10^{17} cm^{-3} and 3×10^{17} cm^{-3}), respectively. and the concentration of laser dye rhodamine B at (1×10^{-5} M). They found of

emergence of spikes and the increase in their number by used a 50 nm diameter with increasing the concentration compared with other sizes. They found that the transition from the incoherent to a coherent type of random laser were done, and the spectrum of this laser began growing up and narrow with increasing the incident energy more and more, separate narrow peaks appeared in the emission spectrum were appeared, meaning that the photon reverts back to the first scatterer forming a closed loop, indicating the occurrence of a coherent random laser [34].

Also, the same group studied the effect of increasing concentration of Ag nanomaterial of a hexagonal shape with a fixed size (50 nm) on the performance of the random laser. The three emission spectra of concentrations at particles density were (high, mid, low) in cm^3. They found at low pumping energies typically in the region of 0.024 mJ, broad emission of the dye with peak at 582 nm and FWHM of 58 nm. At lower scatterer concentrations (S_1), the coherent random laser was not observed as pumping energy increased, until at 0.061 mJ the spikes started showing up. By changing the Ag particle density in the solution (S_2), it is continuously varied the amount of scattering which means the possibility of the emergence of coherent random laser early this is evident. Where the Ag particle density is ~ 6×10^{17} cm^{-3} as well as to the early appearance of the spikes compared to the sample S1. When increasing the density of Ag nanomaterial again to become 9×10^{17} cm^{-3} (S_3), it was noticed a great improvement in the performance of the random laser. [35].

1.4 Organization of thesis

This section gives a synopsis of the thesis, displaying the most important topics as follows:

Chapter One provides an introduction to the random laser, most important advantages in addition to its applications, and experimental studies and research that dealt with the topic of random laser. In particular, the studies that focused on the impact of nanomaterials on the random laser action were highlighted.

The 2nd chapter provides an introductory level foundation to theoretical, experimental, and computational concepts used throughout the thesis.

Chapter Three deals with the practical side of this thesis, focusing on the materials that will be used in this work and show casing their most important properties and composition. Afterwards, the techniques used in the preparation of nanomaterials will be addressed. The random media prepared for testing the performance of the random laser will be included. In this chapter, some experimental schemes or devices are employed as well.

Chapter Four presents the results obtained from all measurements, and the discussions on them.

Finally, chapter Five presents a short explanation and a summary of the most important conclusions of our work, and the recommendations for future research.

1.5 Aims of the Research

The main objective of this research is to Achieve extended random laser wavelength emission in the (visible –NIR) region. To verify this aim, several steps had been employed as bellow :

1- Synthesis different types and shapes of nanoparticles by different methods used as scattering center in random laser mediums.

2- Preparation liquid samples contained from laser dye as (Rhodamine Rh-640, MB and LDS 821) at different concentration, with different concentration of nanoparticles as (Fe_3O_4 SMNPs, Ag NWR, and Au NRS) and study the linear optical properties include absorption and fluorescence spectral to specify the best random laser medium that causes highest fluorescence emission.

3- Study the Morphology and structural properties for the prepared nanoparticles using XRD and FE- SEM.

4- Study and test the performance of random laser systems under different nanostructures in terms of type, concentration and shape.

5- Study and test the performance of random laser systems with and without applied external magnetic field.

6- Study and test the effect of energy transfer between dyes (Rh-640–MB) on the performance of random laser systems.

Chapter Two

Concepts

This chapter introduces the theory of Random Laser

2.1 Introduction

The theoretical principles which are considered in this chapter, includes the detailed description of the scattering, random media as light propagation through random media. The important parameters relate with the random laser as (spontaneous emission seeding in cavity, light amplification, laser threshold, random laser action, the parameters controlled random lasing and types active medium of random lasers), have been described in this chapter.

2.2 The Fundamentals of Random Laser

Understanding the random lasers in the best possible way requires basic knowledge of conventional lasers since both systems have many features in common, for example, the working principle is the same where the emitted photons induce other photons to be emitted by the stimulated emission process, and when the gain exceeds the losses, the lasing process occurs [36]. The only exception is the difference indicated earlier, which is that the random laser has no optical cavity in the sense of a conventional laser and this function, which was being performed by mirrors, is now achieved by multiple scattering centers and that the resulting spectrum random lasing is typically emitted in all directions [37].

Unlike the conventional laser, in random laser, the scattering process plays a crucial role in the optical feedback mechanism [38]. Here the scattering particles form an optical cavity instead of the conventional mirrors [39]. Therefore, if there are many centers of scattering, then the light in the gain medium will change its direction thousands of times randomly until it can leave the medium [40]. Thus; the multiple scattering that the photon will encounter within the sample will increase the time it

remains in the gain medium and thus increase its amplification time [41]. Through this process, the scattering centers act as a resonator to trap the light in the gain medium [42]. Accordingly, it becomes not necessary to add reflectors to retain the light inside the medium because the scatterers perform this function very efficiently. Thus, the term of random laser is used to describe the system that includes these disorders introduced to the gain medium [43]. The random laser occurrence can be regarded as a two-stage integrative process: the first is to re-propagate emitted photons from the scattering centers, and then these photons are amplified by the stimulated emission process in the gain medium as a second stage [44]. There are two basic parameters of length that are associated with the random laser. One is mean path length. It is the average distance a photon travels in the gain medium before leaving it. The second one is generation length. It is the average distance that a photon travels before generating another photon by stimulated emission [45]. Let's imagine photon propagates in the gain medium, when the mean free path is larger than the generation length, every photon generates a new photon before escaping the medium [46]. This scenario leads to a chain reaction in which one photon generates two photons, the two photons generate four photons, and so on. So that, the number of photons depends on the time the photon spends within the medium and the length of period time depends in turn on the strength of the scattering centers [47]. Fig.(2.1) shows the main difference between the traditional laser and random laser.

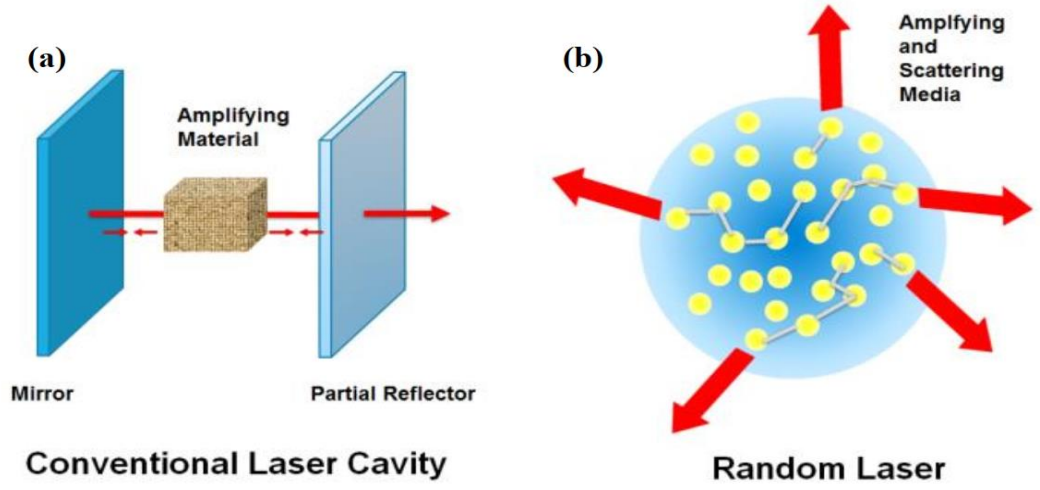

Fig. (2- 1) Schematic diagram of (a) conventional laser and (b) random laser [48].

2.3 Random laser classification

It is clear that the process of amplifying light in random laser is done by stimulated emission and that this process would not have continued had it not been for the feedback provided by multiple scattering of light [49]. Depending on the type of this feedback, the random laser can be divided into two types: (i) random lasers with incoherent (non-resonant) feedback (ii) random lasers with coherent (resonant) feedback [50]. In the case of incoherent random lasers, the intensity feedback can occur but it is not sensitive for phase (incoherent) and an independent frequency (non-resonant), while in the case of a coherent random laser, field or amplitude feedback can be provided where the phase is sensitive (coherent) and the frequency is a dependent (resonant) [51]. These two types will be discussed in more detail.

2.3.1 Incoherent feedback

If a light wave is incident on weakly scattered medium or even strongly scattered medium but the area of pumping pulsed is small [52], the photons

will experience multiple scattering but not for a long time, and then, some of them may escape through the front window into space, while the rest will leave the active volume to un-pumped volume. After a short period and because of the random directionality, a portion of these photons that are still within the disordered medium may return to the effective volume for more amplification [53]. This return process provides intensity or energy feedback. In this case, the trajectory of light is open, which means that the scattered photon does not return to the original position of its scattering, for this reason, the phase of scattered light in this type of random laser does not take into consideration, therefore, it can be called a non-resonant random laser and the photons are emitted as amplified spontaneous emission process [54].

When increasing the pumping rate, the photon intensity grows rapidly, and a narrowed emission peak within few nanometers is produced on broad fluorescence background at the center of the gain spectrum at the threshold [53]. In this type of random laser the scattering mean free path (l_s) which represents the average distance between two successive scattering events is much greater than the wavelength of the emitted photon but is much smaller than the sample thickness L $(L > l_s > \lambda)$ [55]. As a result of the resonance feedback absence, the system sends a stable spectrum with a fixed number of modes (usually one or two) and a bandwidth that is narrowed by about an order of magnitude (typically reaching 25-35 nm). Accordingly, the output spectrum is a smooth narrowed amplified spontaneous emission (ASE) [56]. Therefore, this model does not involve interference effects and explain the peaks in the diffusive scenario, which involves non-resonant feedback and the distribution of photons satisfies the Bose-Einstein distribution [57].

$$P(n) = \frac{\langle n \rangle^n}{[1+\langle n \rangle]^{n+1}} \quad \ldots\ldots\ldots\ldots\ldots\ldots\ldots\ldots\ldots\ldots\ldots\ldots\ldots\ldots\ldots\ldots \textbf{(2. 1)}$$

Where n is the average photons number.

2.3.2 Coherent feedback

The spectral characteristics of this type of random laser differ significantly from the first type [58]. Under certain conditions of pumping and gain, the spectra of the samples show several very narrow peaks (bandwidth FWHM~ 0.1 nm) installed on an incoherent base. These very narrow modes are temporarily coherent and fluctuate strongly in both frequency and intensity [59]. In this type of feedback, the strong scattering in the active medium plays an important role where the multiple scattering increases the path length and thereby increasing the dwell time of light in the gain medium, and thus enhancing the light amplification by the stimulated emission process [60], also, the strong scattering increases the possibility of light returning to the position of its first scattering [61]. This means after series of multiple scattering, the light returns to its first scattering position, forming a closed-loop that serves as a ring cavity for light and thus providing coherent feedback for lasing oscillation [62]. Interference along this closed-loop leads to standing wave patterns with a high degree of light trapping which means this kind of random laser, enables spatial coherence [63]. In this laser the scattering mean free path (l_s) is equal or less than the reciprocal wave-vector $kl_s \leq 1$ ($l_s \leq \lambda^{-1}$) which is known as the Ioffe-Regel criterion [64]. This system produces photon localization, which is equivalent to Anderson's localization proposed by Philip Anderson to interpret conductor-dielectric transitions in

electronic transport [65]. In this type, the photon number distribution $P(n)$ satisfies the Poisson distribution [54],

$$P(n) = \frac{\langle n \rangle e^{-\langle n \rangle}}{n!} \quad \ldots\ldots\ldots\ldots\ldots\ldots\ldots\ldots\ldots\ldots\ldots\ldots\ldots\ldots \quad (2.2)$$

where $\langle n \rangle$ is the average photon number. The laser spikes in the emission spectrum are the main characteristic of this type of random laser. These spikes, which are very narrow spectral features, are caused by the recurrent modes occurring in the random medium of this system. One can be distinguished between a coherent random laser and a non-coherent random laser through the emission spectrum containing spikes in the coherent laser while the incoherent laser is a single spectrum. Fig.(2-2) shows the difference between these two types of random laser, and also compares them with the conventional laser.

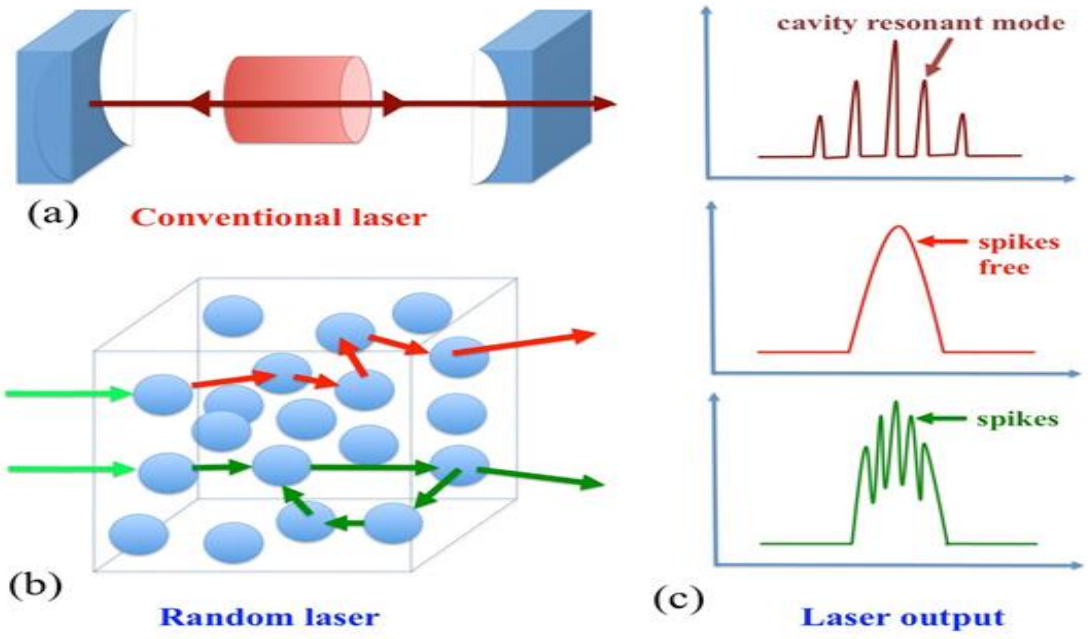

Fig. (2- 2) (a) Conventional laser cavity,(b) random laser cavity illustrating the incoherent feedback (red arrows) and coherent feedback (green arrows), (c) illustration of spectral outputs of a conventional laser and a random laser [66].

2.4 Characteristics of random laser

2.4.1 Optical Gain

Optical gain is one of the elements needed for the random lasing system besides multiple light scattering. The gain material becomes active when it is excited by a high energy pump source. Light may interact while propagates with an amplifying or gain material. Lasing action takes place when the light is sufficiently amplified before it leaves the framework, providing that gain overcomes loss, [67]. The light waves are multiplied scattered and amplified in an amplifying disordered medium. The amplification process is described by the Eq. (2.3)

$$l_{amp} = \sqrt{l_t l_g}/3 \quad \text{..... (2. 3)}$$

where l_g represents the gain length and l_{amp} refers to the amplification length. The amplification length is defined as the average distance between the beginning and ending point for paths of length, *lg* while the gain length refers to the path length over which the intensity is amplified by a factor e [68]. As light travels in a straight line in a medium without scattering, the Eq. (2.4) defines that amplification length should equal to the gain length.

$$l_{amp} = l_g \quad \text{..... (2. 4)}$$

Random lasing works the best upon the availability of sufficient scattering and the scattered light is well amplified to balance the loss as it leaves the gain medium [68]. The emitted photons propagate and being amplified within the active gain region, until they escape from the region. Thus, to balance the loss before photons escapes the medium, the Eq. (2.5) represents the necessary condition of random lasing so that the light is adequately amplified [68].

$l_s \geq l_g$ ..... **(2. 5)**

2.4.2 Lasing threshold:

The threshold, an important characteristic of lasing, has been extensively studied. For random lasers, the threshold depends on the scattering mean free path of photons in the random media and the luminescence efficiency of the gain media. Usually, the threshold is reached when the pump transition is bleached (saturated). Such bleaching increases the penetration of the pump and results in a longer scattering mean free path [69]. The threshold power can be lowered significantly when the scattering mean free path is equal to or less than the stimulated emission wavelength, as demonstrated in the ZnO random laser [70]. The concentration of scatters can influence the threshold, and it has been pointed that the threshold is proportional to $N^{-1/2}$. It was experimentally demonstrated that the threshold was lowered by more than two orders of magnitude, when the concentration of the scattering particles were increased [70]. The threshold also depends on the refractive index of the scatters compared to that of the surrounding media, and is lowered when the RI of the scatters is increased or the RI of surrounding media is decreased [71]. Recently, for realization further lower the lasing threshold, metal nanoparticles have been used as the scatters, which can induce surface plasmon resonance (SPR) and spatially confine the light near the surface to enable high gain. The metal nanoparticles have large scattering cross section. When the SPR wavelength is optimized to match with the lasing emission wavelength, plasmonic scattering is the strongest and the random laser has the lowest threshold [72].

2.4.3 Scattering mean free path

The scattering mean free path l_s is defined as the average distance that light travels between two consecutive scattering events, and is given by:

$$l_s = 1/\rho\sigma_s \quad \text{..... (2.6)}$$

Where, ρ and σ_s are the number density and the scattering cross-section of scattering particles respectively [73].

The transport mean free path l_t is defined as the average distance over which the scattered light is randomized. The relationship between the transport and the scattering mean free path is given by:

$$l_t = l_s/(1 - \cos\theta) \quad \text{.....(2. 7)}$$

where cosθ is the average cosine of the scattering angle, such that for Rayleigh scattering, $l_t = l_s$. There are three regimes for light scattering in random media [73]:

A- Localization regime ($l_s \leq \lambda$),

B- Diffusive scattering regime ($\lambda < l_s < L$)

C- Ballistic scattering regime ($l_s \geq L$)

Where, λ is the wavelength and L is the sample length.

Therefore, the most appropriate approach for calculating the scattering cross-section (σ_s) is the Rayleigh model, according to the following equation [73] :

$$\sigma_s = \frac{128\,\pi^5\,r^6}{3\,\lambda^4}\left(\frac{n^2-1}{n^2+2}\right)^2 \quad \text{.....(2. 8)}$$

where *r* is the radius of the scattering particle, and *n* is the refractive index. In the past two decades, lasing in random nanostructures has been extensively investigated using both theoretical and experimental studies. Based on the different feedback and gain mechanism provided by random nanostructures, many types of random lasers have been proposed and demonstrated.

2.4.4 Transition from Incoherent to Coherent Random Laser

In random laser, it is crucial to distinguish between the amplified spontaneous emission ASE (incoherent random laser) and lasing emission (coherent random laser), but the most important of all is the possibility of the transition from a non-coherent random laser to a coherent random laser [74]. To explain this transition, it is useful to use Fig.(2-3) where the scattering centers density increases from left to right while the bottom-to-top represents the pump power increasing [75]. When the scattering centers are weak, as shown in the first image at the bottom of the first column, which represents an incoherent laser state, the photon travels within a random medium of little density in terms of the scattering centers. Therefore it is difficult to form a closed path for not meeting the Ioffe-Regel criterion ($kl_s \leq 1$) which means the scattering mean free path (l_s) is much larger than the emission wavelength ($l_s \gg \lambda$) and thus what happens is an amplification of spontaneous emission or lasing with non-resonant feedback [60]. Therefore; at low scattering concentration and weak excitation, the emission spectrum is broad and low [76]. When pumping rates increase from low to higher values, it is noted that the emission spectrum begins to narrow and its intensity increases as it is observed in

the first column from bottom to the top. However, the possibility of the photon returning and forming a closed-loop which is still weak [46].

Now, with increasing the concentration of the scattering centers, as shown in the Figure (2-3), from left to right, and in order. It is observed that the width of the emission spectrum becomes very narrow and its intensity increases significantly more than the previous state above the pump threshold [77]. With increasing the concentration of nanoparticles, the scattering mean free path becomes close and close to the emission wavelength ($l_s \approx \lambda$) which increases the possibility that the photon will return to its first point of scattering, forming a closed path [78]. More sharp peaks appear when the pump intensity increases further and these discrete peaks result due to light returning to the first scattering position.

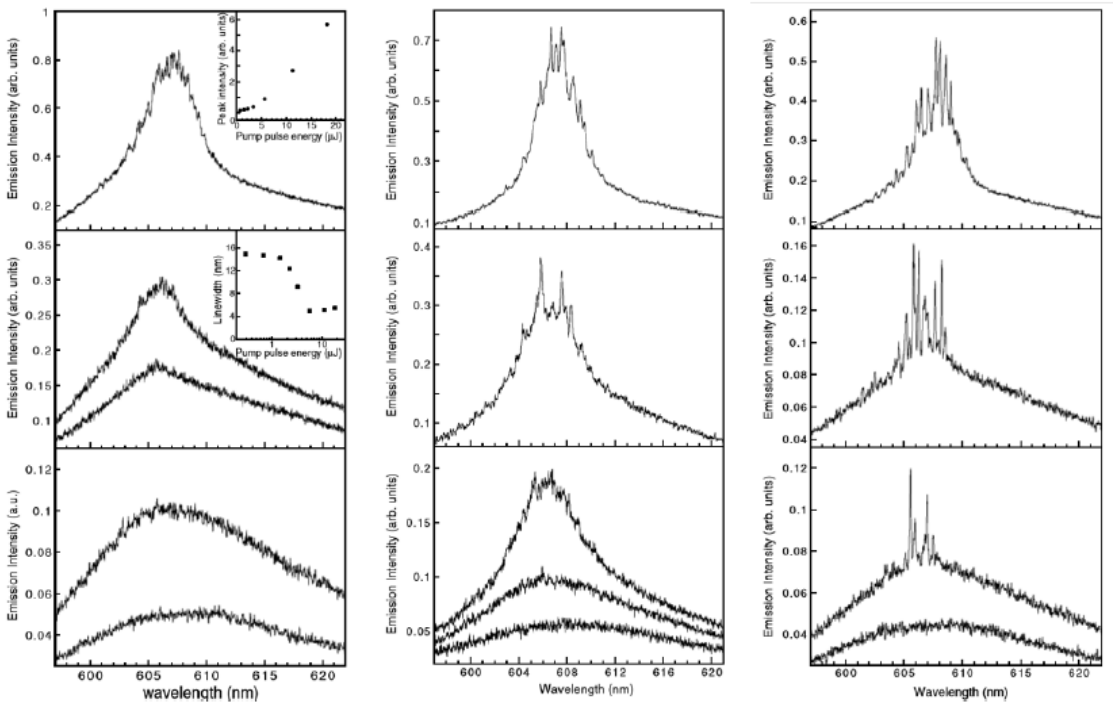

Fig. (2- 3) Evolution of random laser with increasing scattering centers from (left to right) and increasing the pumping power from (bottom to top) [75].

Laser oscillation can occur in these loops which serve as a resonator [79]. The discrete lasing modes correspond to the number of closed loops that formed in the gain medium. Also, one can note the number of modes in the second column is less than those in the third column under the same pumping power. This is due to that the concentration of scattering centers in the third column more than that in the second [60].

Finally, it can be reported that the transition from an incoherent laser state to a coherent laser depends mainly on the concentration of scattering centers and to a lesser degree on pumping sources and that the transformation process is done gradually [74].

2.5 Random Laser Applications

It is possible to employ random lasers in many fields owing to their distinctive characteristics such as operating at a specific wavelength. Alternatively, the fabrication cost of these lasers is low, and they have flexible shape with substrate compatibility [80]. Redding et al. [2] has indicated the applicability of the random lasers in bioimaging, producing speckle-free light with high intensities. In this way, one can be able to fabricate an integrated on-chip random spectrometer device [81]. For image quality tests, random lasers have also shown promising results, outperforming all the other sources of light. In this regard, the proof of concept was provided by comparing between the performances of random lasers and other light sources for speckle generation, image quality, and contrast-to-noise ratio tests. Notably, for the speckle generation tests, non-speckle patterns were formed by the random laser and light-emitting diodes (LEDs), whereas they produced higher contrast-to-noise ratios after performing the corresponding tests. When it comes to medical area, random

laser are capable of detecting tumor and performing photodynamic therapy [82]. In addition, Song et al. reported the applicability of random lasers for sensing purposes, light with a wavelength of 690 nm has been utilized to excite bone specimens soaked with a dye emitting at a wavelength of 800 nm. Thus, it has been possible to detect nanoscale structural stacks in a mechanical biosensor, resulting from the random lasing characteristics in the bone specimens [83]. On the other hand, Wan Ismail et al. has provided evidence on applicability of the aggregation of gold NPs for the measurement of an extremely low concentration of dopamine. This was enhanced by Cu ions for random lasers, having incoherent feedback. In this regard, emission peak linewidth, emission peak shift, lasing threshold and signal-to-noise ratio were affected, so that a dopamine detection limit of ~1 $\times 10^{-7}$ M was obtained as the detection indicator [84]. Furthermore, under mechanical tests, emission peak wavelength of the random lasers shifted by pressuring the bone specimens. According to Vardeny et al. [85], human tissues can have strong scattering, allowing for the support of the random lasing when penetrated with a laser dye solution with a high concentration. It has also been possible to employ random lasers in order to map cancerous tissues. This was achieved by portraying the affected spectral emission for both the healthy and cancerous tissues. In this respect, the tissues were separately immersed in Rhodamine 6G dye, followed by flattening them between the slides of the microscope. By pumping the specimens using Nd: YAG laser (532 nm, 100 ps, and 800 Hz), emission spectra were obtained.

2.6 Optical properties of nanomaterials

Nanometer-scale metal particles exhibit optical properties of great aesthetic. technological, and intellectual value. At a fundamental level, optical absorption spectra provide information on the electronic structure of small metallic particles. Colloidal solutions of the noble metals, copper, silver, and gold show a very intense color and exhibit a strong absorption band, which is remarkably different from the bulk material as well as for the individual atoms. Also, the significant reduction in the size of nanomaterials affects their optical properties [86].

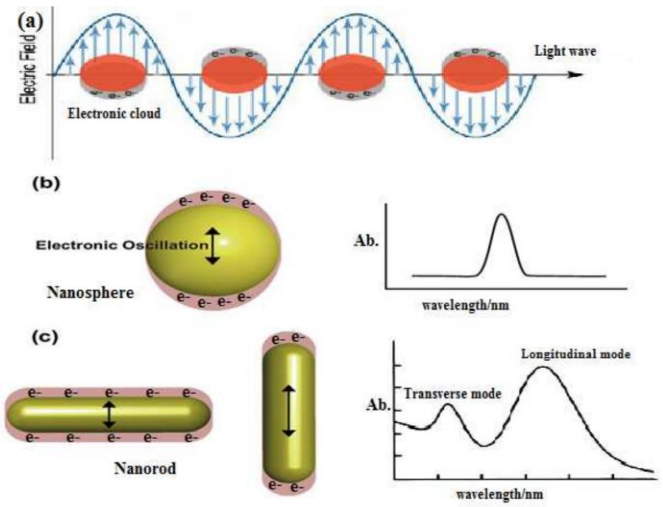

Fig. (2- 4) Schematic representation of (a) localized surface plasmon resonance, (b) electric oscillation of nanoshere, and (c) nanorod with respective extinction spectrum due to LSPR and TSPR [86].

The change in optical properties is caused by two factors, the quantum confinement of electrons within nanoparticles and the surface plasmon resonance.

When the metallic nanoparticles are irradiated by electromagnetic light wave, the free electron in the metals are in driven by the alternating electric field with collectively oscillate in a phase with the incident light (Fig. (2-4)). When the dimensions of a metal are reduced, boundary and surface effects become very prominent, and for this reason the optical properties of MPs are dominated by collective oscillation of conducting electrons in response to an incident electromagnetic radiation, which is typically known as surface plasmon resonance (SPR). The linear and nonlinear optical properties of such materials can be finely tailored by controlling the crystal dimensions, the chemistry of their surfaces and fabrication technology becomes a key factor for the applications [87].

The free electrons in metal (specially, the 'd' electrons in silver and gold) travel through the material. The mean free path in gold and silver is ~50 nm. In particles smaller than ~50 nm, no scattering is expected from the bulk [88]. This means that the interactions with the surface dominates. When the wavelength of light is much larger than the nanoparticle size it sets up standing resonance conditions as represented in Fig. (2-5).

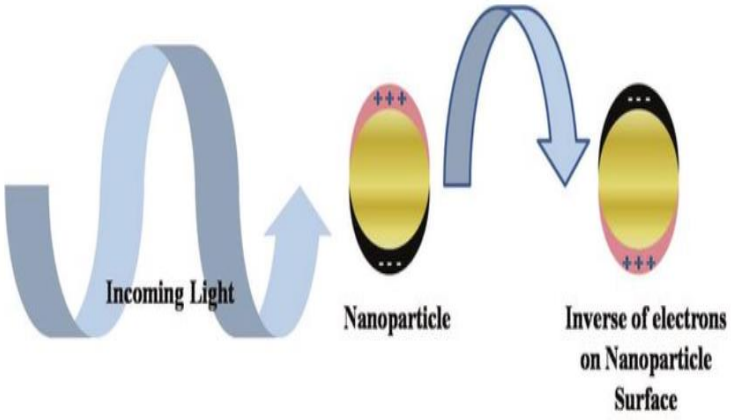

Fig. (2- 5) Origin of surface plasmon resonance due to coherent interaction of the electrons in the conduction band with light [89].

Light in resonance with the surface plasmon oscillation causes the free-electrons in the metal to oscillate. As the wave front of the light passes, the electron density in the particle is polarized to one surface and oscillates in resonance with the light's frequency causing a standing oscillation. The resonance condition is determined from absorption and scattering spectroscopy and is found to depend on the shape, size, and dielectric constants of both the metal and the surrounding material [90]. This is referred to as the surface plasmon resonance (SPR), since it is located at the surface. As the shape or size of the nanoparticle changes, the surface geometry changes, causing a shift in the electric field density on the surface. This causes a change in the oscillation frequency of the electrons and generates different cross- sections for the optical properties including absorption and scattering.

2.7 Nanomaterials have been used in optical feedback applications

2.7.1 Gold Nanorods

Gold nanorods are microscopic gold nanoparticles that are elongated along one direction and resemble a rod shape. There are different methods for the synthesis of gold nanorods. Some of them are (i) Seed-mediated growth method (ii) Electrochemical method (iii) Template method (iv) Electron beam lithography method. These methods synthesized nanorods with different aspect ratio and their properties depend upon the aspect ratio. Because of the tunable optical properties of gold nanorods, they are suitable for a wide range of applications, from information processing to medicine. Gold nanorods are effectively used for the development of optical imaging techniques, cancer detection, and therapy [91]. Radiative processes such as photoluminescence emission of nanomaterials can be profoundly modified by their interaction with plasmonic nanostructures. Collective oscillation of conduction (free) electrons in metallic gold nanorods cause the formation of plasmon resonance as shown in Fig. (2-4). Depending on the size of of gold nanomaterials, the peak resonance wavelength may be varied at the range of (500-900) nm, which is spectrally overlapped with the dye emission wavelength (Fig.(2-6)) [92].

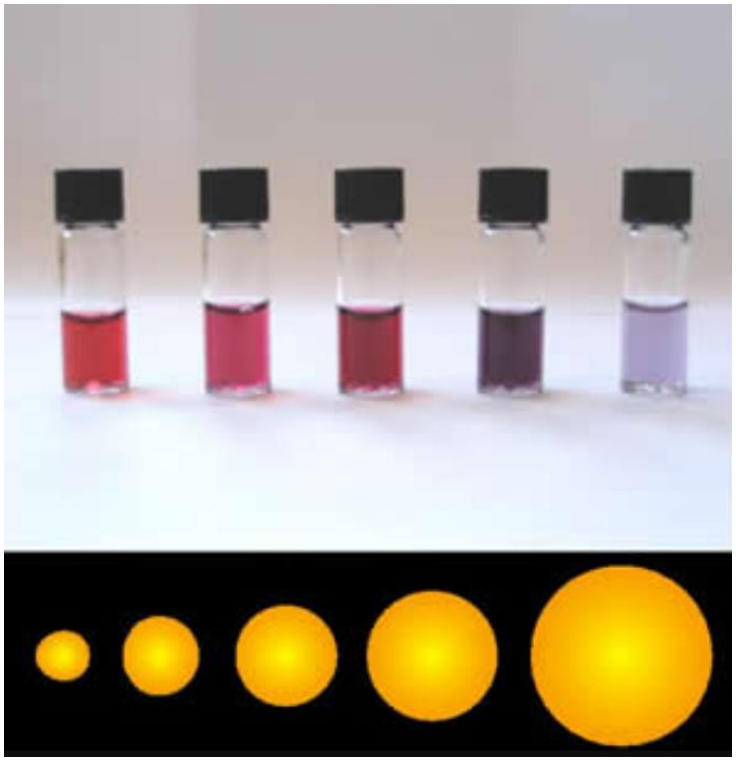

Fig. (2- 6) Suspensions of gold nanoprods of various sizes. The size difference causes the difference in colors [93]**.**

2.7.2 Silver nanowire :-

Ag nanowire is a metallic type of nanostructure in the form of a wire with the diameter of the order of a nanometre. More generally, nanowires can be defined as structures that have a thickness or diameter constrained to tens of nanometers or less and an unconstrained length. Silver NWRs have attracted a lot of attention in the electronics, chemistry, physics, biology, and medicine fields because of their unique properties that depend strongly on the composition, size, shape of metal nanostructure [94]. The ability to control the size and shape of metal nanostructures provides a great opportunity to check the electrical and optical properties of these materials

and opens up prospects for use in different applications as random laser systems [95].

Ag nanostructures contain a set of properties that can be adjusted or improved by controlling their shape. Ag has the highest thermal and electrical conductivity among the metals. It also has unique optical properties, and this is evident in its major role in photography. The nanosilver's advantages over other noble metals in relation to its physical and chemical properties are: stability at ambient conditions, low cost than other noble metals such as gold and platinum, broad absorption band in the visible region of the electromagnetic spectrum, chemical stability, and non-linear optical behaviour [96].

Silver nanowires have been shown to significantly enhance light scattering with different gain materials, because the interactions between the emission centers and the surface plasmons can be controlled in the visible range from 442 to 785 nm [97]. Depending on the size and shape of silver nanomaterials, the peak resonance wavelength may be varied at the range of (380-470) nm [98].

2.7.3 Fe_3O_4 magnetic nanoparticles

Iron (III) oxide is the chemical compound with formula Fe_3O_4. It occurs in nature as the mineral magnetite. It is one of a number of iron oxides. It contains both Fe^{2+} and Fe^{3+} ions and is sometimes formulated as $FeO \cdot Fe_2O_3$. This iron oxide is a black powder. It exhibits permanent magnetism and is ferromagnetic [99]. Its most extensive use is as a black pigment. For this purpose, it is synthesized rather than being extracted from the naturally

occurring mineral as the particle size and shape can be varied by the method of production.

The physical and chemical properties of magnetic nanoparticles largely depend on the synthesis method and chemical structure. In most cases, the particles range from 1 to 100 nm in size and may display superparamagnetism [100].

Magnetic nanoparticle clusters that are composed of a number of individual magnetic nanoparticles are known as magnetic nanobeads with a diameter of 50–200 nanometers [101]. Magnetic nanoparticle clusters are a basis for their further magnetic assembly into magnetic nanochains. The magnetic nanoparticles have been the focus of much research recently because they possess attractive properties which could see potential use in catalysis including nanomaterial-based catalysts, biomedicine and tissue specific targeting, magnetically tunable colloidal photonic crystals, microfluidics, magnetic resonance imaging, magnetic particle imaging, data storage, environmental remediation, ferroofluids and optical filters [102].

Various chemical synthetic routes have been employed to produce magnetite nanoparticles with desired physical and chemical properties, such as coprecipitation of aqueous ferrous (Fe^{2+}) and ferric (Fe^{3+}) salt solution by the addition of a base [103].

2.8 Enhancing light matter interaction by Plasmonic structure

In the last few decades, researchers have been making efforts to understand the light-matter interaction and now they emerged a new research field called “Plasmonics”. Plasmons are the quantization of charge oscillations of free electrons in materials such as metals, in response to incoming light. When these oscillations are restricted to a meta-dielectric interface, and light interacts with particles that are much smaller than its wavelength, a local charge oscillation around the particle is produced, which is known as localized surface plasmonic resonance (LSPR) [104].

In general, the optical phenomenon which arises (from the) interaction between an electromagnetic wave and free electrons in a metal is called LSPR. The plasmonic nanoparticles show a number of interesting properties when light is confined at the nanoscale dimension. Some of the optical properties are; large enhancement in the electromagnetic field, high photothermal conversion efficiencies, great spectral responses, etc. [105]. Although there are a number of existing plasmonic materials, the most common materials are noble metals like gold and silver. Gold nanostructures with its (their) exciting localized surface plasmon property fascinates may (many) researchers and became an interesting field of research. The free electrons in a gold nano nanostructure are driven by the electric field and subjected to the collective oscillation at a resonant frequency. At this resonant frequency, the incident light is absorbed by the nanostructure and a number of incident photons are scattered, or released in all directions with the same frequency, while the others were absorbed. Interestingly, the gold nanostructure’s LSPR peak includes both scattering and absorption components. The spectral position of the plasmon resonance

strongly depends upon the shape and size of the nanoparticles, so that the variation in shape allows spectral tuning of the plasmon resonance to overlap the emission spectrum of the desired active medium [106].

2.9 Photophysical process

Fluorescence as a phenomenon is part of a larger family of related luminescent processes in which a susceptible substance absorbs light, only to reemit light (photons) from electronically excited states after a given time. Photoluminescent processes that are generated through excitation, whether this is via physical, mechanical, or chemical mechanisms, can generally be subdivided into fluorescence and phosphorescence. Fig. (2-7) shows the schematic representation of the fluorescence phenomenon in the classical Bohr model. Absorption of a light quantum (blue) causes an electron to move to a higher energy orbit. After residing in this "excited state" for a particular time, the fluorescence lifetime, the electron falls back to its original orbit and the fluorochrome dissipates the excess energy by emitting a photon (green) [107].

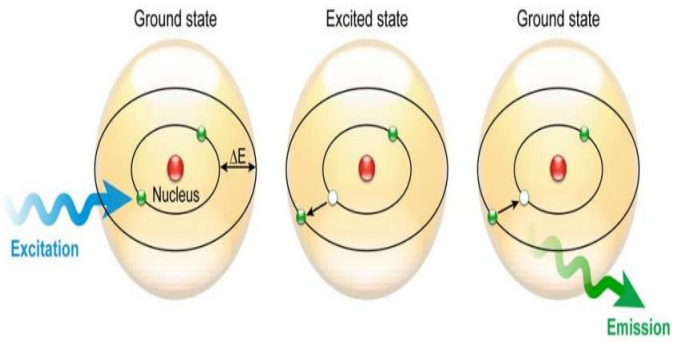

Fig. (2- 7) Fluorescence principle [107]**.**

Compounds that display fluorescent properties are generally termed fluorescent probes or dyes and de facto the term fluorochrome is most appropriate. Often fluorochrome and fluorophore are used interchangeably. Strictly taken the term fluorophore refers to fluorochromes that are conjugated covalently or through adsorption to biological macromolecules, such as nucleic acids, lipids, or proteins. Fluorochromes come in different flavors and include organic molecules (dyes), inorganic ions (e.g., lanthanide ions such as Eu, Tb, Yb, etc.), fluorescent proteins (e.g., green fluorescent protein), and atoms (such as gaseous mercury in glass light tubes). Recently, inorganic luminescent semiconducting nanoparticles, quantum dots, have been introduced as labels for biological assays, bio-imaging applications, and theragnostic purposes, the combination of diagnostic and therapeutic modalities in one and the same particle [108]. Fluorescence follows a series of discrete steps of which the outcome is the emittance of a photon with a longer wavelength, a process which can be visualized in more detail via the Jabłoński diagram in Fig. (2-8) [109]. When light of a particular wavelength hits a fluorescent sample, the atoms, ions or molecules therein absorb a specific quantum of light, which pushes a valence electron from the ground state $_GS_0$ this initial state is an electronic singlet in which all electrons have opposite spin and the net spin is 0, into a higher energy level, creating an excited state $_ES_n$. This process is fast and in the femtosecond range and requires at least the energy $\Delta E = E_{ESn} - E_{GS0}$ to bridge the gap between excited and ground states in order for excitation to occur. The energy of photons involved in fluorescence and generally a quantum of light can be expressed via Planck's law [110]:

$$\boldsymbol{E = h \cdot v = h \cdot \frac{c}{\lambda}} \quad \text{.....(2. 9)}$$

where E is the quantum's energy (J), h is Planck's constant (J.s), v the frequency (s^{-1}), λ is the wavelength of the photon (m), and c is the speed of light ($m.s^{-1}$). However, there are several excited state sublevels (vibrational levels) and which level is reached primarily depends on the fluorescent species' properties. Irradiation with a spectrum of wavelengths generates numerous allowed transitions that populate the various vibrational energy levels of the excited states, some of which have, according to the Franck-Condon principle, a higher probability to occur than others (the better two vibrational wave functions overlap, the higher the probability of transition) and combined form the absorption spectrum of the fluorescent dye. After excitation to the higher energy level E_{Sn}, the electron quickly relaxes to the lowest possible excited sublevel, which is in the picosecond range. The energy decay from dropping to a lower vibrational sublevel occurs through intramolecular non-radiative conversions and the converted heat is absorbed via collision of the excited state fluorescent molecule with the solvent molecules. Emission spectra are usually independent of the excitation wavelength because of this rapid relaxation to the lowest vibrational level of the excited state, which is known, as Kasha's rule [111]. In most cases, absorption and emission transitions involve the same energetic levels as schematically shown in Fig. (2-8). For this reason and the fact that excitation is instantaneous, involving electrons only and leaving the heavier nuclei in place, many fluorochromes display near mirror image absorption and emission spectra (mirror image rule), although many exceptions exist. External conversion depletes the excited state through interaction and energy transfer to the solvent and/or solute. Intersystem crossing is the slowest energy dissipation pathway, because the electron has to change spin multiplicity from an excited singlet state to an

excited triplet state (Fig. (2-8)). This is essentially a spin forbidden transition, but in some fluorochromes favorable vibrational overlap between the two states makes the transition weakly allowed.

The mutual effect between radiation and matter is one of the basic operations behind many phenomena occurring in the universe. Transmitted light waves through any medium interact with the medium particles. This interaction can be described via several processes so called photophysical processes; in these processes, the main route of energy relaxation of an excited dye molecule is either radiative or non-radiative transition.

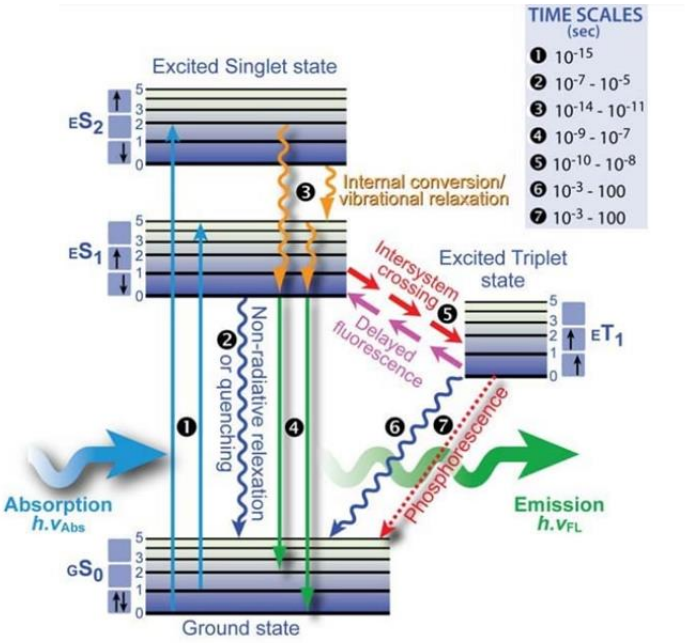

Fig. (2-8) Jablonski diagram illustrating the processes involved in the creation of an excited electronic singlet state by optical absorption and subsequent emission Processes [107]**.**

2.9.1 Fluorescence energy transfer

Fluorescence energy transfer is one type of photo-physical prosses that is transfer of the excited state energy from a donor (D) to an acceptor (A) [112]. This transfer occurs without the appearance of photon and is primarily a result of dipole-dipole interaction between the donor and the acceptor. The rate of energy transfer depends upon the extent of overlap of the emission spectrum of the donor with the absorption spectrum of the acceptor, the relative orientation of the donor and acceptor transition dipoles and the distance between these molecules [113]. The nonradiative energy transfer occurs as a result of dipole dipole coupling between the donor and the acceptor, and does not involve the emission and reabsorption of photons. The other process is radiative process, which depends upon other properties of the sample, such as size of the sample, container, optical densities of the sample at the excitation and emission wavelengths and the precise geometric arrangements of the excitation and emission axes [114]. In contrast to these trivial factors, nonradiative energy transfer depends upon the molecular details of donor acceptor pairs. It is important to note here that the phenomenon of energy transfer also contains molecular information, which is different from revealed by other phenomena such as solvent relaxation, excited state reactions, and fluorescence quenching of fluorescence polarization. These other spectral properties of fluorescence reveal primarily the interactions with the other molecules in the surrounding solvent shell. The important parameter for energy transfer that nonradiative energy transfer is effective over distance ranging of 50A. The intervening of solvent or other macromolecules has little effect on the efficiency of the energy transfer, which depends primarily on the D-A

distances. S_o, briefly the transfer of electronic energy from one molecule to another generally occurs in one of the following two ways [114].

1- Radiative energy transfer mechanism.

2-Non-Radiative energy transfer mechanism: which includes

a- Resonance energy transfer.

b- collision energy transfer.

Energy transfer in a mixture of dyes has been established as an effective mechanism for extending the wavelength of lasing, tenability, enhancement of power of the dye laser and low pump power requirement; dye lasers have some limitations as the dye solution used as an active medium absorbs energy from the excitation source in a very limited range and So the emission band also has these limitations. If a dye laser has to be used as an ideal source its spectral region needs to be extended. In order to extend the spectral region of operation mixtures of different dye solutions/dye molecules embedded in solid matrices are being used. The work on energy transfer between different dye molecules in such mixtures in various solvents and solid matrices is, therefore, of great importance. The use of such energy transfer in dye lasers is also helpful in minimizing the photo-quenching effects and thereby, increasing the laser efficiency. The energy transfer is manifested by a quenching of donor emission, an increased emission of acceptor excited via the donor, a decrease in donor photobleaching rate, and a decrease in donor lifetime [115]. Fig. (2-9) shows the energy level scheme of the resonant transitions of a donor-acceptor pair.

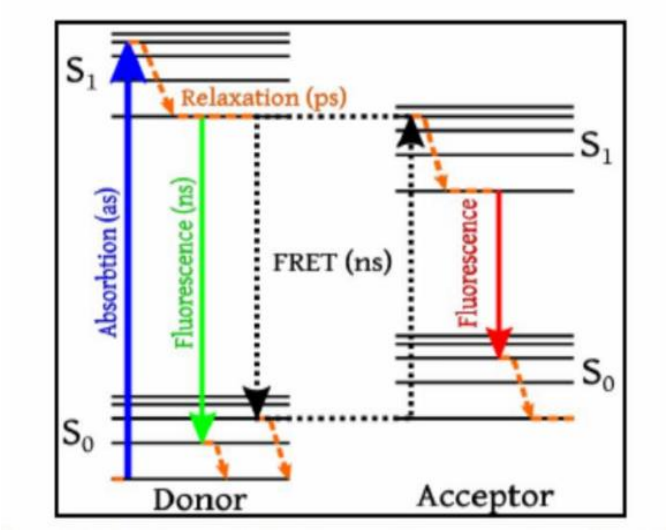

Fig. (2- 9) Energy level scheme of the resonant transitions [116].

Forster has developed a theory for non-radiative energy transfer in terms of the resonance dipole-dipole interaction mechanism, and has shown that rate constant for dipole energy transfer K_{ET} between donor D and acceptor A, is given by:

$$K_{ET} = 1.25 \times 10^{17} \frac{\Phi_D}{n^4 \tau_D R^6} \int_0^{\infty} \frac{F_D(\bar{\nu}) \epsilon_A(\bar{\nu}) d\nu}{4} \quad \ldots\ldots\ldots\ldots\ldots\ldots\ldots (2.10)$$

where Φ_D is the quantum yield of donor emission, τ_D is the lifetime of the emission, n is the solvent refractive index and R is the distance in nm between D* and A, $F_{D(\bar{\nu})}$ is the emission spectrum of the donor, expressed in wave number and normalized to unity and $\epsilon_{A(\bar{\nu})}$ is the molar excitation coefficient of A at the wave number $(\bar{\nu})$ [117].

The critical transfer distance (R_o) is generally used to indicate the strength of the interaction between donor and acceptor molecules and by definition, is the distance where the rate constant for energy transfer K_{ET} is equal to the rate constant for fluorescence by donor in the absence of acceptors $1/\tau$. Eq. (2-9) can re-written as [118]:

$$K_{ET} = \frac{1}{\tau_D}\left(\frac{R_0}{R}\right)^6 \quad \text{..... (2. 11)}$$

substituting equation (2.8) into equation (2.7) gives:

$$R_o^6 = 1.25 \times 10^{17} \frac{\Phi_D}{n^4} \int_0^\infty \frac{F_D(\bar{v})\epsilon_A(\bar{v})d}{4} \quad \text{..... (2. 12)}$$

The conditions favoring energy transfer are a large overlap between fluorescence spectrum of the donor and the absorption spectrum of acceptor, a large value of ϵ_A and a large value of fluorescence quantum yield of donor Φ_D.

The Stern–Volmer plots can be used to derive the radiative and non-radiative rate constants, as illustrated in [119], [120]:

$$\frac{\emptyset_D}{\emptyset_{DA}} = 1 + K_{AD}\tau_D[A] \quad \text{..... (2. 13)}$$

$$\frac{I_D}{I_{DA}} = 1 + K_{SV}[A] \quad \text{..... (2. 14)}$$

Where I_D and I_{DA} are the fluorescence intensities of the donor in the absence and presence of acceptor, respectively; K_{SV} and K_{ET} are the total and nonradiative transfer rate constants respectively and [A] acceptor concentration ,φ_D and φ_{DA} the corresponding quantum yields; τ_D the fluorescence lifetime of the donor without acceptor which can be calculated from Bowen and Woks relation [121] :

$$\frac{1}{\tau_D} = 2.88 \times 10^{-9} \times n^2 \times (\bar{v}^2) \int \varepsilon(\bar{v}) d\bar{v} \quad \text{..... (2. 15)}$$

Where the area under the curve of the molar extinction coefficient of donor vs wave number is $\int \epsilon(\nu)\, d(\nu)$, n is the refractive index, and ν_o is the peak absorption spectrum value in cm^{-1}.

Eq. (2-12) can be rewritten as follow:

$$\frac{\tau_D}{\tau} = 1 + K_{AD}\tau_D[A] \quad \ldots\ldots\ldots\ldots\ldots\ldots\ldots \quad (2.16)$$

Where $\tau = 1/2\tau_{fm}$, $[A]_h = [A]_{1/2}$: half-value concentration, which is given by:

$$[A]_{1/2} = 1/K_{SV} \quad \ldots\ldots\ldots\ldots\ldots\ldots\ldots \quad (2.17)$$

From Eq. (2-15):

$$K_{SV} = \tau_D K_{AD} \quad \ldots\ldots\ldots\ldots\ldots\ldots\ldots \quad (2.18)$$

Then the critical transfer distance between donor and acceptor is

$$R_0 = \frac{7.35}{\sqrt[3]{[A]_{1/2}}} = 7.35(K_{SV})^{1/3} \quad \ldots\ldots\ldots\ldots\ldots \quad (2.19)$$

Resonance transfer is often the dominant mechanism of energy transfer in concentrated solutions and can occur over intermolecular distance of (10-100) °A [122].

Chapter Three

Experimental Part

This chapter introduces the Materials, experimental and practical concepts used throughout the thesis

3.1 Introduction

In this chapter, the properties and characteristics of materials used in our experiments to generate random laser with specific outputs will be discussed. The ways and methods used in preparing the research materials will also be covered. Then, the random media will be reviewed depending on the type, size, concentration and shape of the nanomaterials used as scattering centers in the random laser system. The experimental setups which employed whether to test the performance of the random laser or to calculate some of its related parameters will also be demonstrated.

3.2 Outline of the Experimental Part

The schematic diagram in Fig.(3.1) illustrates the flow chart that will be focused on in our experimental work to improve the performance of the random lasers. It includes the elements that make up the random medium (gain medium, scattering centers, host medium, and supporting materials). Then, the optical and structural properties of these components are measured and examined. After, different random media will be formed in terms of type, shape, size, and concentration of the nanomaterial to test the performance of the random laser under the influence of these parameters associated with the dispersion centers.

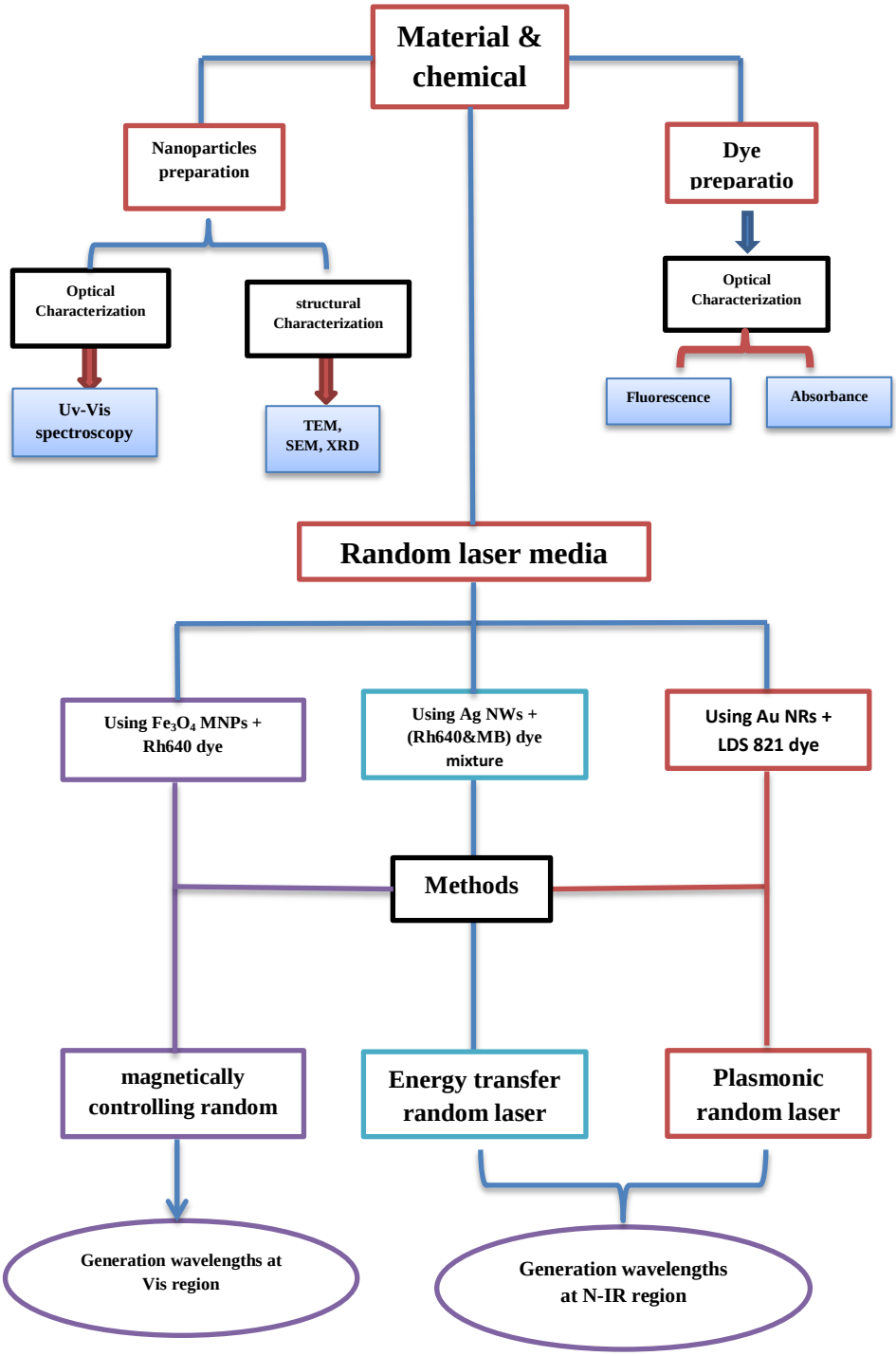

Fig. (3-1) Flow chart of the experimental part in this project.

3.3 Nanoparticles preparation

Three types of nanomaterial have been prepared by different methods will be discussed in following details

3.3.1 The formation mechanism of the magnetic nanoparticles (Fe_3O_4)

3.3.1. a-Chemical method

CO-Precipitation method is the most widely applied technique for preparing Fe_3O_4 magnetic nanoparticles due to it is more versatile, economical where it does not require any advanced equipment. The method used to prepare the Fe_3O_4 magnetic nanoparticles colloidal solutions of ferrofluid can be summarized as follows:

- Materials and Method

All the reagents used for the synthesis Fe_3O_4 were analytical grade and used without further purification. Ferric chloride [$FeCl_3$], ferrous chloride [$FeCl_2$], sodium hydroxide [NaOH] were purchased from India. Deionized water was used throughout the experiments.

The synthesis of Fe_3O_4 magnetics nanoparticles were prepared by co-precipitation of ferric and ferrous salts under the presence of N_2 gas. 16.25 g of $FeCl_3$ and 6.35 g of $FeCl_2$ were dissolve into 200 mL of deoxygenated distilled water. The pH of the solution varied from 1.5 to 2.0. After stirring for 60 minutes, chemical precipitation was achieved at 30 ^{0}C under vigorous stirring by adding of 2 M NaOH solution under presence of N_2 gas. The pH of the solution raised from 2 to 8.0. The color of the iron solution changed slowly from light brown, through dark brown, and finally to black, indicating the formation of magnetite nanoparticles (Fig.3-2, Supporting Information).

The reaction system keep at 70 ^{0}C for 3 h and pH solution ± 12. Completed precipitation of Fe_3O_4 expected at pH between 8 and 14 [123]. After the system was cooled to room temperature, the precipitates were separated by a permanent magnet and washed with deoxygenated distilled water until pH neutral. Finally Fe_3O_4 was washed with acetone and dried in oven at 60-70 ^{0}C. The relevant chemical reaction can be expressed as follows Eq. (3.1):

$$Fe^{2+} + 2Fe^{3+} + 8OH^- \rightarrow Fe_3O_4 + 4H_2O \quad \text{.....(3. 1)}$$

Fig. (3-2) The formation of Fe_3O_4 magnetic nanoparticles.

3.3.1 .b- Pulsed laser ablation in the liquid phase

Because of lack of control on the stability of the magnetic nanomaterial, pulsed laser ablation technique in aqueous medium were used as a post processing introduced to make a colloidal suspensions of Fe_3O_4 magnetic nanoparticles to meet the requirement. After completing the preparation of

the samples in the form of a solid solution, take of 0.5 g from the samples and immerse in (2 ml) of distilled water. The Nd:YAG laser of wavelength (1064) nm with a number of pulses (200) and energy is (200 mJ) at a frequency of (6) Hz for the ablation source. Laser ablation occurs in the liquid phase by the interaction of the (high energy) laser beam with the interface between the solid target and liquid, which causes to evaporate the target into a small amount in the surrounding liquid as the removed parts from the target [124].

The plasma column is also generated as in Fig. (3-3), which shows the drawing of the plasma cloud formed by the laser beam from the target of the material. It consists of different thermal layers and a state of atomic ionization as a result of high temperatures (T), and high pressure (P), and high density (Fig.(3-4)), at the solid-liquid interface. Thus, the plasma is trapped by the liquid and produces a shock wave that travels through the target, which in turn produces additional pressure in the plasma. As a result of the liquid quantitative confinement effect, the dispersed parts form a dense layer near the liquid-solid interface [125]. And the white arrows indicate that when the distance from the laser spot increases, the temperature (T), pressure (P) and the concentration of the removed substance (CM) decrease, while the concentration of the solution increases [124].

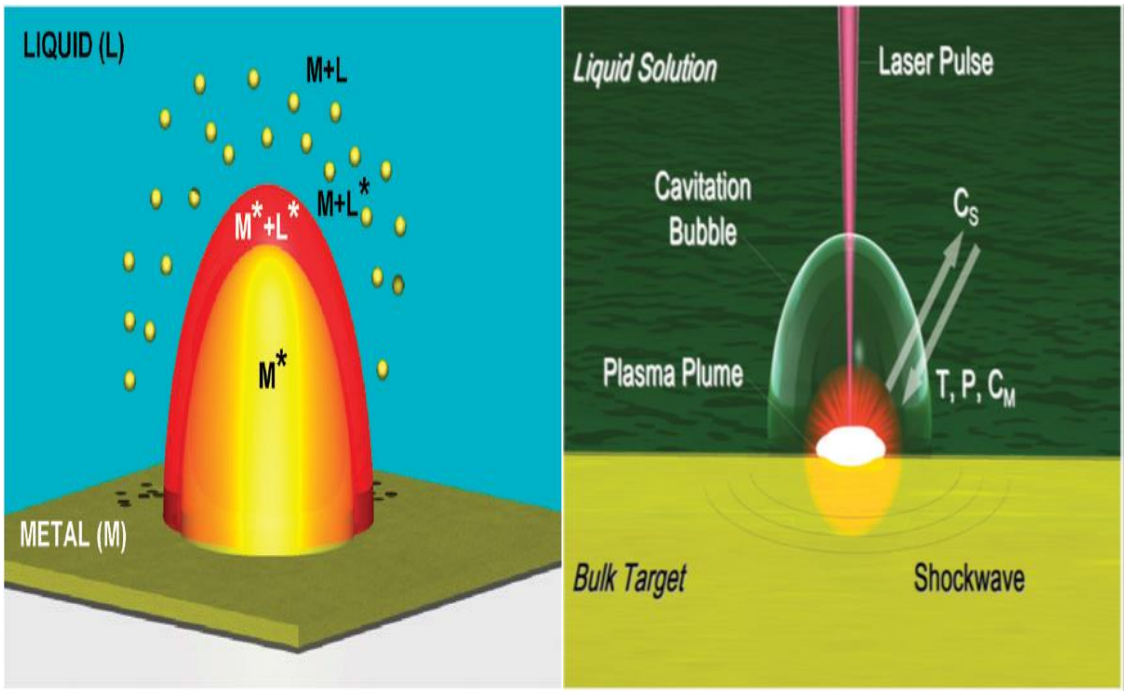

Fig. (3-3) The steps of the preparation of Fe_3O_4 SNPs by laser ablation [126].

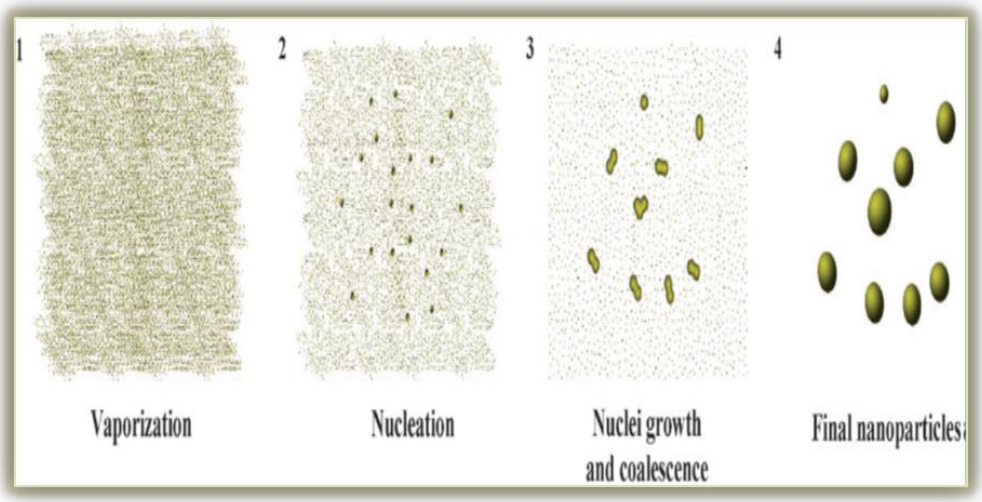

Fig. (3-4) The stages of nanoparticle formation (evaporation - nucleation - nuclei growth - nanoparticles) [126].

3.3.2 Synthesis of the silver nanowire by seed-mediated growth method

In this study, the seed-mediated growth method were used to synthesis of Ag NWs. First, the small metal particles were prepared and later used as seeds for the preparation of nanowires. The silver seeds were prepared by reduction of silver ions with sodium borohydride in the presence of sodium citrate dehydrate as stabilizer. These silver seeds were added into the solution containing more silver salt, an ascorbic acid (weak reducing agent) and cetyltrimethylammonium bromide (CTAB). under specific of temperature of solution. the procedures with supporting chart described as follow (Fig. (3.5)) [127]:

1- 10 ml aqueous solution containing 0.25 mM $AgNO_3$ and 0.25 mM sodium citrate dehydrate was prepared.

2- A 20 ml of aqueous solution containing 0.1 mM CTAB have been prepared.

3- A 0.1 mM of freshly ascorbic acid has been prepared

1- a varied amount of 1 mM NaOH have been prepared

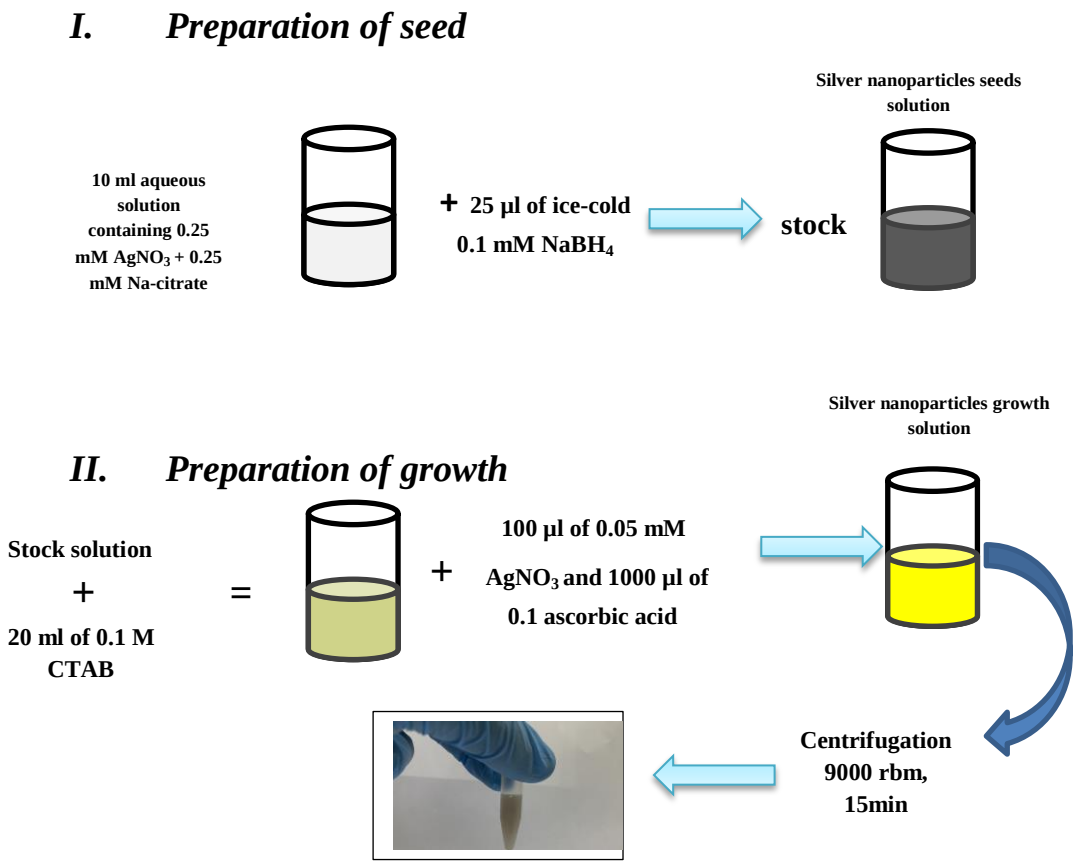

Fig. (3- 5) The procedures of synthesis of the silver nanowire by seed-mediated growth method.

3.3.3 The synthesis of Gold nanorods:

3.3.3 *a-Materials*

The following precursors were used as reagents in the experiments: chloroauric acid trihydrate ($HAuCl_3H{\cdot}4H_2O$, 99%, Acros Organics), ascorbic acid (99.5%, Alpha Chemical), CTAB (96%, Sigma Aldrich), silver nitrate ($AgNO_3$, >99%, Sigma Aldrich), and sodium borohydride ($NaBH_4$, 99%, Sigma Aldrich). All solutions used in this study were prepared using distilled water. The properties of chloroauric acid trihydrate shown in Table (3-1).

3.3.3 *b-Method (Seedless growth)*

Fig. (3-6) schematically depicts the seedless synthesis process of gold NRs. To prepare the solution, the following procedure was utilized: $HAuCl_3H{\cdot}4H_2O$ (6 mM, 800 µL) and CTAB (200 mM, 4 mL) were mixed in a 20 mL glass vial, resulting in a yellowish brown solution. In continuance, ascorbic acid (100 mM, 80 µL) was added to the previous solution, and stirred until the color of the solution changed to colorless. Silver nitrate (10 mM, 80 µL) was also added and shaken for 10 s. Next, ice-cold freshly prepared sodium borohydride (1 mM, 20 µL) was added to the solution and vortexed for 5–10 min. The final solution was maintained at room temperature for 3 h, making its color more intense. After finishing the reaction, the excess CTAB was removed from the gold NR dispersion using a centrifugation process (14000 rpm, 1 h). The supernatant was then separated, and the precipitate was redispersed twice in distilled water using an ultrasonic bath [128].

Table (3- 1) Properties of chloroauric acid ($HAuCl_4.3H_2O$) [129].

Another name	Hydrogen tetrachloroaurate
Chemical structure	$HAuCl_4.3H_2O$
Molar mass	393.833 g/mol
Appearance	Orange-yellow needle-like crystal
Density	2.89 gm/cm^3
Melting point	245 ^oF
Solubility in water	350 gm $HAuCl_4.3H_2O$/ 100 gm H_2O
solubility	alcohol, ester, ether, ketone

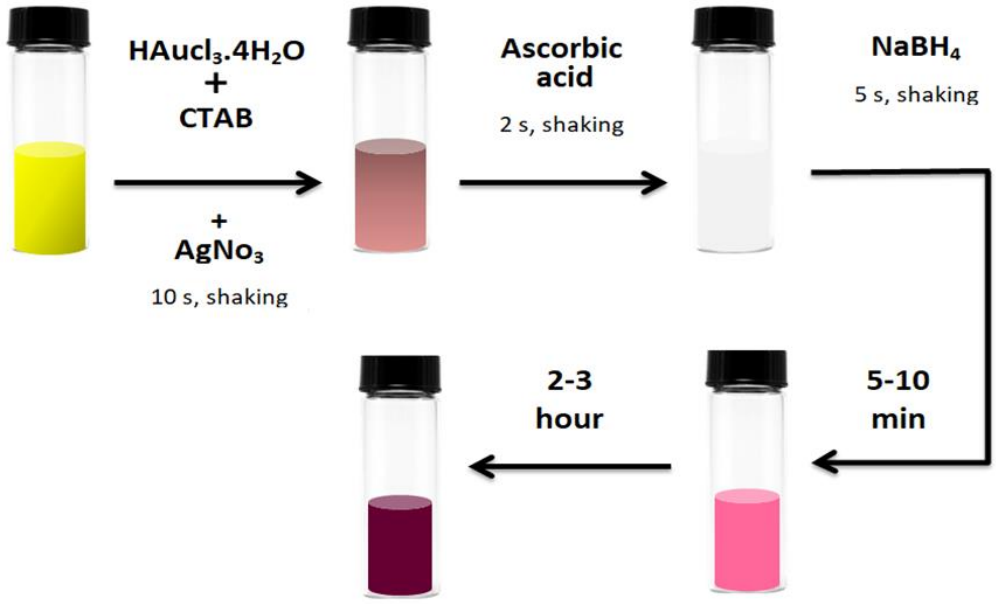

Fig. (3-6) The schematic representation of the seedless synthesis of gold NRs.

3.4 Random Laser Sample preparation

3.4.1 Preparation of Ferrofluid

Three magnetic ferrofluid concentrations have been used in this study. Nanofluid is composed by taking methanol as base fluid and ferric-oxide (Fe_3O_4) as nanoparticles. The ferric-oxide magnetic nanoparticles (Fe_3O_4) which prepared by Co-pricipition method. The three concentrations of magnetic ferrofuid (1, 0.5, 0.1) mg/10ml based-methanol were placed for 30 minutes in an ultrasonic path device in order to get a ferrofluid suspentions, regular separation, uniform distribution and prevented particle aggregation as illustrated in Fig.(3-7).

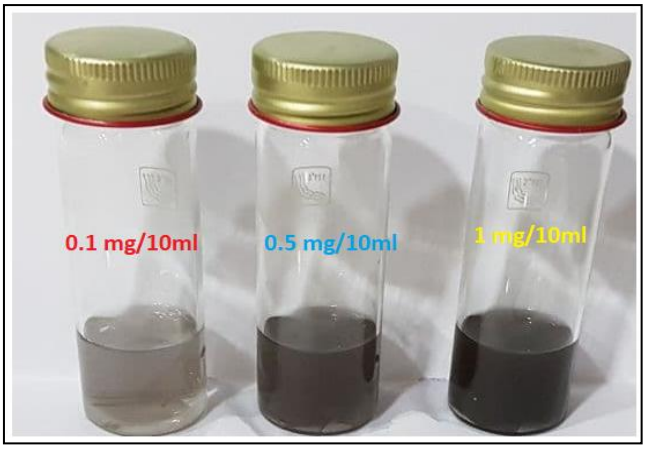

Fig. (3-7) Ferrofluid suspensions with different concentrations prepared by dispersing Fe_3O_4 NPs in methanol solution.

3.4.2 Preparation of the mix dye (Rh-640) and Fe_3O_4 SNPs

The dye samples of the random laser were prepared as follows: the dye used in this experiment (Rh-640, a dark green crystal powder in appearance with a concentration of 5×10^{-4} M, purchased from Sigma Aldrich) was dissolved in methanol in order to obtain the host medium of random laser (Fig.(3-8a)). Next, Fe_3O_4 SNPs (1.3×10^{17} cm^{-3} in density, synthesis by co-precipitation method) was mixed with the dye solution (Fig.(3-8b)). Two samples of the random medium were then prepared by doping 70% of Rh-640 dye with 30% of Fe_3O_4 SNPs (sample-1), and 50% of Rh-640 dye with 50% of Fe_3O_4 SNPs (sample-2). These samples consisting of the dye and SNPs were ultrasonically dispersed in methanol for 30 min before each experiment.

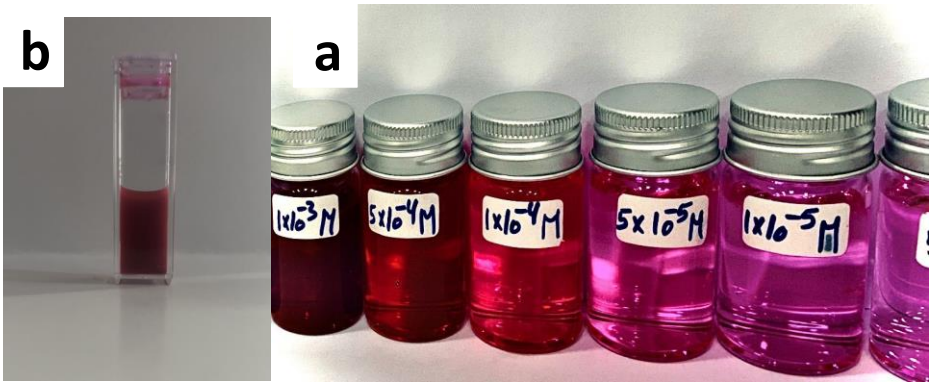

Fig. (3-8) a- Picture of Rh640, synthesized in Methanol with different concentrations, b- The mixture of Rh640: Fe_3O_4 SNPs random media.

3.4.3 *Preparation of Mix dyes (Rh-640: MB) and Ag NWs*

Ag nanowires (length 50 microns, diameter 50 nm) used as scatterer. Rhodamine 640 (Rh-640) and Methylene blue (MB) laser dyes as host medium. The silver NWs its dissolving with methanol by continuously stirring the solution for 30 min and has a concentration of approximately 9 $\times 10^{17}$ cm^3 , shown in (Fig. (3-9a)). It is noted that all samples were not mixed with any surfactant to preserve energy transfer efficiency. The concentration of Rh-640 and MB dyes was fixed at (1×10^{-5} M and 1×10^{-3} M) respectively. Then, preparation of three different samples by mixture of Rh-640/MB dyes, S_1 (1:1), S_2 (1:2), and S3 (1:5to examine transfer energy between two dyes) as shown in Fig. (3-9b). They also prepared another three samples to be examined by random laser by mixture fixed ratio from Rh-640/MB with different concentrations of AgNWs .

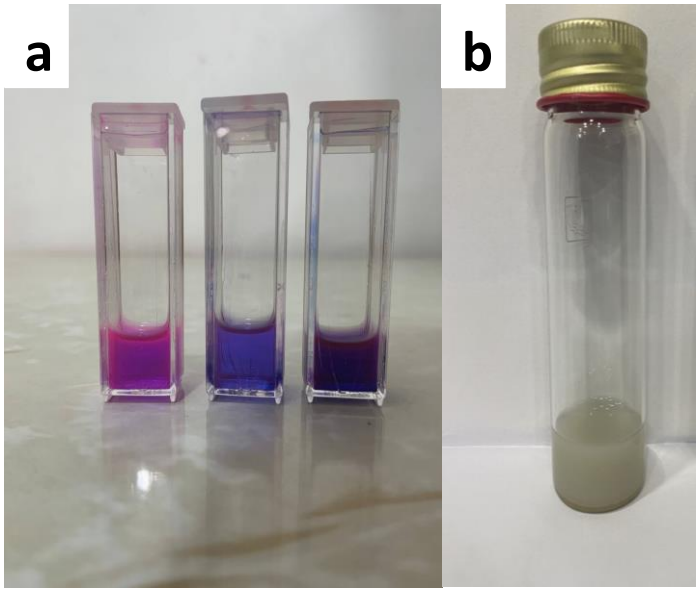

Fig. (3-9) Picture Rh640:MB: Ag NWs, prepared in Methanol solvent with different concentrations.

3.4.4 *Preparation of mix LDS 821 dye and Au NRs*

The Au nanorod were synthesized by seedless method, using a CTAB - assisted the reaction as mentioned above. The two samples prapared of Au nanorod had (lengths ± 18.8 µm, diameter ± 6.3 nm) and (lengths ±22.3 µm, diameter ± 7.2). After complete the synthesis, the excess CTAB was removed from the samples, it was necessary to dislodge the liquid by centrifuging. Following a purification cycle of wash–centrifuge–redisperse, the quasi-spherical Au nanoparticles were removed. Then, the solid was stored in methanol to form the Au nanorod suspension as shown in Fig.(3-10 a). The Au nanorod concentration was approximately 18.5 mg⁄mL.

the random lasing medium was obtained by mixing 0.5 mL of the Au-nanorod ink, shown in Fig. (3-10 a), and adding 1×10^{-4} M concentration of LDS 821 dye dissolved in methanol. Au nanorods concentration became

0.185 mg⁄mL. The dilute nanorod suspension was used to reduce the effect of light scattering on lasing resonance, shown in Fig.(3-10 b).

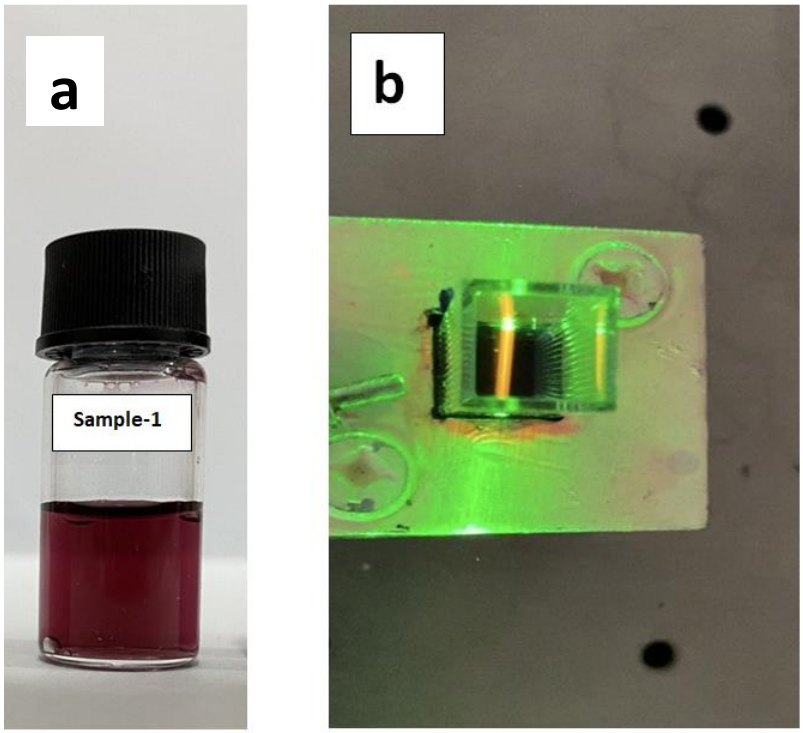

Fig. (3-10) (a) Au nanorod ink in methanol solvent with concentration of 18.5 mg⁄mL for two samples. (b) random lasing medium of Au nanorod dilution at concentration of 0.185 mg⁄mL and LDS 821 dye at concentration 1×10^{-4} M.

3.5 Random laser measurements

3.5.1 Experiment setup to dermination of scattering mean free path in Fe_3O_4 SNPs suspension

The experimental setup used for magneto-optical measurements of the ferrofluids is schematically depicted in Fig.(3-11). The ferrofluid suspensions were placed in a quartz cuvette with a thickness of about 10 mm at the magnetic system center, and kept inside a solenoid. The magnetic field was changed between 25−250 G by varying the current passing through the coil using a dc power supply. The direction of the magnetic field was parallel to the light propagation. A Gaussian diode laser with a wavelength of 532 nm and an output power of 35 mW was employed as the light source. The output of the transmitted light intensity was split into two equal separate beams using a beam splitter. The first output (part I) from the transmitted power was connected to a digital power meter and the second output (part II) was projected on a screen in order to observe diffraction pattern modes.

In this respect, the ferrofluids were exposed to the magnetic field transverse to the direction of the light source, so that the magnetic particles dispersed in the methanol solution experienced a force, attracting them toward one side of the cuvette. In turn, this formed a chain of magnetic NPs. The moving direction of the NPs would depend on the magnetic field strength applied, and on the transmitted intensity of the light source across the ferrofluid.

The magnetic field would affect on the concentration of the nanomaterial be affecting the change in the transmitted intensity, and this in turn would lead to the change in the rate of the scattering mean free path according to the following equation [130].

$$l_{s2} = l_{s1}\ {}^{\ln(T_1)}\!/_{\ln(T_2)} \quad \text{..... (3. 2)}$$

l_{s1} and l_{s2} are scattering mean free paths without and with a magnetic field applied, respectively. The associated transmissions are T_1 and T_2.

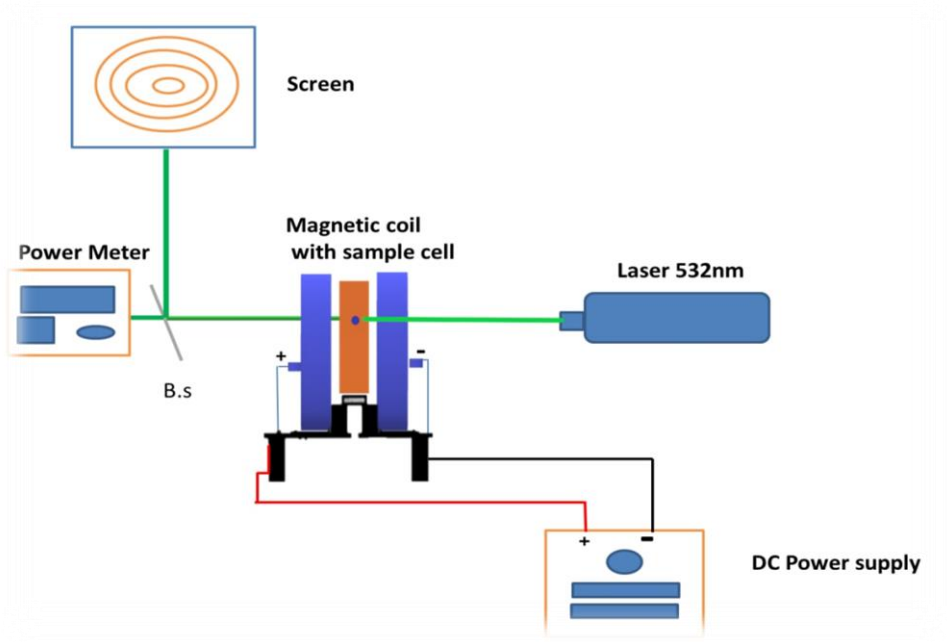

Fig. (3-11) Schematic representation of the experimental setup used for magneto-optical measurements of ferrofluids.

3.5.2 Experimental setup of performance Rh640: Fe_3O_4 NPs random laser under magnetic field (magnetically controlling random laser)

The experimental setup used for magnetically controlling the random laser is schematically depicted in Fig.(3-12). The random suspension media were placed in a quartz cuvette with a thickness of about 10 mm at the magnetic system center, and kept inside a solenoid. The magnetic field was fixed at 125 G. A Q-switched frequency-doubled Nd:YAG laser (532 nm, 5 ns pulse duration, 10 Hz pulse repetition rate) was oriented at 90^o with respect to the normal to the cuvette face. The dye laser emission from the front face of the cuvette was collected using a lens (f = 5cm) oriented at 30^o with respect to the normal to a fiber-coupled spectrometer. The direction of the magnetic field was parallel to the light propagation.

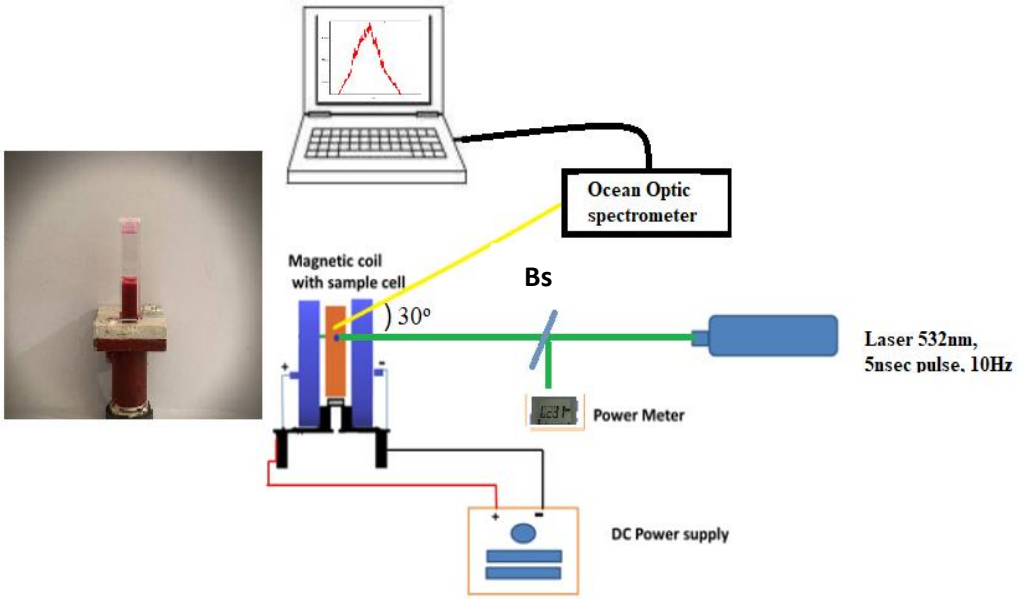

Fig. (3- 12) The schematic representation of the optical setup used for controlling the random laser under an external magnetic field in disordered solutions containing dye-doped Fe_3O_4 SNPs.

3.5.3 Experimental setup Performance of Rh640:MB:Ag NWR random laser using Energy transfer mechanism

The experimental arrangement for the RL based on energy transfer mechanism is shown in Fig. (3-13). During the experiment, each sample was inserted into the glass cuvette with a 10 mm inner diameter (10 mm thickness) and 45 mm height. A second harmonic generation (SHG) at 532 nm was employed to excite the Rh-640 dye solutions. The energy ranged from 1. to 10 mJ. The laser beam impinging normally of the center of cell. The emissions from the samples were collected by using a fiber-coupled spectrometer (Ocean Optics USB2000+UV-VS-ES with 0.3 nm spectral resolution) and the fiber probe was placed at a fixed distance (typically 2 cm) at angle 300 from the center axis of the cell by the rotatable arm. The Pump laser power incident on the sample was controlled using appropriate neutral density filter (NDF).

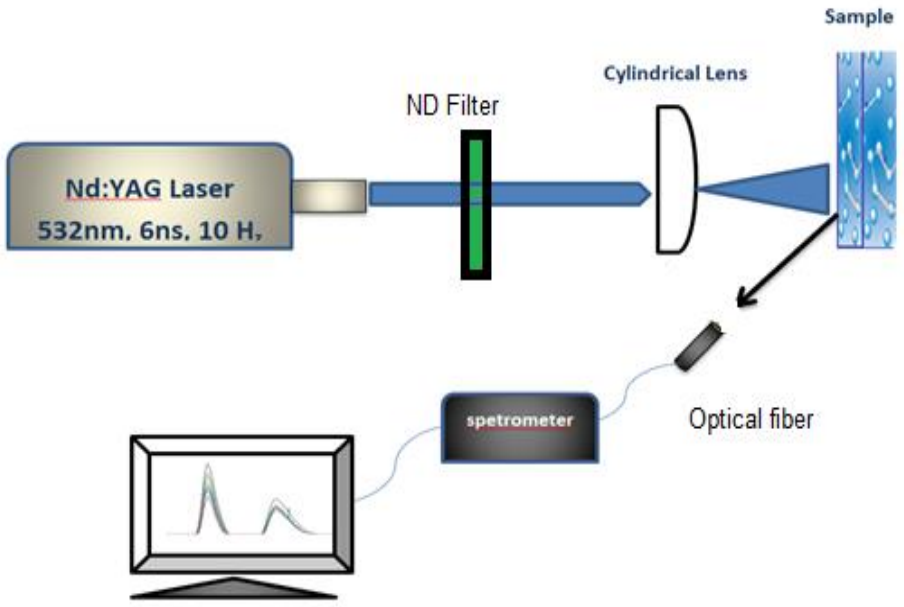

Fig. (3- 13) The experimental arrangement for the RFRL characterization.

3.5.4 *Experiment setup Performance of (LDS 821 dye:Au NRs) random laser*

For the random laser experiments, the suspensions were placed in a 1 cm quartz cuvette. The pump source for the experiments was a Q-switched frequency doubled Nd:YAG laser operating at 10 Hz pulse repetition rate with 4 ns pulse width. The front face of the random laser cuvette was irradiated at an incident angle of 90^{o} normal to the front face. The emission light at an angle of 30^{o} to the cuvette's front face was collected by a lens and delivered to a fibre-coupled spectrometer (Ocean Optics USB2000 + UV-VS-ES with ~1 nm spectral resolution). The optical setup geometry used is shown in Fig (3.14)

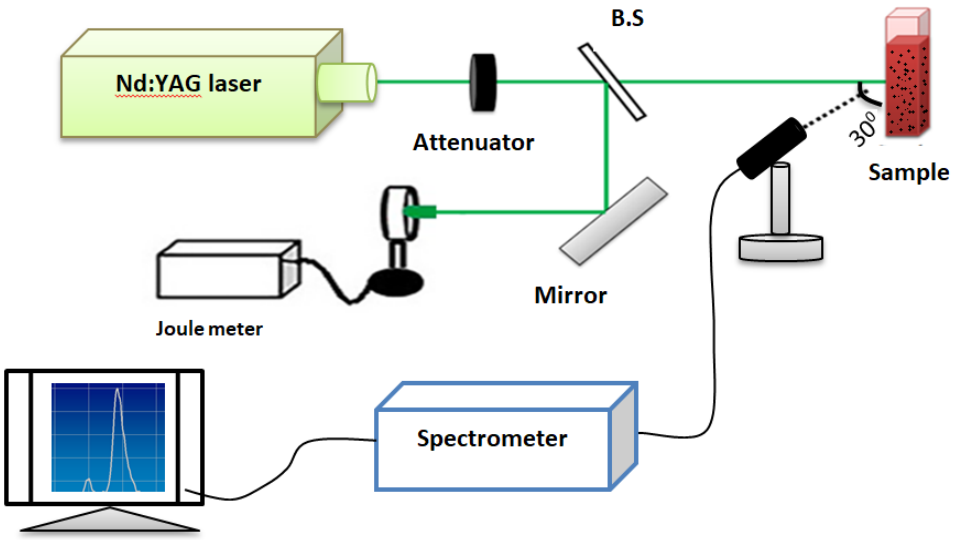

Fig. (3- 14) Experimental setup of plasmonic Nanorods for Random Lasing performance.

Chapter Four

Results & Discussions

This chapter introduces the results of experimental details of the work carried out in this thesis.

4.1 Introduction

In this chapter, the characterizations of the prepared samples were determined by different parametric tests, such as XRD, FE-SEM, TEM and FTIR. The spectroscopic studies including absorption and fluorescence spectra will be discussed, and studied the spectra depening on the dye concentration and amount of nanoparticles. From the obtained results, the optimum concentration was determined. The output from the selected samples has been examined and detected using the laser beam profile tests. For the same optimum concentration, the measurement of mean free path (ℓ_s) and quantum yield have been conducted and the results are also presented.

4.2 Optical Properties of Laser Dyes and Nanoparticles

4.2.1 Absorption & Fluorescence Spectrum of Rh640 Dye

Fig. (4.1) shows different concentrations of the Rh640 dye dissolved in methanol have been studied (1×10^{-5}, 5×10^{-6}, 1×10^{-6}) M. It is very clearly and as it appears from the figure that with increasing the concentration of the dye in the solution, the absorption spectrum increases and regularly in a certain range of wavelengths around (490-607 nm) with its maximum peak at 570 nm. Whereas, it is known that the dye solution has a lower absorption spectrum at wavelengths less than 490 nm, and for the region of wavelengths greater than 607 nm, the absorbance minimizes to the lowest, regardless of the dye concentration according to Beer-Lambert law.

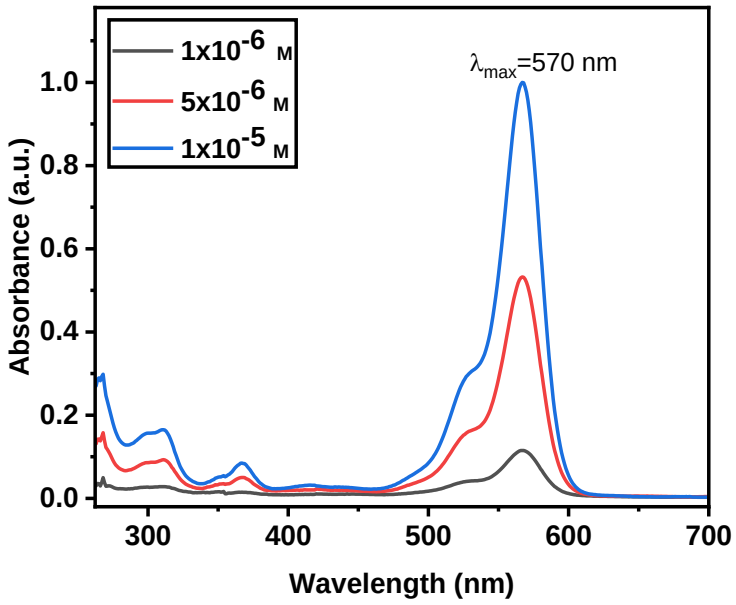

Fig. (4- 1) Absorption spectra of Rh640 dye dissolved in methanol with different concentrations.

besides studying the absorption spectrum of prepared solutions of Rh640 dye (in methanol) with a particular concentrations in the previous section, the fluorescence spectra curves for those concentrations were illustrated in Fig.(4.2) at 532 nm wavelength excitation.

For the intensity of the fluorescence spectrum, it is common, and as literature shows, it increases with increasing dye concentration, and this is evident in the above figure when moving from a lower concentration 1×10^{-6} M to a higher concentration 1×10^{-5} M, where the intensity of the fluorescence spectrum is clearly increased (i.e, Beer-Lambert law). Dye concentration 1×10^{-5} M shows the best fluorescence spectrum and therefore strengthens our selection as the best suitable concentration for random laser action based on the absorption spectrum.

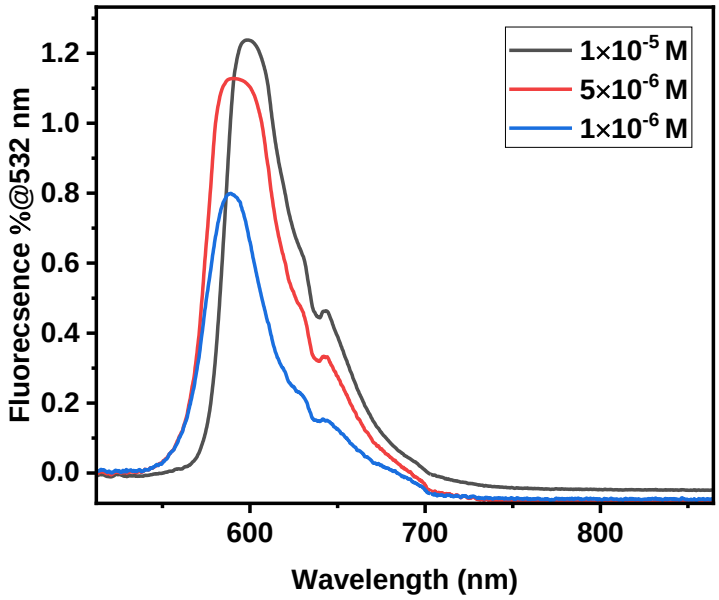

Fig. (4- 2) Fluorescence spectrum of Rh640 in methanol at different concentrations

Moreover, increasing the dye concentration causes the fluorescence spectrum to shift towards longer wavelengths (redshift). It is shifted from 587 nm at concentration of 5×10^{-6} M to 600 nm at concentration of 1×10^{-5} M. Thus, the displacement amount towards the longer wavelengths (red shift) is about 13 nm. Which means that the fluorescence of laser dye has moved to red shift. The redshift in the fluorescence spectrum of the Rh640 dye due to its increased concentration can be attributed to the fact that the dipole moment of the excited state is higher than that of the ground state and these results got supported by [131].

4.2.2 Absorption & Fluorescence Spectrum of MB Dye

Fig. (4-3) illustrates the UV-VIS absorbance spectra of pure MB. The maximum absorbance takes place over red spectral range with a certain characteristic peak at 653 nm.

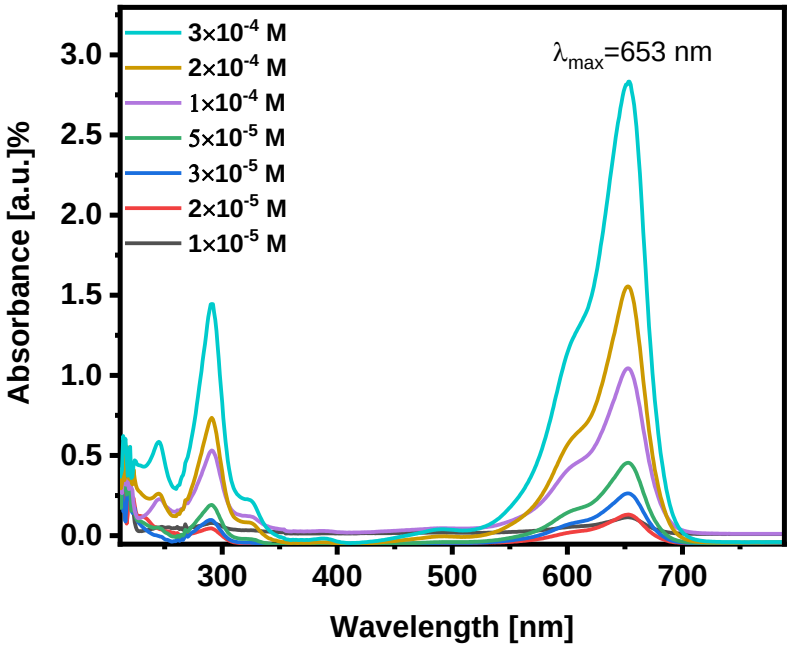

Fig. (4- 3) Absorption spectra of MB dye dissolved in methanol with different concentrations.

Furthermore, a couple of UV characteristic emissions appear at 250 nm and 291 nm too. Furthermore, the figure displays the spectral absorbance in terms of MB concentration, which lucidly demonstrates a linear function at 653 nm as shown. When the concentration increases, then the absorbance elevates, however no spectral shift appears.

Moreover, Fig. (4-4) demonstrates the corresponding overlapping area of the normalized absorption and fluorescence emission spectra. The stokes

shift of 27 nm is obtained for MB at 3×10^{-4} M which shows a significant overlapping leading to the lucid re-absorption events [132].

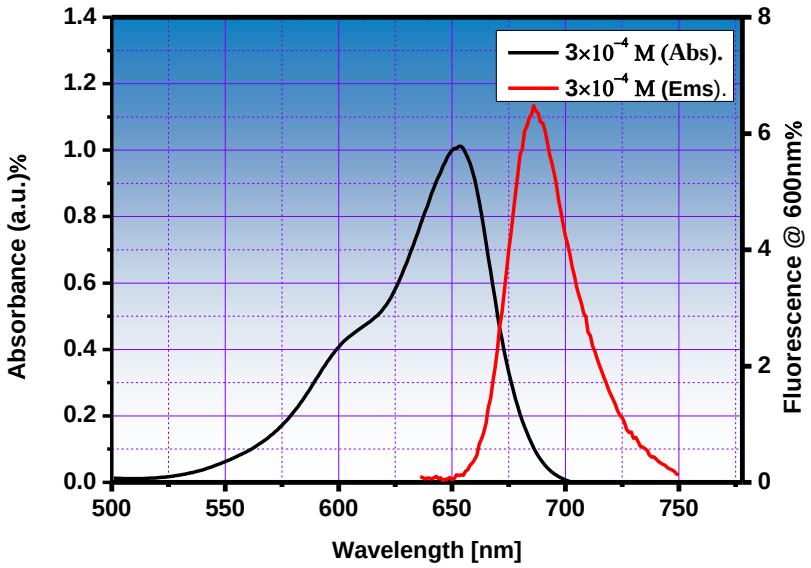

Fig. (4- 4) Fluorescence and absorption spectrum overlap of MB in methanol at 3×10^{-4} M concentrations.

4.2.3 Absorption & Fluorescence Spectrum of LDS-821 Dye

A four different concentrations (1×10^{-4}, 5×10^{-4} , 1×10^{-5} and 5×10^{-5})M of LDS 821 laser dye (MW= 460.98 g/mol , product of USA , exciton) had been prepared in methanol. Fig. (4-5) shows the absorption spectrum for these samples. The wide absorption band of the LDS 821 dye allow the efficient pumping at 532nm by Nd:YAG laser used in the random laser experiments. The absorption peak ranges from 431-725 nm and maximam peak at 575 nm.

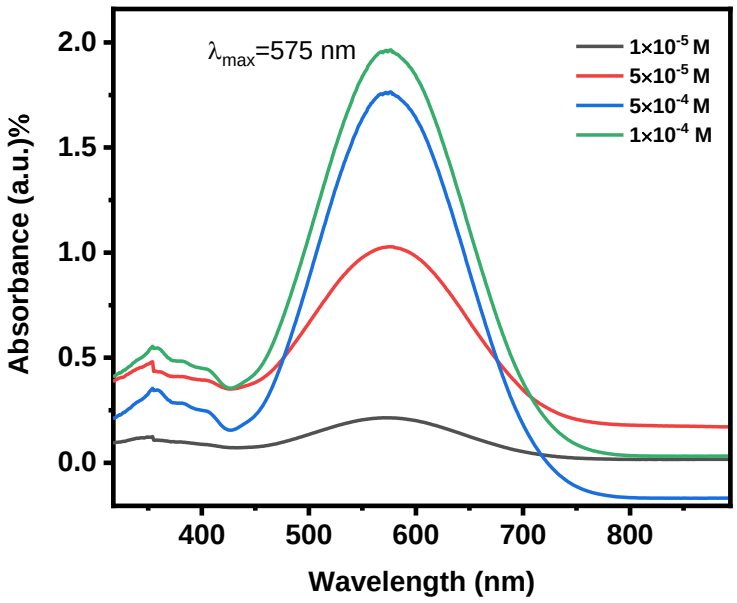

Fig. (4- 5) Absorption spectra of LDS 821 dye dissolved in methanol with different concentrations.

Fig. (4-6) shows the fluorescence emission obtained from LDS 821 dye. The FWHM of around 74-160 nm. The fluorescence spectra have the wavelength ranging from 670 to 844 nm and maximam peak at 781 nm. Furthermore, as known that the fluorescence increases with increasing dye concentration, and this is evident in the above figure when moving from a lower concentration 5×10^{-5} M to a higher concentration 1×10^{-4} M, where the intensity of the fluorescence spectrum is clearly increased. But the verse is reflected in relation for the concentration 1×10^{-3}, where a disappear fluorescence is observed with an increase in the concentration of the dye, and this can be attributed to the appearance of dimers as supported by [133].

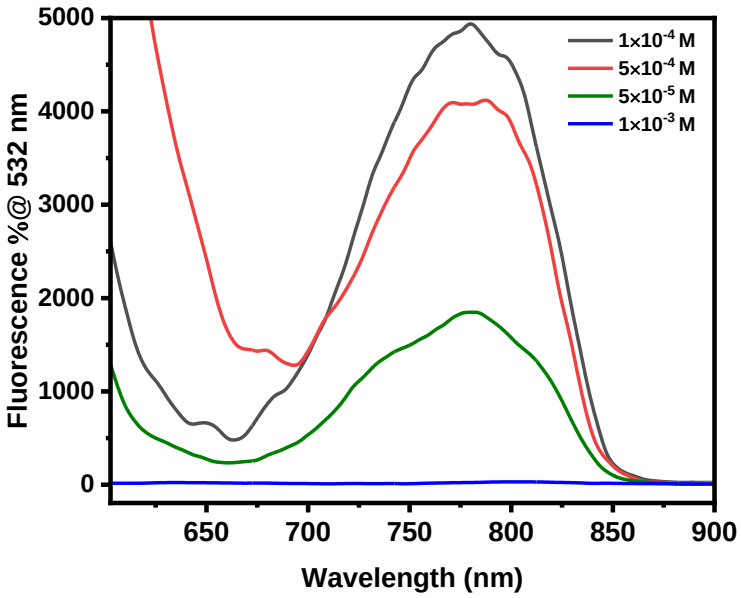

Fig. (4- 6) Fluorescence spectrum of LDS 821 dye in methanol at different concentrations.

4.3 The Random Laser Under Different Operation Conditions

4.3.1 Fe_3O_4 SNPs random laser

4.3.1.1 *Morphology and Structure of Fe_3O_4 SNPs*

Morphological and structural characteristics of the Fe_3O_4 SNPs synthesized by a co-precipitation method are shown in Fig. (4-7).

From FE-SEM image in Fig. (4-7) (a), these SNPs are observed to have spherical-like morphology. According to the inset of Fig. (4-7) (a), the size distribution of the SPNs is found to range between 20 and 40 nm. Additionally, the mean size of the Fe_3O_4 SPNs is about 27 nm and take spherical shape. Furthermore, there are some aggregation of nanoparticles. The X-ray diffraction (XRD) pattern of the SNPs is depicted in Fig. (4-7) (b), indicating the reflections of (220), (311), (400), (422), (511), (440), and

(622) planes at 2θ°~ 30.4°, 35.6° , 43.5°, 53.9°, 57.4°, 63.0°, and 75.0°, of the cubic structure of spinel Fe_3O_4, respectively, according to the standardized JCPDS card (no. 01-075-0449). The crystal structure of the SNPs is then confirmed to be from magnetite (Fe_3O_4) without the presence of impurity or secondary peaks. Based on the Scherrer formula [123], the crystallite size along the main peak (i.e., (311)) is calculated to be about 22 nm, which is in accordance with the mean size observed using the FE-SEM analysis.

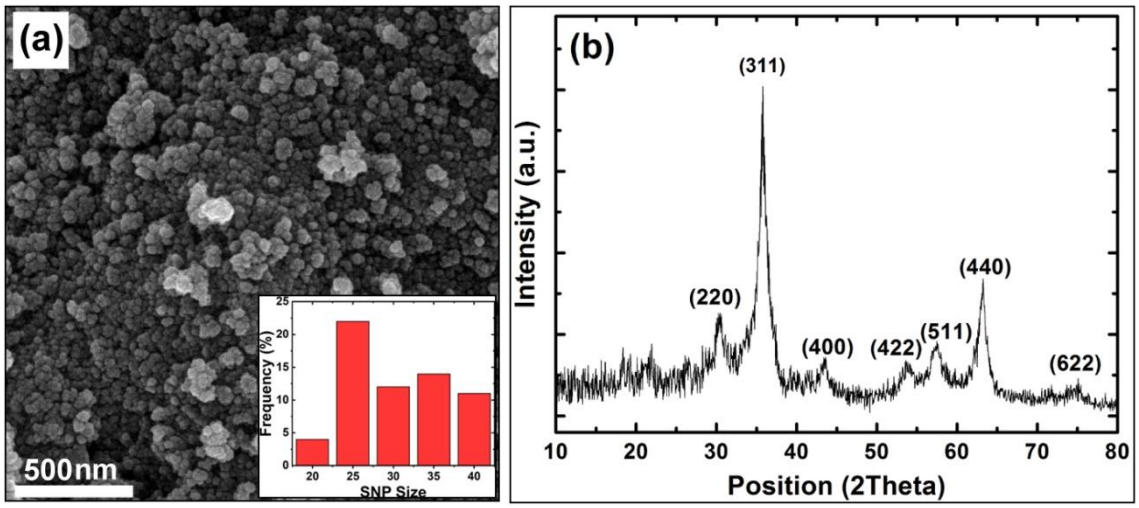

Fig. (4- 7) FE-SEM image of Fe_3O_4 SNPs together with the corresponding size histogram as the inset. (b) XRD pattern obtained from Fe_3O_4 SNPs.

4.3.1.2 Optical absorption of Fe_3O_4 nanofluids

UV-Vis spectra of Fe_3O_4 nanofluids with different concentrations (1, 0.5, and 0.1 mg/10ml) are shown in Fig. (4-8) (a). The light absorption taking place in the wavelength range of 290–550 nm (i.e. blue shift) can be attributed to the colloidal Fe_3O_4 NPs, which decreases with decreasing the nanofluid concentration. These findings are consistent with earlier research

[134]. In fact, the absence of sharp absorption peak and/or the slight absorbance values of the nanofluids arise from the low concentration of the Fe_3O_4 NPs. Therefore, the nanofluid with the middle concentration (0.5 mg/10ml) was selected for the subsequent experiment.

Since the agglomeration and stability of NPs may affect the properties of nanofluids, UV-Vis spectrometry was carried out for different decay times (ranging from 0 to 30 min) at the concentration of 0.5 mg/10ml, and the results obtained are shown in Fig. (4-8) (b). As observed, the intensity of the absorption edge is continuously reduced and shifted to a longer wavelength (i.e red shift) with increasing the decay time. Accordingly, the highest decay time (30 min) was found to be suitable for performing the magneto-optical measurements, which will be presented in the following sections.

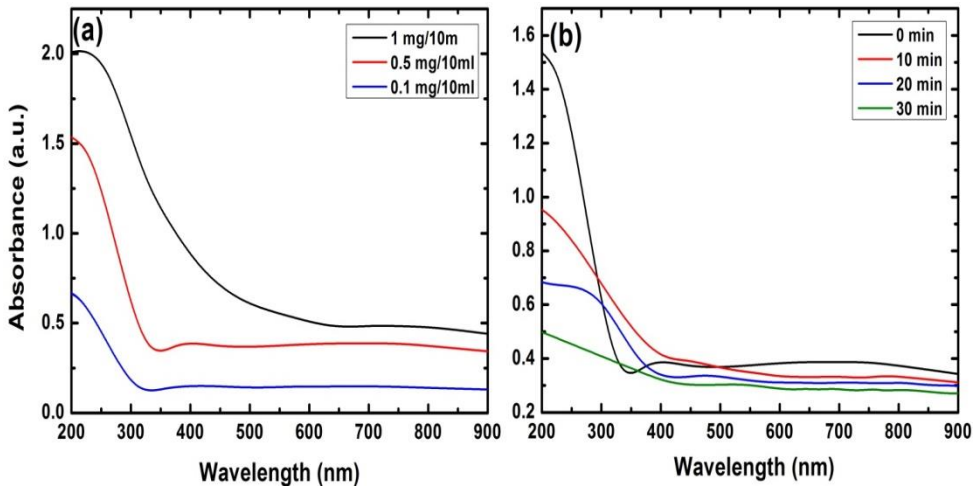

Fig. (4-8

Fig. (4- 8) UV-Vis spectra of: (a) Fe_3O_4 nanofluids with different concentrations, and (b) Fe_3O_4 nanofluid with a concentration of 0.5 mg/10ml at different decay times.

Fig. (4-9) shows the absorption spectra of the magnetically controllable random laser samples were measured. The absorption spectra studied for pure Rh-640 dye with a concentration 5×10^{-3} M, pure Fe_3O_4 SNPs with a concenration of 1.3×10^{17} m^{-3}, and 50% Rh-640:50% Fe_3O_4 mixture. From these results, one can infer that the pure Rh-640 dye possessed a wide absorption spectrum (500–630 nm) with a maximum absorption peak at the wavelength of 540 nm. In the case of the pure Fe_3O_4 SNPs, one can observe that the maximum absorption occurred at the wavelength of 350 nm. Furthermore, the absorption decreased in the wavelength range between 350–800 nm. The spectrum of the dye-Fe_3O_4 SNP mixture was indicative of a reduction and a shift to a higher energy (a blue shift), without overlapping with the pump laser wavelength of 532 nm, and the absorption and emission spectra of pure Rh-640 laser and Fe_3O_4 SNPs. In turn, this can lead to the formation of strong scattering centers for the dye-doped SNPs.

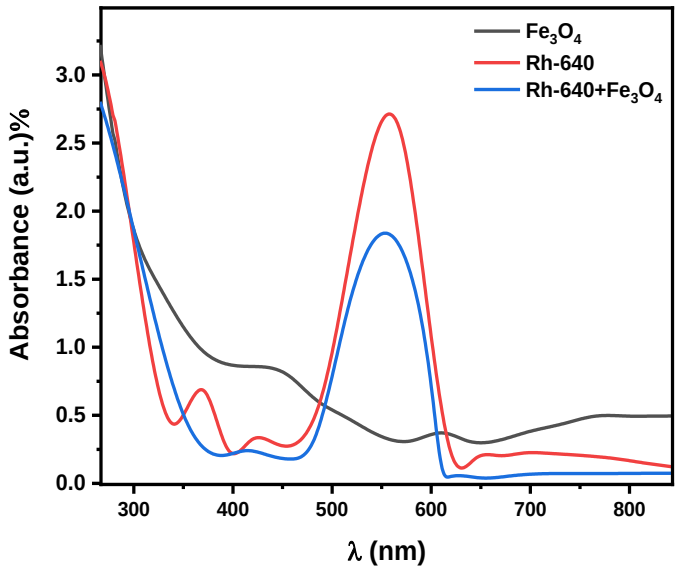

Fig. (4- 9) UV-Vis absorption spectra of pure Rh-640 dye, pure Fe_3O_4, and 50% Rh-640:50% Fe_3O_4 mixture.

Fig. (4-10) shows the comparison between spontaneous emission spectra of pure Rh-640 dye and Rh-640 dye-Fe_3O_4 SNP mixture under a pumping energy of 7 mJ recorded using a spectrofluorometer (Shimadzu, RF-5301 PC, Japan). It is observed that the peak of the emission spectrum of pure Rh-640 dye was at the wavelength of 600 nm, and that the spectrum of the mixture broadened towards a longer wavelength (a red shift) with significant differences in the amplitude and band width.

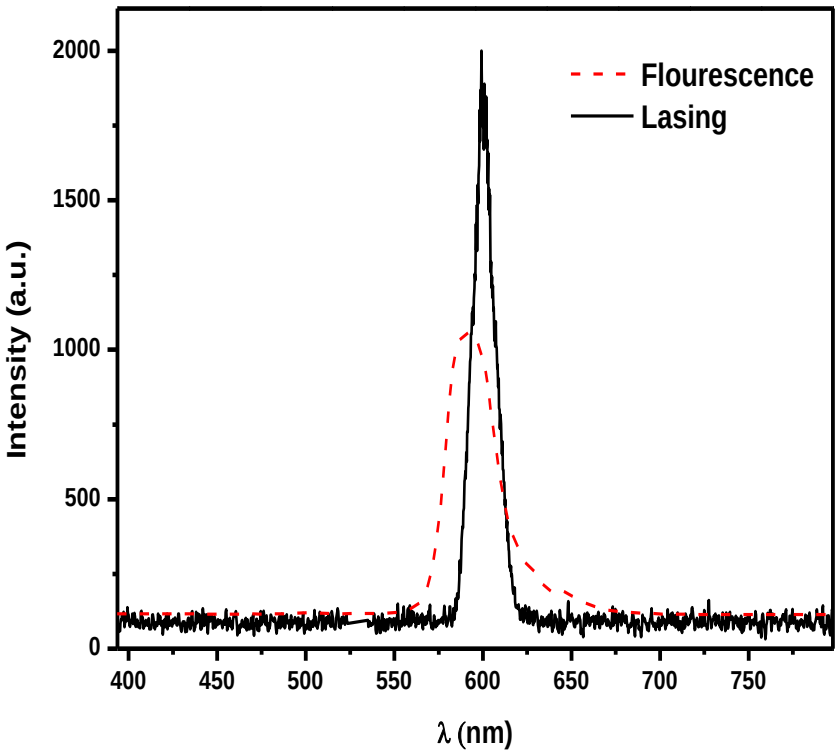

Fig. (4- 10) Spontaneous emission spectra of pure Rh-640 dye solution (the dashed red line) and Rh-640:Fe_3O_4 mixture (the solid black line).

4.3.1.3 Magneto-optical measurements

Fig. (4-11) shows the normalized transmitted light intensity as a function of applied magnetic field for these three concentrations of ferrofluid. In the case of the lowest concentration (0.1 mg/10ml), the transmitted light intensity is slowly reduced with increasing the magnetic field, taking a long period of time. Alternatively, at the middle concentration (0.5 mg/10ml), the transmitted light intensity drastically decreases as a function of time.

In this case, the transmitted light intensity further decreases with increasing the magnetic field. At the highest concentration (1 mg/10ml), it is observed that the transmitted light intensity initially increases slightly with time, and then decreases with increasing the magnetic field. Thus, the ferrofluid concentration and the magnetic field can concurrently affect the transmitted light intensity. The decrease in the transmitted intensity with increasing the concentration may be assigned to the competition between the attraction among the Fe_3O_4 NPs, and to the role of the solvent in their movement. Consequently, the effective concentration of the ferrofluid for the magnetically controllable light intensity is found to be 0.5 mg/ml, leading to a decrease in the rate of the transmitted light intensity with the ideal time of the experiment.

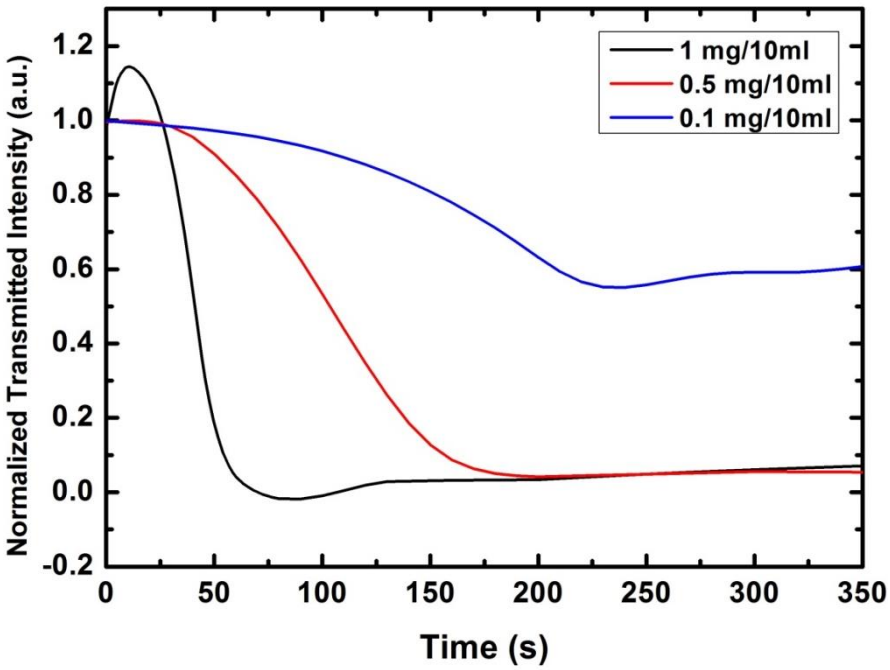

Fig. (4- 11) The normalized transmitted light intensity as a function of time when increasing the applied magnetic field between 25−250 G for Fe_3O_4 nanofluids with different concentrations.

In order to understand the influence of magnetic field on the magneto-optical properties, the normalized transmitted intensity of the ferrofluid with a concentration of 0.5 mg/10ml was investigated as a function of time for constant magnetic fields of 25, 50, and 125 G, as shown in Fig. (4-12). As can be inferred, three regions appear in the transmitted intensity-time curves. In the first region labeled as the first critical magnetic field (H_{C1}), the optical transmittance decreases with time. Increasing the magnetic field strength rapidly reduces the transmitted intensity. In the second region (H_{C2}), the transmittance stabilizes at a certain period of time, depending on the value of the magnetic field applied. In the third critical magnetic field (H_{C3}) region, an increase in the transmittance occurs, pertaining to the strength of the magnetic field. This change in the value of the optical transmittance is due to the movement of the magnetic NPs and their

assembly into chains with different shapes and sizes, involving the roles of the applied magnetic field and response time. It is also notable that the valley position of the three curves shifts by varying the magnetic field. These results agree with those reported in the literature [135].

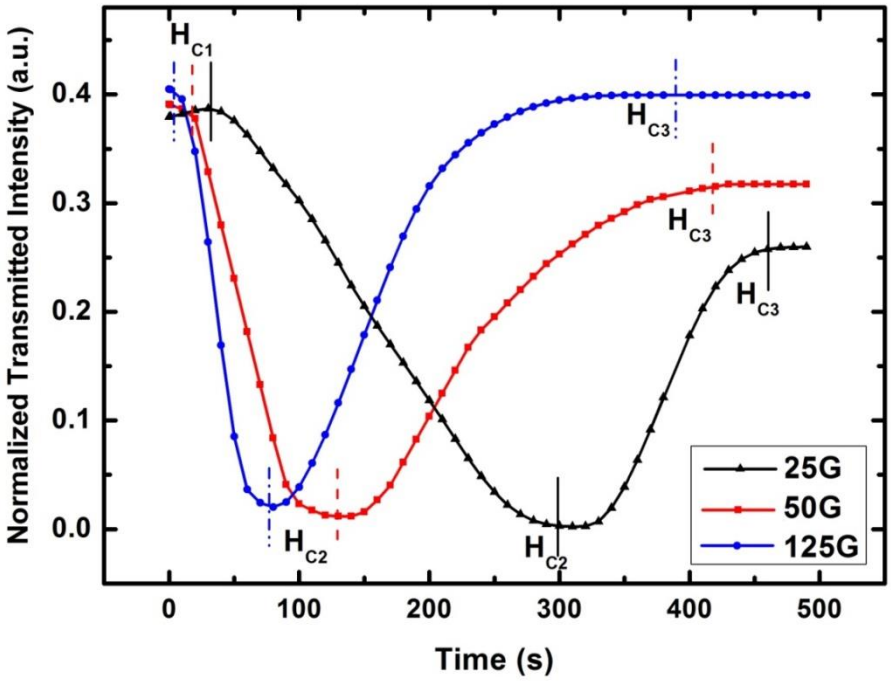

Fig. (4- 12) Normalized transmitted intensity as a function of time required at different critical magnetic fields for the Fe_3O_4 ferrofluid with a concentration of 0.5 mg/10m.

4.3.1.4 Effect of applied magnetic field on diffraction ring patterns

Fig. (4-13) displays diffraction ring patterns recorded on the screen by the digital camera for Fe_3O_4 nanofluids with two concentrations of 0.5 and 1 mg/10ml under different applied magnetic fields ranging from 0 to 50 G. For the ferrofluid concentration of 0.5 mg/ml (Fig. 4-13 (a-d)), three kinds of ring patterns are observed experimentally when increasing the applied magnetic field. Increasing the concentration to 1 mg/10ml (Fig. 4-13 (d-f)) leads to an increase in the overall random distribution area of the beam

spot. This phenomenon is associated with the redistribution and assembly of the NPs, clearly affecting the beam spot passing through them.

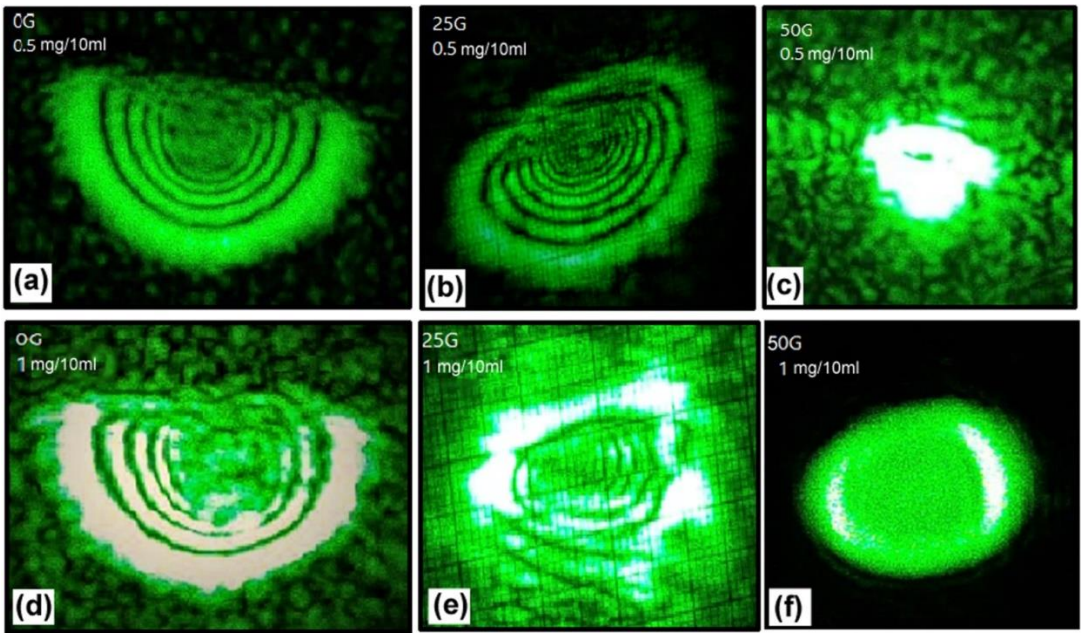

Fig. (4- 13) The variation in diffraction patterns of Fe_3O_4 nanofluids with concentrations of: (a–c) 0.5 mg/10ml, and (d–f) 1 mg/10ml in the presence of different magnetic field strength (0–50 G).

4.3.1.5. Effect of response time on scattering mean free path

As mentioned earlier, the spherical-like Fe_3O_4 NPs dispersed in methanol had a mean diameter of about 30 nm. Moreover, the wavelength (λ) of the incident beam of the diode laser was 532 nm. According to Eq. (2.7), the scattering cross-section (σ_s) is found to be (5.45×10^{-20} m ^{2}) by taking into account the density (ρ_s= 5.91 10^{18} m^{-3}) and refractive index (n= 1.236) of Fe_3O_4 NPs. Basically, the SMFP parameter (l_s) represents the average distance that a photon travels between two scattering events, being one of the most important path lengths closely related to random laser mechanisms. By considering an effective concentration of 0.5 mg/10 ml,

the l_s value is calculated to be 141 µm based on Eq. (2.6). in order to calculate the SMFP associated with transmissions intensity without and with a magnetic field applied, one should use Eq. (3.2). Fig. (4-14) shows the variation of l_{s2} as a function of response time for a constant magnetic field and nanofluid concentration of 0.5 mg/10ml. As observed, the value of l_{s2} continuously decreases from 152 to 49 µm with increasing the response time from 25 to 200 s.

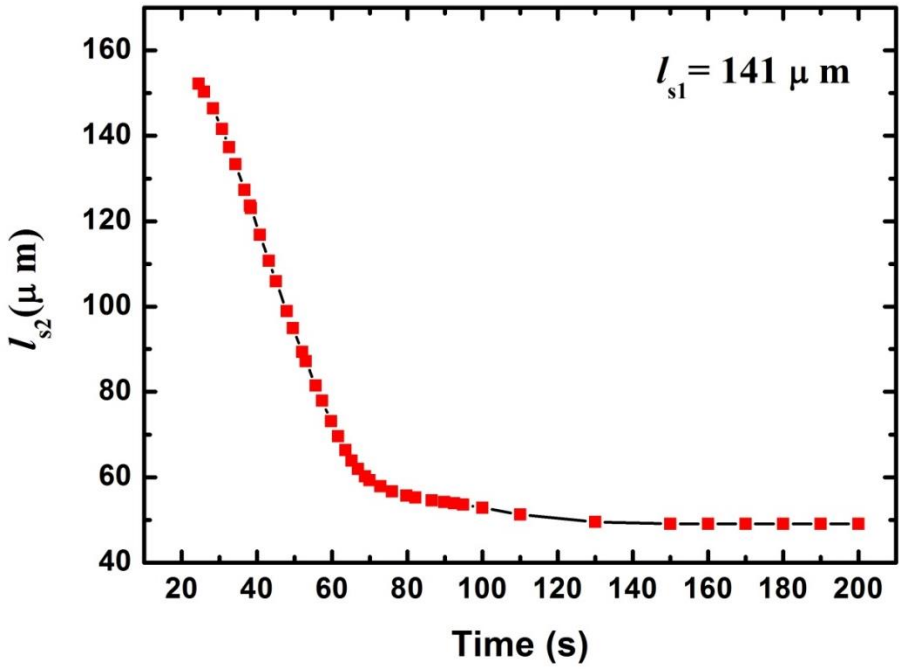

Fig. (4- 14) The variation of scattering mean free path (l_{s2}) as a function of response time under a constant applied magnetic field for Fe_3O_4 nanofluid with a concentration of 0.5 mg/10ml.

4.4. Lasing characteristics of magnetically controllable random laser

4.4.1 The effect of magnetic field and concentration

The effect of magnetic field on laser parameters of Rh-640 dye solution with two different concentrations of Fe_3O_4 SNPs was investigated, and the results obtained are shown in Fig. (4-15). The evolution of emission spectra of sample-1, consisting of 70% Rh-640 (with a concentration 1×10^{-5} M), and 30% Fe_3O_4 SNPs (with a particle density of 2.87×10^{17} cm^{-3}) at different pumping energies (ranging between 1–7 mJ) (a) in the absence and (b) in the presence of a magnetic field (125 G). Moreover, the peak intensities and full width at half maximum (FWHM) values were extracted as a function of pumping energy (Fig. (4-15) (c) (d)).

As inferred from Fig. (4-15) (c), no reasonable change in the slope occurred due to the absence of the magnetic field and lower scattering of SNPs. Therefore, a noticeable threshold activity cannot be observed. However, by applying an external magnetic field, a significant change in the threshold energy was seen as it tended to be optimized in order to surpass the loss and consequently achieve the RL emission (Fig. (4-15) (b)). Meanwhile, FWHM values changed between 25.2–21.5 nm with increasing the pumping energy from 1 to 7 mJ in the absence of the magnetic field. Under the applied magnetic field of 125 G, increasing pumping energy from 1 to 7 mJ decreased the FWHM from 17 to 15 nm. Accordingly, while the magnetic field and pumping energy influence both FWHM and peak intensities of the emission spectra, and threshold energy.

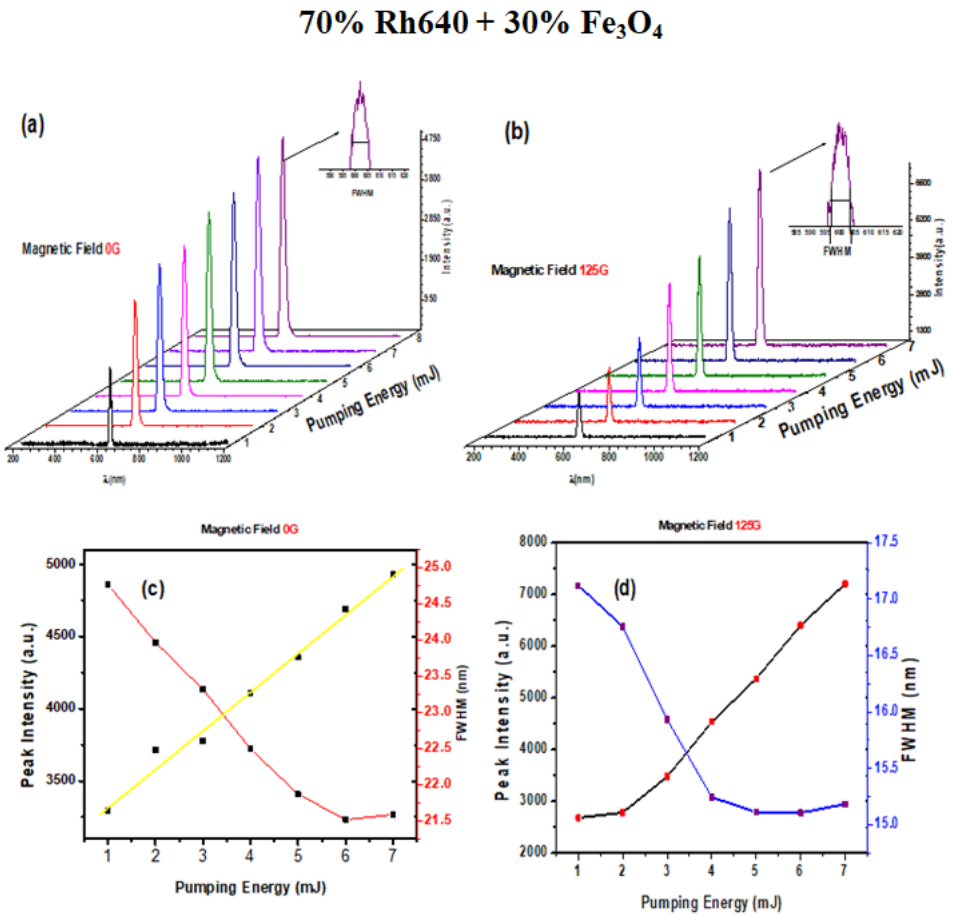

Fig. (4- 15) The emission spectra of 70% Rh-640 dye-30% Fe_3O_4 SNP mixture at different pump energies in: (a) the absence and (b) the presence of a magnetic field (125 G). The variations of peak intensity and FWHM as a function of pumping energy in: (c) the absence and (d) the presence of a magnetic field.

On the other hand, Fig. (4-16) shows the emission spectra of sample-2, consisting of 50% Rh-640 dye and 50% Fe_3O_4 SNPs at different pump energies (1–7 mJ) in the absence and presence of the magnetic field. Increasing the concentration of scattering centers enhanced the random lasing behavior, followed by the increase in the peak intensity and the narrowing of bandwidth at 0 G and 125 G, respectively [Fig. (4-16) (a) and (b)]. These results indicate that the effects of pumping energy and magnetic

field on the random laser parameter (including the emission spectrum intensity and FWHM) for sample-2 [Fig. (4-16) (c)] at 0 G were very similar to that explained for sample-1. With the improvement of some parameters, the threshold energy was reduced to 1.89 mJ (Fig. (4-16) (d)) whereas it was 2 mJ for sample1 at 125 G.

For better clarity, increasing the concentration of scattering centers initiated an improvement in the random lasing behavior, leading to the increases in the peak intensity, narrowing of bandwidth, and decrease in the threshold energy. In fact, the higher concentration necessarily leads to a reduction in the scattering mean free path (l_s), which can be calculated using the following relation: $l_s=1/(\rho\sigma)$, where ρ is the particle density and σ is the scattering cross section. In this way, l_s of the dye-doped Fe_3O_4 SNPs was calculated to be 14.1 mm for sample-1 and 10.4 mm for sample-2. Essentially, two scattering regimes can exist based on the magnitude of l_s: the weakly scattering regime ($l_s \geq L$) and the diffusive regime ($L > l_s > \lambda$), in which L is the sample size (10 mm) and λ is the emission wavelength (600 nm). Therefore, l_s obtained in this study is indicative of dye-doped Fe_3O_4 SNPs with weak scattering behavior. It should be noted that, another factor affecting the value of l_s is the magnetic field, as according to the literature [136]. Tables (4-1) and (4-2) show improvements in the value of random laser parameters by changing the magnetic field from 0 to 125 G for the two samples, thereby indicating enhancements in the amplification of the random laser.

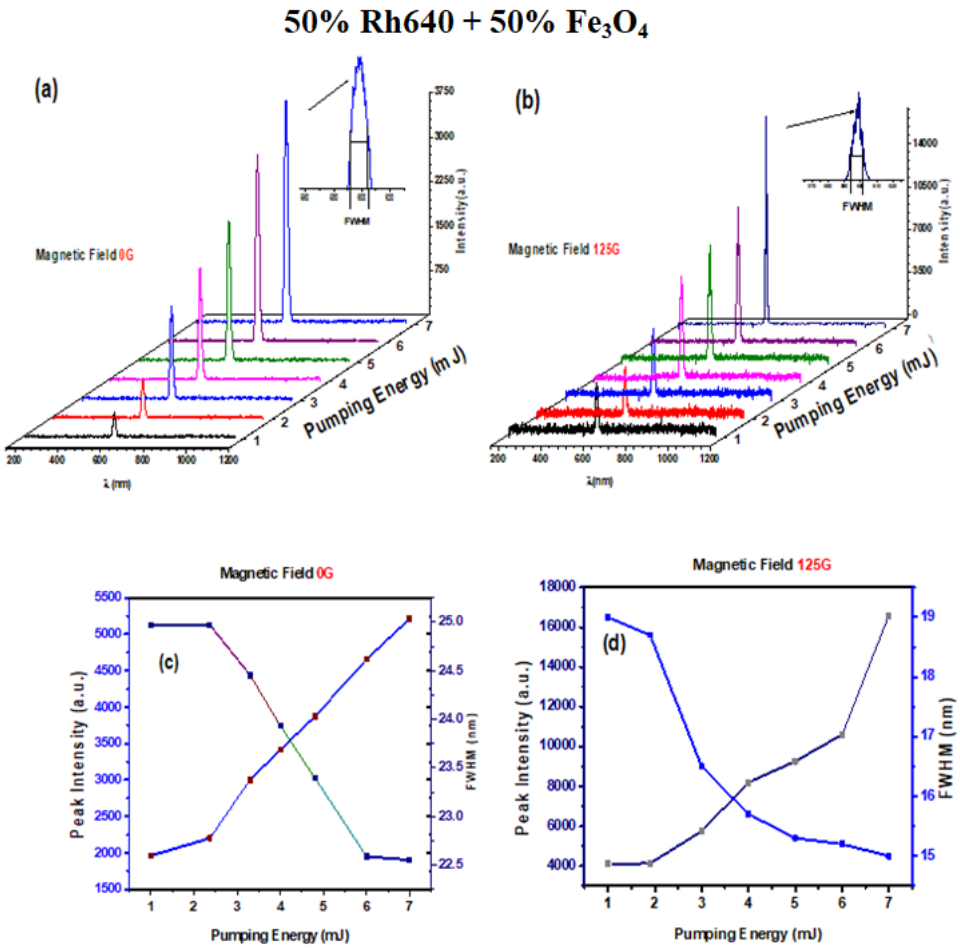

Fig. 4- 16 The emission spectra of 50% Rh-640 dye-50% Fe_3O_4 SNP mixture at different pump energies in: (a) the absence and (b) the presence of a magnetic field (125 G). The variations of peak intensity and FWHM as a function of pumping energy in: (c) the absence and (d) the presence of a magnetic field.

Table (4- 1). Random laser parameters by changing the magnetic field from 0 to 125 G (Sample-1)

Magnetic field (Gauss)	Threshold pumping energy $_{Pth}$ (mJ)	$FWHM_{below}$ (nm)	$FWHM_{above}$ (nm)
0	3.1	25	21.5
125	2	17.5	15

Table (4- 2). Random laser parameters by changing the magnetic field from 0 to 125 G (Sample-2)

Magnetic field (Gauss)	Threshold pumping energy $_{Pth}$ (mJ)	$FWHM_{below}$ (nm)	$FWHM_{above}$ (nm)
0	2.8	25	22.5
125	1.89	19.1	15

4.4.2 The effect of response time on the emission wavelength

Generally, the wavelength emission spectra of dye lasers are affected by the concentrations of the scattering centers (NPs), leading to shifts that might be in the direction of red or blue shifts, and a jump from blue to red shifts depending on the NP and dye concentrations (being high, low, or moderate), respectively [137]. Fig. (4-17) shows the investigation of the effect of the response time (0–30 s) on the emission wavelength in the presence of the applied magnetic field (125 G). It is clear that red shifts (about 6 nm) took place with increasing the response time from 0 to 25 s. Furthermore, a jump to the blue shift was observed with the increase in the response time from 25 to 30 s. This wavelength shift was supposed to be caused by Fe_3O_4 SNPs that can form chains and change their concentration along the direction of the external magnetic field with increasing the response time.

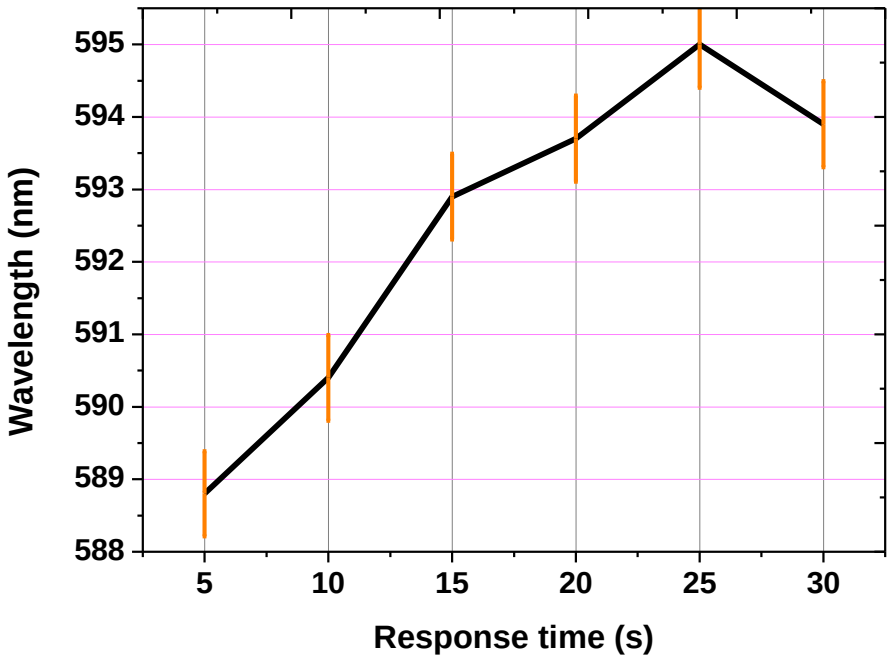

Fig. (4- 17) The tuning of wavelength by varying the response time of magnetic field at a constant pumping energy (6mJ/pulse).

4.4.3 Transition from incoherent to coherent random laser under external magnetic field

In random laser systems, it is possible to transit from incoherent to coherent modes. This is mainly indicated when spikes appear and their number increases in the corresponding emission spectrum. According to Figures (4-15), (4-16),(4-17) and (4-18), it can be noticed that effect of the magnetic field, pumping energy, and the concentration of the dye-doped SNPs on the appearance of the spikes and the increase in their numbers to more than 10 spikes with a FWHM of approximately 1 nm. Alternatively, Fig. (4-18) (b) shows the following three regions: Region (I), representing the amplified spontaneous emission; and Regions (II) and (III), indicating the change in the intensity of emission spectra and FWHM. The change in Region (II) may represent a transition from the amplified spontaneous emission to

incoherent random laser. Moreover, the occurrence of the superlinear change of Region (III) could arise from a transition from incoherent to coherent random laser modes.

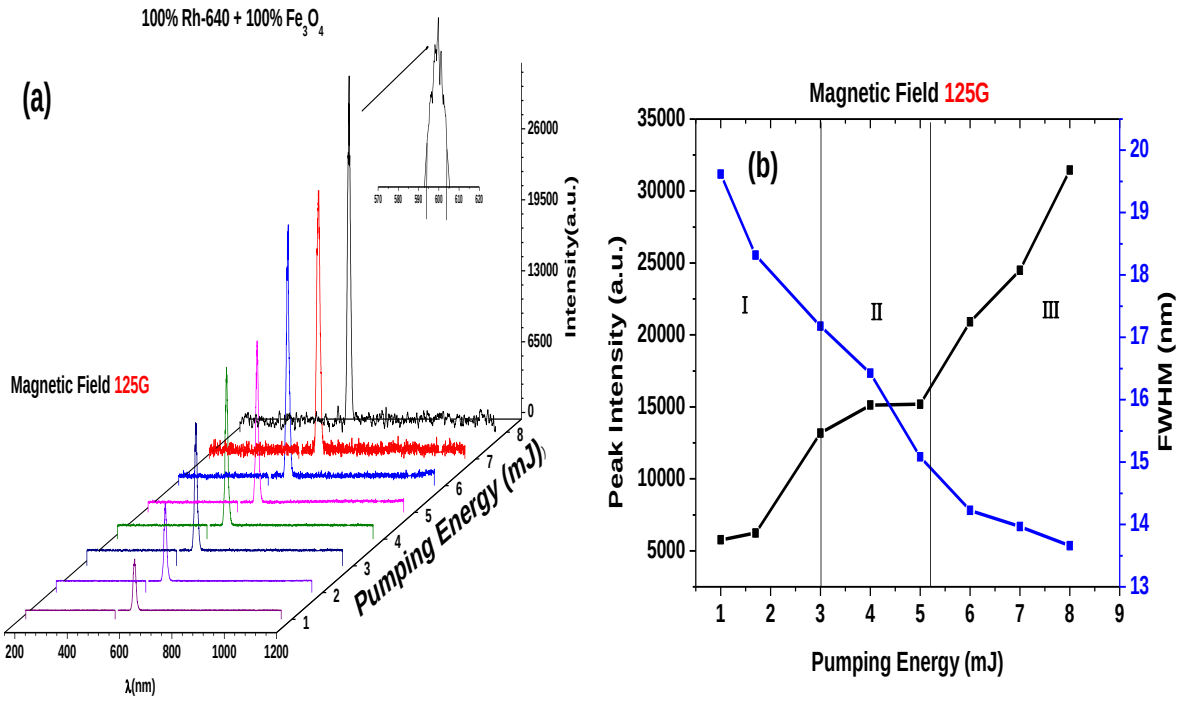

Fig. (4- 18) (a) The emission spectra and (b) variations of peak intensity and FWHM as a function of pumping energy in the presence of a constant external magnetic field of 125 G.

4.5. Ag Nanowires Random Laser Based Resonance Energy Transfer

4.5.1. Morphology and Structure of Ag Nanowires

Fig. (4-19-a) and (4-19-b), shows the absorption spectrum of Ag nanowires as synthesized by seed-mediate growth. After that Prepared a concentration of (1.1×10^{11} cm^{-3}) without and with Rh640/MB dye (1×10^{-5})/(2×10^{-4}) M, using methanol as solvent for all samples. Two absorption bands can be seen in Fig. (4-19) (a), which correspond to the longitudinal and transverse Plasmon bands [138]. The longitudinal Plasmon band has a center wavelength of 380 nm, while the transverse Plasmon band has a center wavelength of 348.8 nm. Fig. (4-19) (b), shows the absorption spectrum of the mixture (40% Rh-640 with 40% MB + 20% Ag NWR), which shows three absorption spectra bands centered at 380, 560, and 650 nm, respectively.

From FE-SEM analysis of silver nanowires as synthesized, shown in Fig. (4-20-a) ,the average mean size of the sample was found to be 50 nm in diameter of and a length of less than 50 microns. The Energy-Dispersive X-ray (EDX) profile showed a strong signal for silver NWs composition, shown in Fig. (4-20-b).

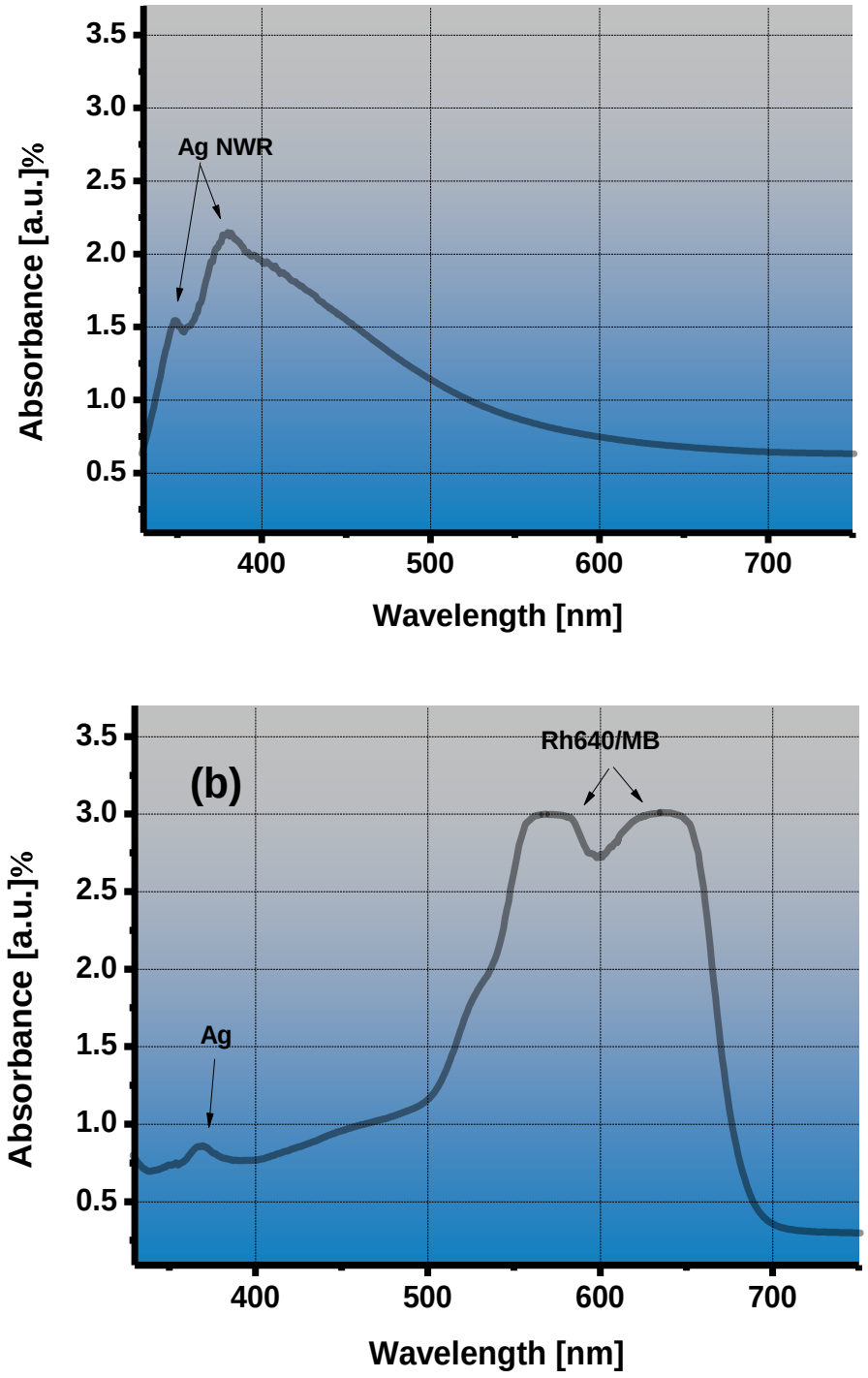

Fig. (4- 19) The absorption spectrum of (a) pure Ag NWS and (b) Ag NWS with dye mixture Rh-640 /MB

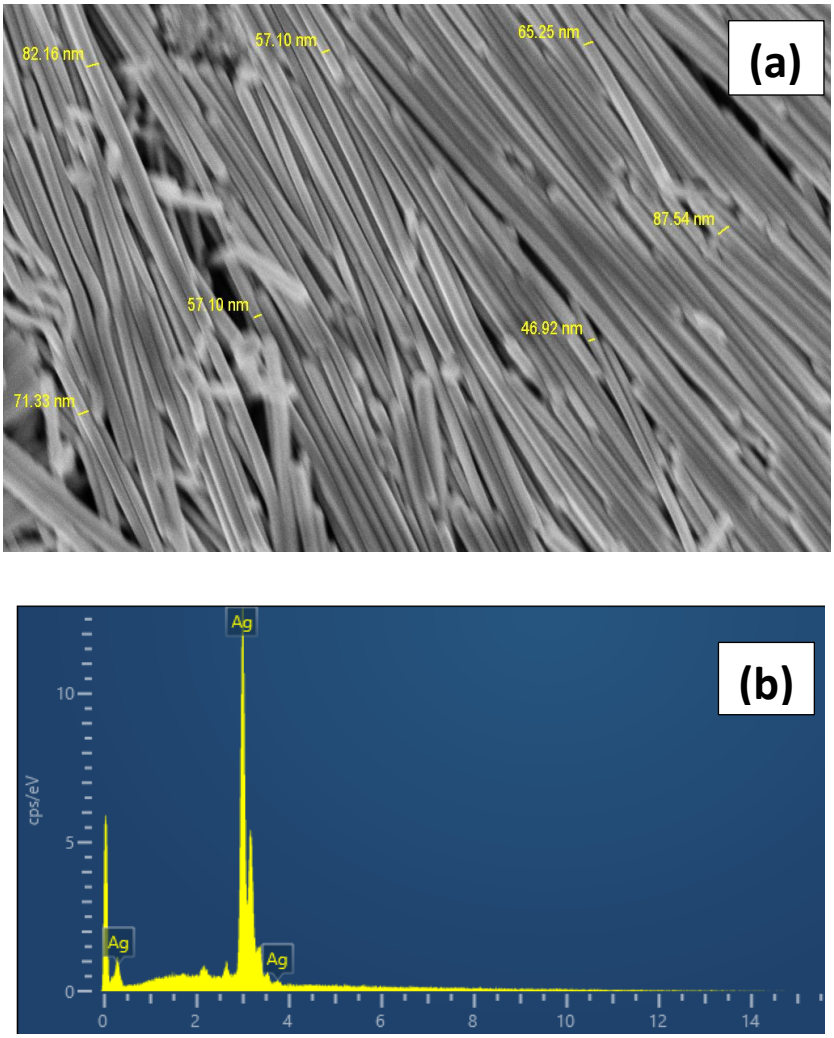

Fig. (4- 20) a- Image of Ag nanowires taken with a field emission scanning electron microscope (FESEM) ,b- EDX (energy-dispersive X-ray spectroscopy) image of Ag NWs.

On the other hand, Fig. (4-21) shows The spectral overlapping area between the absorption and fluorescence emissions of dyes mixture: (Rh640) as donor and (MB) as acceptor, where used in the random laser energy transfer experiment. Through Fig. (4-21), the revealed a broadband absorption and fluorescence emission band for the dyes mixture. Furthermore, The Rh640 fluorescence spectra overlap with the absorption

spectra of MB. This suggests that energy can be transferred between these two dyes in both radiative and nonradiative ways.

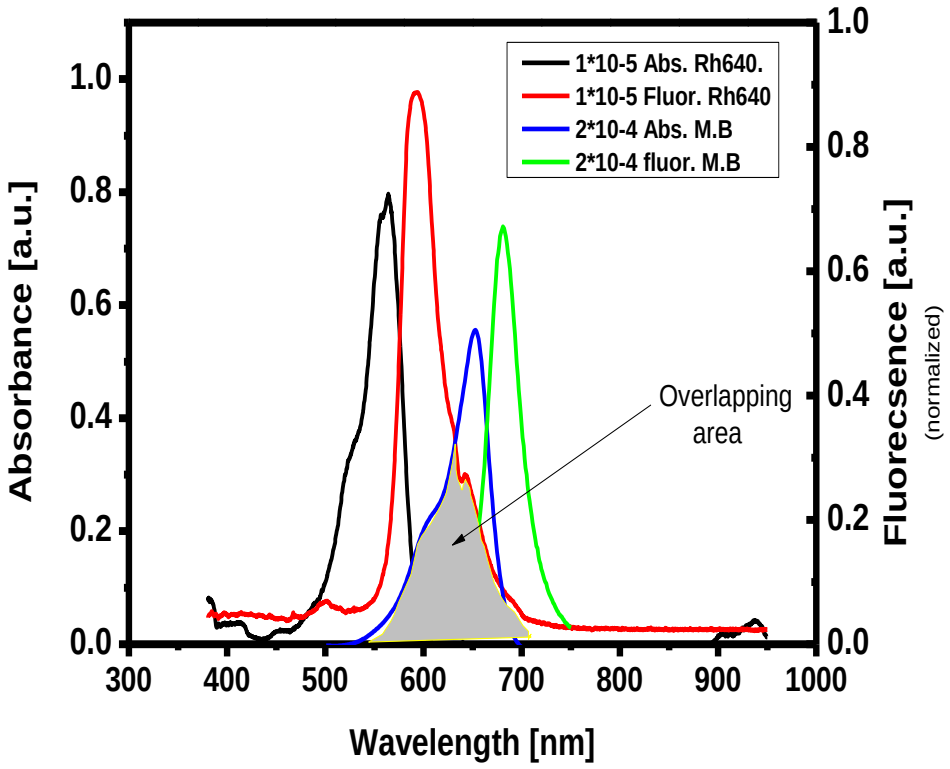

Fig. (4- 21) Spectral overlapping between absorption spectra of Rh640 (black line), MB (blue line) and the fluorescence spectra of Rh640 (red line), methylene blue (green line).

4.5.2 Variation of transfer efficiency with acceptor concentration

As illustrated seen in Fig. (4-21), poor absorbance of methylene blue dye at 532 nm can be overcome by using this dye as acceptor along with an efficient donor [139]. The donor should have significant absorption at 532 nm and emission band of the donor should overlap with absorption band of the acceptor. Rh640 dye satisfied both these requirements and therefore Rh640 dye at optimized concentrations of 1.65 x 10^{-3} M was mixed with MB dye at concentration 4.5 x 10^{-3} M to make donor-acceptor pair. Fig. (4-22) (a-c) shows the fluorescence spectra of dyes mixture Rh640 and MB at ratio 1:1, 1:2, 1:5. At mixture dye (2:1) [Fig. (4-22) (a)], observed the intensity of Rh-640 it is maximum and the intensity of MB it is reduce, this mean the self-reabsorption occur in this ratio, the result agreement with [2]. Mixture dye (1:5) lead to improving of intensity spectra of MB this indicted the efficient energy transfer in this mixture [Fig. (4-22) (b)]. Finally, it should also be note that the bleaching effects on intensity of the Rh-640 and MB, at mixture ratio (1:1) .the energy transfer from 1:1 is effective to give dual wavelength [Fig. (4-22) (c)].

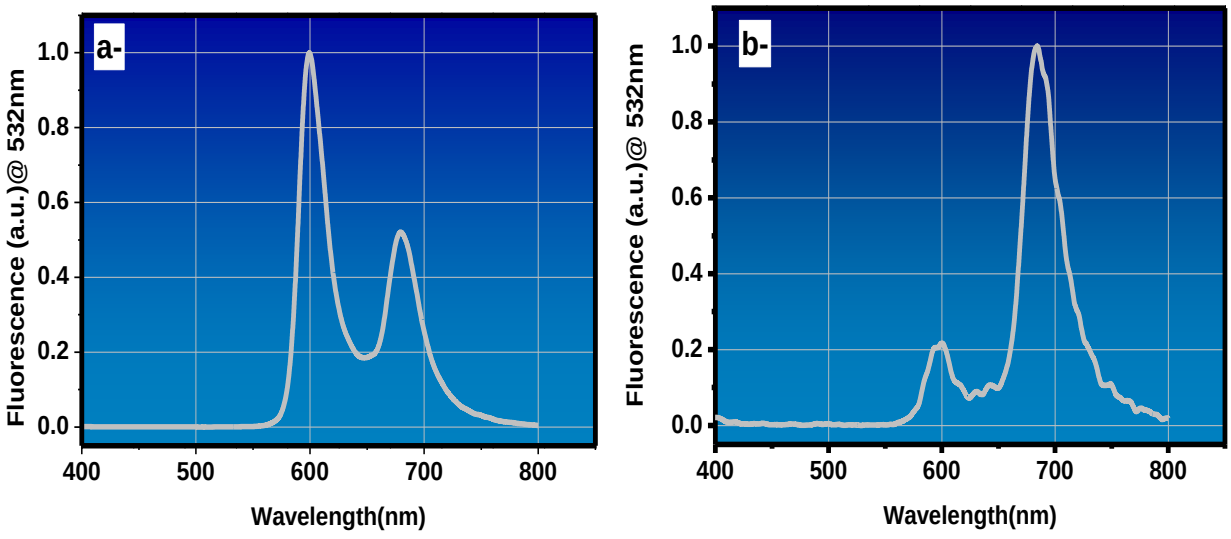

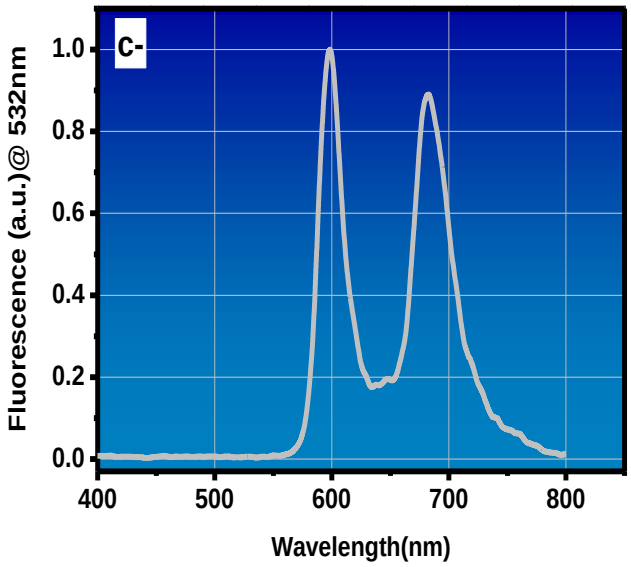

Fig. (4- 22) Fluorescence spectrum for the mixture of Rh-640 / MB dye solution with different dye ratio combination; (a) 1:2 (b) 1:5 (c) 1:1.

The I_D/I_{DA} ratio in relation to various MB dye acceptor concentrations is shown in Fig. (4-23).To calculate the Stern-Volmer constant, compare the fluorescence intensity of the donor (Rh-640) in the presence and absence of the acceptor (MB dye) or the slope of the figure's best-fit straight lines.

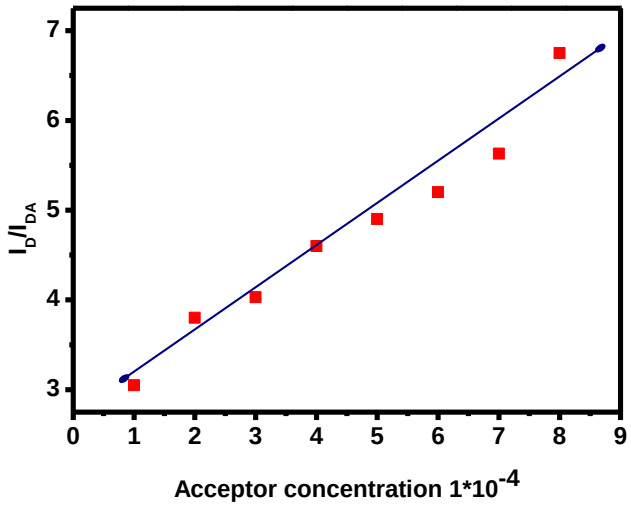

Fig. (4- 23) shows the I_D/I_{DA} ratio versus acceptor concentrations for MB dye.

Eqs. (2.13) (2.14) (2.15) are used to calculate the values of $[A]_{1/2}$, R_o, and K_{AD}. are listed with the value of K_{SV} in Table (3-2). The radiative lifetime (τ_D) of 1 x 10^{-5} M was calculated from Rh-640 using Eq. (4) , and its value was found to be about 3.7 ns. The $\emptyset_D/\emptyset_{DA}$ of quantum yields of the donor in the absence and presence of acceptor and energy transfer (E) were calculated at varying concentrations of (MB) acceptor dye by using Eq. (2-18), respectively. These values are listed in Table (1) too.

According to the studies, for a fixed donor (Rh-640) concentration, the energy transfer efficiency increases with the concentration of the acceptor (MB) and approaches (0.9) at a high concentration, giving the energy transfer mechanism the dominating mechanism. These findings are in agreement with those of a group of studies, including Baha T.chiad et al [140]. and Wan Zakiah Wan Ismail et al [22].

Table (3- 2) shows the energy transfer parameters for the Rh-640:MB dyes.

Donor Dye- Rh-640 - concentration (1×10^{-5} M)					
K_{SV} (M^{-1})	**$[A]_{1/2}$ (M)**	**R_o (A^o)**	**K_{AD} (M^{-1} Sec^{-1})**	**τ_D(ns)**	
4944	**0.22×10^{-3}**	**120**	**1.336×10^{12}**	**3.7**	
Accepter Dye –MB- Concentration (mM)				**$\emptyset_D/\emptyset_{DA}$**	**E**
0.2				**2**	**0.73**
0.4				**3**	**0.77**
0.6				**4**	**0.8**
0.8				**5**	**0.83**
1				**6**	**0.85**

4.5.3 Dual wavelengths emission in Rh640/MB random laser

Fig. (4-24) shows two intense spectral bands associated with Rh640 and MB were clearly seen, which narrowed down at different pump energy. The emission spectra of a dye solution without Ag NWs is shown as a red line, and in the presence of Ag NWs as a black line. Using a single-wavelength 532 nm pulsed laser beam as wavelength excitation, the first excitation was to Rh640 dye, producing two peaks at wavelengths of 580 nm and 700 nm, respectively. The excited spectra of Rh640 has a wide linewidth (about 32nm), this is important requirement for excites MB dye. This is a strong indication that the energy transfer from the Rh640 donor was sufficient to support random lasing to the MB acceptor, and the residual energy in Rh640 was enhanced by scattering feedback. This cause shown the Rh640 dye has a stimulated emission. The linewidth of each spike is smaller than 1 nm, and the number of spikes were approaching 30 appeared on the top of spectrum which indicates typical coherent lasing occurs. The threshold were 2.1 mJ for Rh640 dye and 3 mJ for MB dye. In fact, these are basic characteristics of random laser. Also, it can be observed that effective concentration of Ag NWs for both emission from dyes was not similar in the wavelength tunability, ranged from (570–598) nm (i.e blue shift) for donor Rh640, and from (700-720) nm for acceptor MB (i.e red shift), this was occurred due to optical elongation leads to increasing a birefringence.

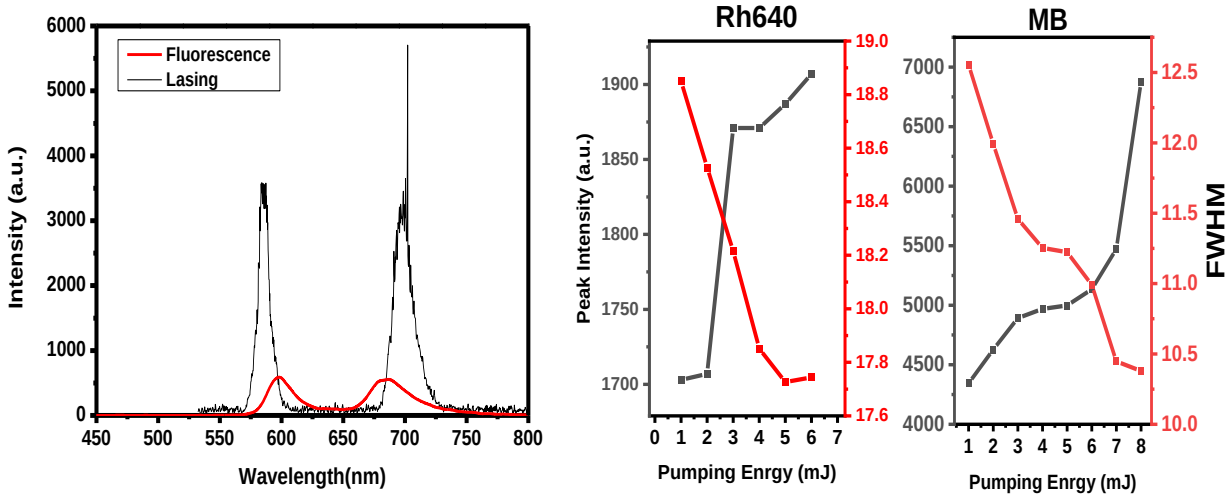

Fig. (4- 24) (a) The emission spectra of Rh640/MB at ratio (1:1) with and without Ag NWs at concentration ($1.1\times10^{11}cm^{-3}$), variation of FWHM and peak intensities of the spectra with respect to pump energies of (b) Rh640 and (c) MB

Fig. (4-25) shows the random laser's coherent emission spectra at the energy efficiently transmitted from the donor (Rh640) to the acceptor (MB). Because of low molar ratio of donor leading to absorbed the 532 nm of energy by the Rh640 dye then mostly transferred to the MB. The emission spectra at 580 nm is reduced dramatically (6 fold lower than of than MB). In this case two dyes are used with scatters to create a single wavelength.

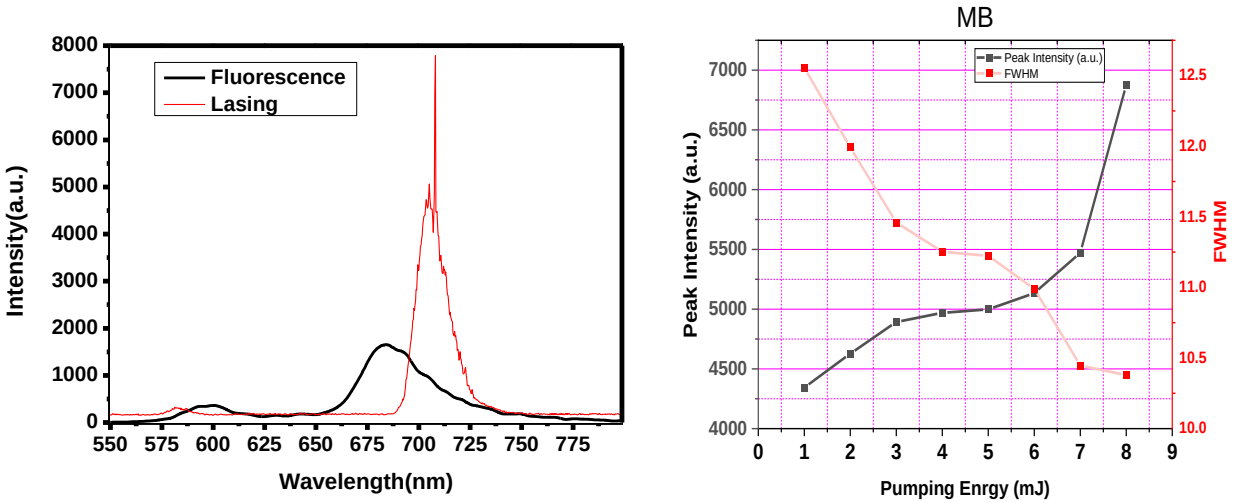

Fig. (4- 25) (a) The emission spectra of Rh640/MB at ratio (1:5) with and without Ag NWs at concentration ($1.1\times10^{11}cm^{-3}$), (b) variation of FWHM and peak intensities of the spectra with respect to pump energies of MB

4-5-4 Effect of pumping power on RET random laser

Figure (4-26), illustrated the emission spectra under 532 nm pulses under various pumping powers, for dye mixture systems based on Ag NWR with R640 and methylene blue at concentrations of 1.65 x 10^{-3} M and 4.5 x 10^{-3} M (i.e. at a molecular ratio between Rh-640 and MB 1:1 and an average distance between the molecules >10 nm). At 0.87 mJ of pumping power (black curves in figure). The findings in (4-26) (a) demonstrate that a tiny amount of energy is transferred from R640 to the gain material MB, causing the gain in some loops for R640 to be more than the loss, but not for methylene blue due to the extended optical paths. The dual-coherent random lasing with two series of sharp spikes at the center wavelengths of 585 and 696 nm with 1.5 mJ and 2 mJ of pumping powers (first and second thresholds, respectively) were observed in Fig. (4-26) (a) (blue curve) and (red curve). Furthermore, by increasing a pumping power more above 2.3

mJ (third threshold), as shown by the purple curve in Fig. (4-26) (a). The system be change rapidly with exhibit a discrete sharp peaks with a red shift about 700 nm. This suggests that the coherent lasing resonances from the two gain materials, which were obtained from the optical gain based on the regulated RET, are affects concurrently under a changing in pumping power.

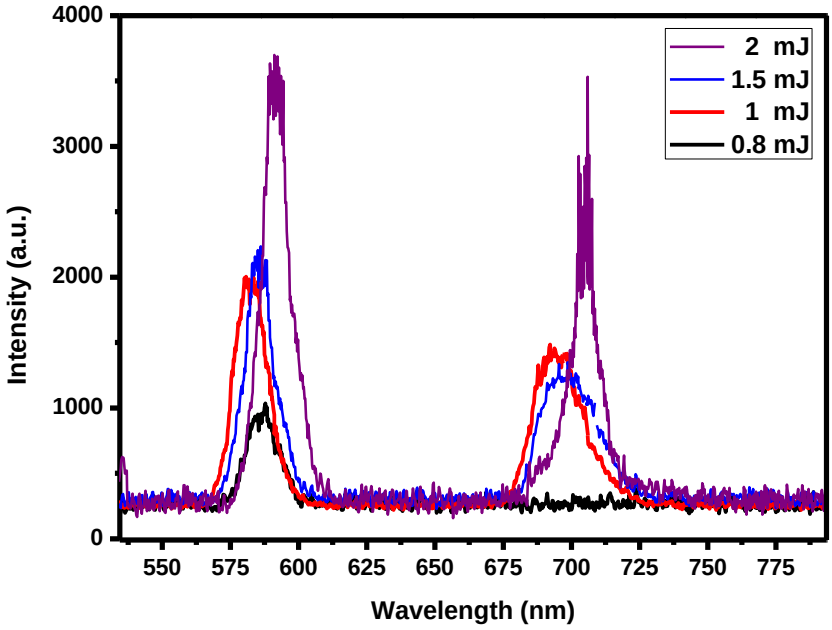

Fig. (4- 26) The dual-color coherent random lasing emission at different pumping power.

Fig. (4-27-a) thresholds behavior of random lasing from R640 and (b) methylene blue with respect to the linewidth and output intensity of the dye mixture RET random laser. Notice that by increasing a pumping power more and more give a decreasing in the linewidith from both dual color Rh640 and MB, were (13-10.5) nm and (22- 12) nm, respectively.

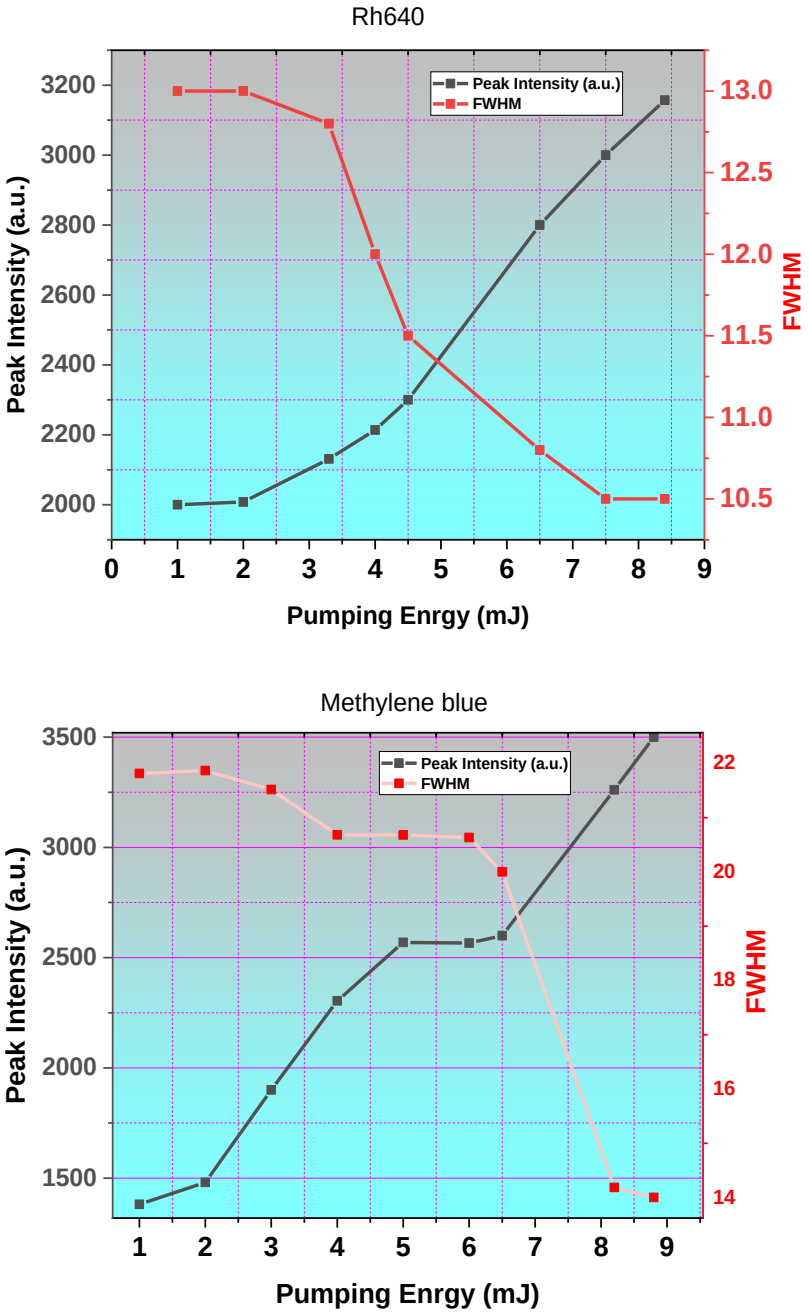

Fig. (4- 27) (a) thresholds behavior of random lasing from R640 and (b) methylene blue with respect to the linewidth and output intensity of the dye mixture RET random laser.

4-6 Gold Nano-Rod Random Laser

4-6-1 Morphology of Gold Nano-Rod

In this type of random laser, Au nanorods have been used as scattering centers in a random medium containing LDS 821 as the gain medium. The Au nanorods with two size: sample-1 (lengths ± 18.8 μm, diameter ± 6.3 nm) and sample-2 (lengths ±22.3 μm, diameter ± 7.2) were synthesis by seedless method. Fig.(4.28) displays the transmission electron microscopy (TEM) of the Au nanorods with two sizes separately.

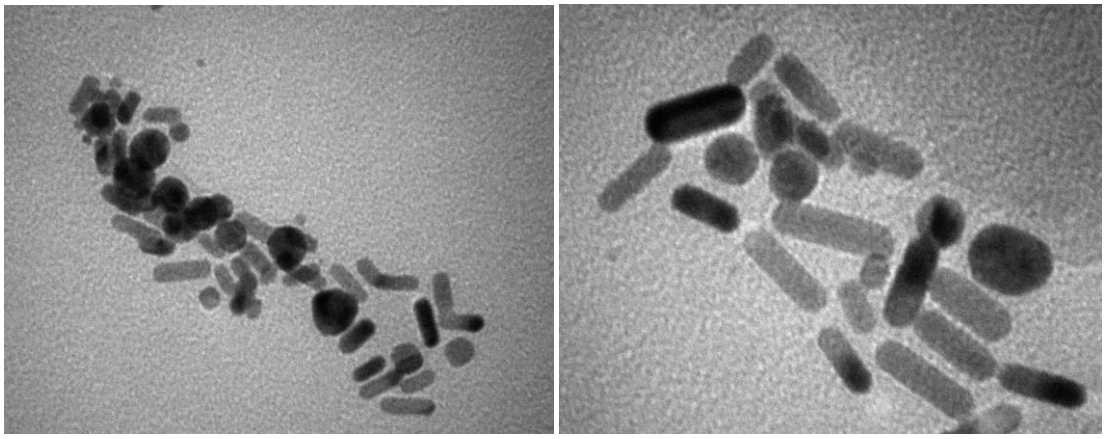

Fig. (4- 28) The TEM images of Au nanorods as collide for different sizes.

Furthermore, the results of the TEM analysis of gold NRs synthesized using different concentrations of $NaBH_4$ (reduction agent). As can be seen in all cases, the nanostructures are in the form of rod-shape with relatively low size distribution in the range of (lengths ± 18.8 μm, diameter ± 6.3 nm) and (lengths ±22.3 μm, diameter ± 7.2) It is interesting to notice that, increasing $NaBH_4$ concentration reduces the size and aspect ratio of the

resulting gold NRs. This occurrence is expectable because the increase in the $NaBH_4$ concentration forms a higher number of seed NPs, which in turn decreases the amount of metal ions involved in the growth of gold NRs.

4.6.2 Absorption spectra of Au nanorods

Fig. (4.29), shows the absorption spectra of two sizes of Au nanorods dissolved in deionized water, respectively. It can be seen that the absorption spectrum of the two sizes of Au nanorods exhibited two relatively sharp surface plasmon resonance (SPR) peaks for each size. These two absorption bands correspond to the longitudinal and transverse plasmon bands. The longitudinal plasmon band is attributed to the absorption and the scattering light spreading over the long axis of the nanorods, while the transverse plasmon band is caused by the same reason, but along the short axis of the nanorods. The same results were obtained by Keerthi G. Nair et. al. [141]. Comparing the two spectra, the centers of the longitudinal plasmon bands are approximately at 517 nm because the length of the two samples of nanowires is a fixed, while the centers of the transverse plasmon band are at 712.1 nm and 720.77, respectively.

UV-visible spectra were obtained to investigate optical characteristics and confirm the synthesis of gold NRs. In this regard, one can observe the characteristic SPR of gold NRs over the wavelength range of visible to near infrared. Also, this indicates that the absorption spectrum is shifted towards longer wavelengths (redshift) by increasing the diameter of the nanomaterial which agreement with [142]. Fig.(4.29) (red line) shows that the absorption spectrum of the Gold nanomaterial of 6.3 nm diameter is

higher than the absorption spectrum of those of 7.2 nm (black line in Fig. 4-29)). This result was supported by [143].

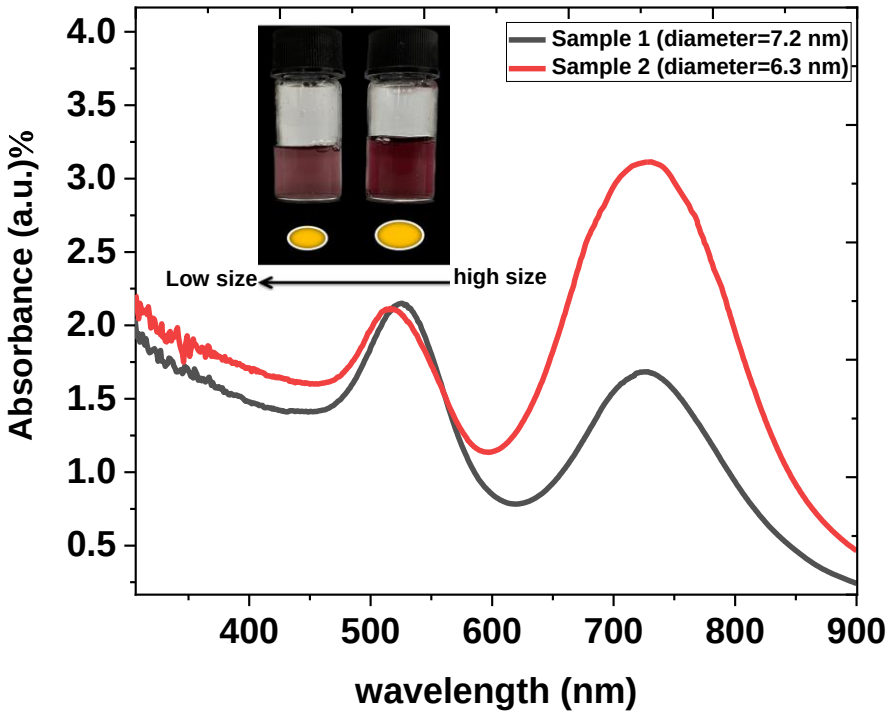

Fig. (4- 29) The absorption spectrum of Ag nanowires of two sizes capped with different concentrations of CTAB.

4.6.3 Lasing characteristics of gold NR random laser

To influences of two sizes of gold NRs, the characteristics of the random laser will be discussed in three different laser media in terms of nanomaterial size at a fixed particle density $1.8\times10^{18}cm^{-3}$ as follows:

Fig. (4.30 a and c) shows the evolution of the random laser emission spectra for the two different dimensions of Au NRs used as scattering centers are sample-1(D= 7.2 nm) and the sample-2 (D = 6.3 nm) with same length at different pumping energies.

Fig.(4.30 a-b) show the evolution of the emission spectra with different pumping energies of the first medium (sample1) at diameter (D=7.2 nm). At the lowest pumping energy 0.038 mJ, it is noticed that there is no random laser emission and what appears, is only a spontaneous emission related to the surrounding environment, and this spontaneous emission had persisted for some higher energy values than 0.038 mJ (see the region I in Fig.(4.30-b). When the pumping energy exceeds the value of E_{th}=0.095 mJ (the first threshold), the FWHM of the peak emission centered around 775 nm had narrowed to several nanometers, meanwhile, the emission intensity increased rapidly. This behavior refers to the emergence of incoherent lasing in the random laser systems. The persistence of this incoherent laser was observed from 0.095 mJ into under the value of 0.15 mJ of pumping energy (see the region II in Fig.(4.30-b). By further increasing the pumping energy into the value of E_{th}=0.152 mJ which is called the second threshold (see the region III in Fig.(4.30-b), the random system begins to exhibit distinct characteristics and several discrete peaks appear in the emission spectrum. The width of these peaks can reach less than 1 nanometer, which is many times narrower than the spectrum of the incoherent random lasing.

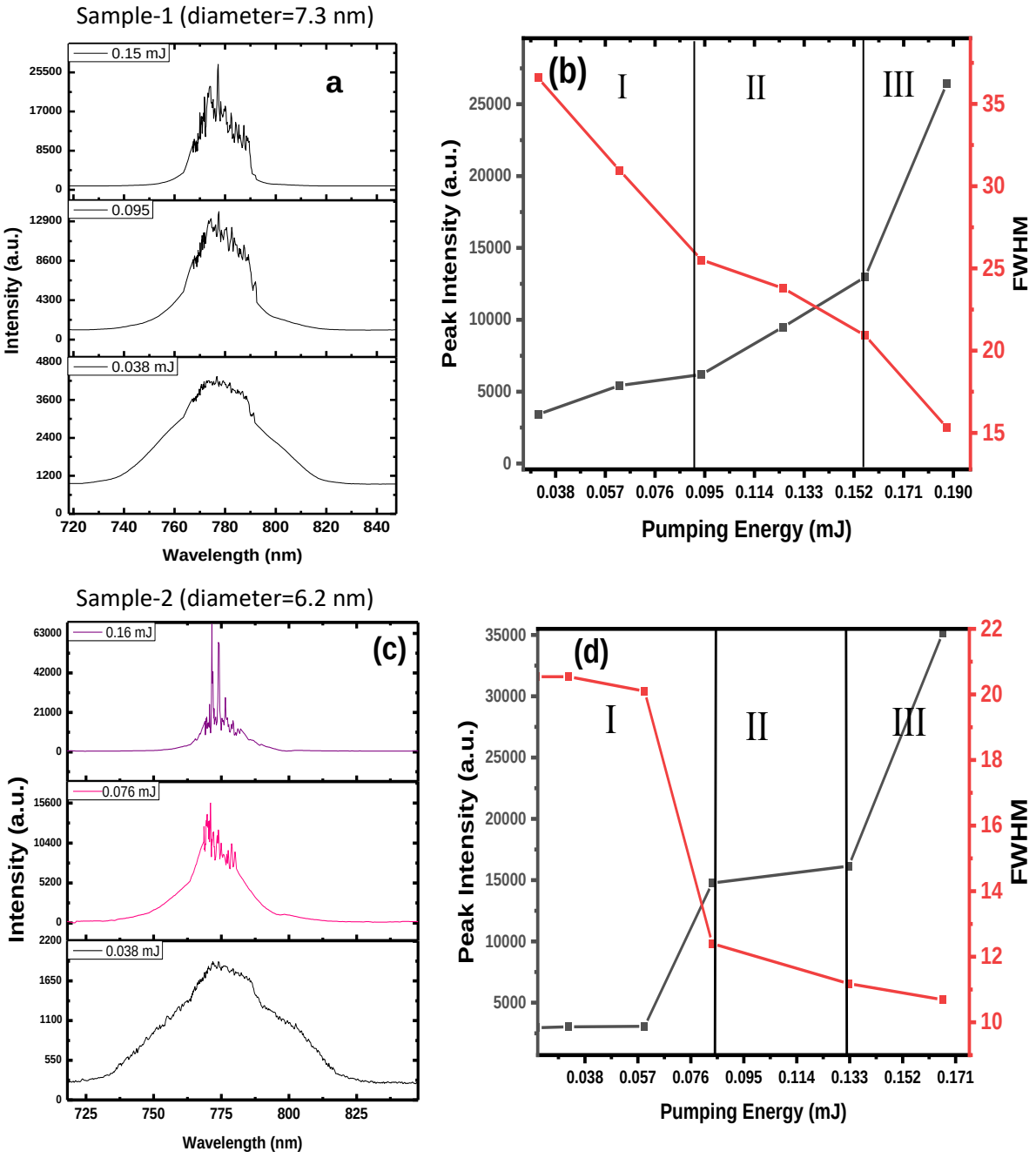

Fig. (4- 30) The evolution of the emission spectra in (left column) and the threshold curves (black line) and FWHM (red line) in (right column) with pumping energy at different sizes of Au nanorods, (a) and (b) at D=7.2 nm, (c) and (d) at D=6.3 nm.

These discrete peaks (spikes) resulting from the recurrent scattering of light represent the turning point from the incoherent to the coherent random laser. This result is compatible with these presented by J. Xia et. al. in [74], as the second threshold is the critical value for the occurrence of the coherent random laser. This result indicates the possibility of achieving the transition from incoherent feedback to coherent feeding by increasing the pumping energy at the same concentration and size of nanomaterial, It is similar to what H. Cao and J. Y. Xu found in their manuscript [144].

To observe the effect of size on the optical features of the random lasing, the diameter 7.2 nm gold nanorods will be replaced by the 6.3 nm nanorods where Fig.(4.30 c-d) represents the emission spectrum of a random laser medium with gold NR its diameter (D = 6.3 nm) as dispersants. At the minimum pumping energy which was 0.038 mJ, it is noted that the spontaneous emission still dominates the scene, but it looks less than in the previous case indicating the approaching appearance of the emission spectrum, the best proof of this is the narrowness region I in the Fig.(4.30-d) compared to it in the Fig.(4.30-b). When the incident pumping pulse energy exceeds the value of 0.057 mJ which represents the first threshold of this medium, the emission peak centered around 780 nm begins to narrower and its intensity rises more rapidly with increasing pumping energy. It has represented the incoherent random laser of the new size, which appears to be more narrow and has higher emission than the previous size see Fig.(4.30-c). Compared to the incoherent random laser of the first size, this laser began to appear at pumping energy of 0.076 mJ and continued to the limit of 0.16 mJ (see the region II in Fig.(4.30-d)). By further increasing the pumping energy to the value of the E_{th}=0.172 mJ which symbolizes the second threshold of this medium (see the region III in

Fig.(4.30-d)), the system turns into a coherent random laser and it shows characteristics that differ from those at the pumping energies less than 0.076 mJ, and also differ from what they were in the first size in terms of early emergence and number of separate peaks of the emission spectrum.

The effect of increasing the Au nanorods concentration on the performance of random laser can be seen in Fig.(4.31), where new concentrations for the diameter of 6.3 nm was 2.1×10^{18} cm^{-3}. For this particle density, it was observed that the emission signal prevailed over the source noise and the incoherent random laser spectrum appeared very early at 0.045 mJ which announcing the first threshold of this laser (see the region II in Fig.(4.31-b)) and it is less than 0.076 mJ and 0.057 mJ which are the first two thresholds of the Au nanorods random laser at a fixed particles density 1.8×10^{18} cm^{-3}. By continuing to increase the pumping energy, the emission spectrum began narrow rapidly to several tens of nanometers, while the peak intensity increased see Fig.(4.31-c), and when the pumping energy surpassed the value of E_{th}=0.081 mJ which exemplified the second threshold of this laser (see the region III in Fig. (4.31-d)). It was certainly regarded as the transform point of a random laser from the incoherent to the coherent type, and it is the best transition threshold for gold nanorods compared to the values shown in Fig. (4-30). Accordingly, it can be said that the properties of random lasers can be improved, as well as there is a great opportunity to shift from the incoherent to the coherent type of random lasers by increasing the concentration of nanomaterials within a certain range.

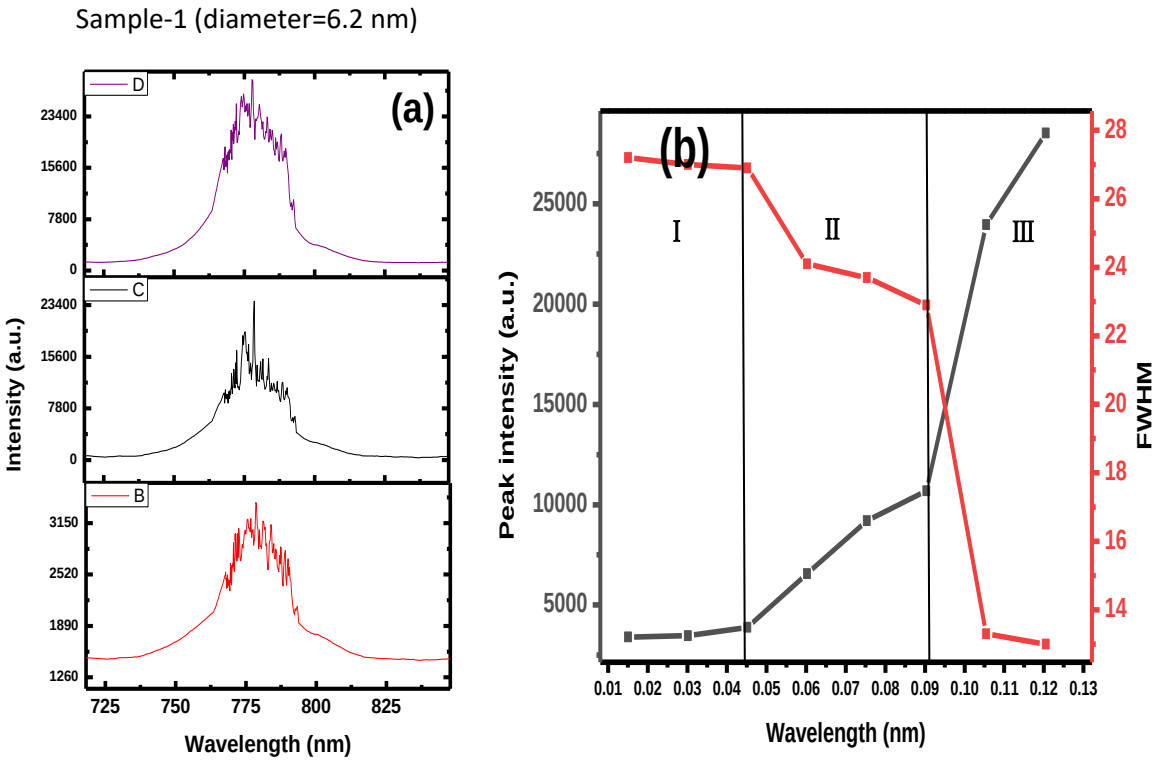

Fig. 4- 31 The evolution of the emission spectra in (left column) and the threshold curves (black line) and FWHM (red line) in (right column) with pumping energy at C=2.1×10^{18} cm^{-3}. concentrations of Au nanorods.

Chapter Five

Conclusions & Future Works

5.1 The Conclusions

1- This study confirmed that the interaction between magnetic NPs in the nanofluids under the exposure of the applied magnetic field can allow a wide control of the intensity and re-diffusing of the laser beam penetrating through them.

2- The absorption spectra indicated that the NPs dispersed in methanol solution had good stability over time

3- The applied magnetic field strength and the nanofluid concentration significantly influenced the transition between the two critical field points (H_{C1} and H_{C2}).

4- The SMFP of SNPs was found to continuously decrease from 152 to 49 μm with increasing the response time from 25 to 200 (s). This indicated that an easy transition may occur from a non-coherent to a coherent random laser if the NPs were used as scattering centers in the effective medium of the random laser.

5- The controllability of the random laser parameters in the presence of the magnetic field was evaluated and confirmed up to acceptable values of the SNPs.

6- Sharp spikes were observed in the emission spectra, resulting from the presence of the applied magnetic field and numerous scattering centers formed by SNPs in the excited region.

7- It was found that the emission strength increased with increasing the density of the scattering centers (SNPs). A linear function was established between the spectral shift and the response time (0.30 s) of the magnetic field.

8- Because of the overlap between the absorption and fluorescence bands, the intensity of the fluorescence emission of Rh640 gradually reduced as the concentration of methylene blue increased, and it was discovered that the FRET efficiency could be regulated by varying the donor-acceptor ratio.

9- Combining two dyes (Rh640:MB) resulted in random laser emission beyond 700 nm and the efficiency of random laser was 85%.

10- The scattering centers Au NRS were effective at the laser threshold, emission laser linewidth intensities, and contrast wavelengths, in addition to delivering positive feedback.

5.2 Suggestions for Future Works

1- Studding another types of Infrared Dye Laser in the 800-1000nm Range as active medium of random laser for examples LDS 950 in Methanol, LDS 925 in Methanol and LDS 867 in Methanol.

2- The use of aromatic hydrocarbons with different ring numbers as hosts of the laser dye and scattering nanoparticles.

3- Studding the effect of the temperature of the active medium of a random laser on the lasing characteristics

4- Use three laser dyes in the 550–880 nm range as cascade-pumped sources for the random lasers.

5- Replacing the scattering Fe_3O_4 SMNPs nanoparticles with different ones, such as Fe_3O_4:Au NRs and Fe_3O_4 & AU NRS coreshell, and investigate how they affect the laser's properties when a magnetic field is present.

References

References

[1] A. S. L. Gomes, A. L. Moura, C. B. de Araújo, and E. P. Raposo, "Recent advances and applications of random lasers and random fiber lasers," *Prog. Quantum Electron.*, vol. 78, no. July, 2021, doi: 10.1016/j.pquantelec.2021.100343.

[2] B. Redding, M. A. Choma, and H. Cao, "Speckle-free laser imaging using random laser illumination," *Nat. Photonics*, vol. 6, no. 6, pp. 355–359, 2012, doi: 10.1038/nphoton.2012.90.

[3] J. F. Galisteo-Lõpez, M. Ibisate, R. Sapienza, L. S. Froufe-Pérez, Ú. Blanco, and C. Lõpez, "Self-assembled photonic structures," *Adv. Mater.*, vol. 23, no. 1, pp. 30–69, 2011, doi: 10.1002/adma.201000356.

[4] A. Lagendijk, "Light diffusion with gain and random lasers," vol. 54, no. 4, pp. 4256–4265, 1996.

[5] C. M. Maguire, M. Rösslein, P. Wick, and A. Prina-Mello, "Characterisation of particles in solution–a perspective on light scattering and comparative technologies," *Sci. Technol. Adv. Mater.*, vol. 19, no. 1, pp. 732–745, 2018, doi: 10.1080/14686996.2018.1517587.

[6] M. A. Noginov, J. Novak, and L. Deych, "Photon motion in a random laser medium with gain: Is it diffusion?," in *Frontiers in Optics*, 2005, p. FWQ2.

[7] H. Cao, "Lasing in random media," *Tutorials in Complex Photonic Media*. pp. 301–358, 2009, doi: 10.1117/3.832717.Ch11.

[8] A. Mitra and R. K. Thareja, "Photoluminescence and ultraviolet laser emission from nanocrystalline ZnO thin films," *Journal of Applied Physics*, vol. 89, no. 4. pp. 2025–2028, 2001, doi: 10.1063/1.1342803.

[9] S. Mujumdar, M. Ricci, R. Torre, and D. S. Wiersma, "Amplified extended modes in random lasers," *Physical Review Letters*, vol. 93, no. 5. 2004, doi: 10.1103/PhysRevLett.93.053903.

[10] T. Okamoto and S. Adachi, "Effect of particle size and shape on nonresonant random laser action of dye-doped polymer random media," *Opt. Rev.*, vol. 17, no. 3, pp. 300–304, 2010, doi: 10.1007/s10043-010-0053-0.

[11] F. P. Schäfer, “Principles of Dye Laser Operation,” pp. 1–85, 1973, doi: 10.1007/978-3-662-11579-4_1.

[12] S. Popov, “Dye photodestruction in a solid-state dye laser with a polymeric gain medium,” *Appl. Opt.*, vol. 37, no. 27, pp. 6449–6455, 1998.

[13] C. S. Wang, Y. L. Chen, H. Y. Lin, Y. T. Chen, and Y. F. Chen, “Enhancement of random lasing through fluorescence resonance energy transfer and light scattering mediated by nanoparticles,” *Appl. Phys. Lett.*, vol. 97, no. 19, pp. 1–4, 2010, doi: 10.1063/1.3515913.

[14] L. Yang, G. Feng, J. Yi, K. Yao, G. Deng, and S. Zhou, “Effective random laser action in Rhodamine 6G solution with Al nanoparticles,” *Applied Optics*, vol. 50, no. 13. pp. 1816–1821, 2011, doi: 10.1364/AO.50.001816.

[15] K. Firdaus, T. Nakamura, and S. Adachi, “Improved lasing characteristics of ZnO/organic-dye random laser,” *Appl. Phys. Lett.*, vol. 100, no. 17, p. 171101, 2012.

[16] B. Kumar, S. K. S. Patel, N. S. Gajbhiye, and R. K. Thareja, “Random laser action with nanostructures in a dye solution,” *J. Laser Appl.*, vol. 25, no. 4, p. 042012, 2013, doi: 10.2351/1.4809615.

[17] T. Zhai *et al.*, “A plasmonic random laser tunable through stretching silver nanowires embedded in a flexible substrate,” *Nanoscale*, vol. 7, no. 6, pp. 2235–2240, 2015, doi: 10.1039/c4nr06632d.

[18] Z. Wang *et al.*, “Two-threshold silver nanowire-based random laser with different dye concentrations,” *Laser Phys. Lett.*, vol. 11, no. 9, 2014, doi: 10.1088/1612-2011/11/9/095002.

[19] J. Ziegler, M. Djiango, C. Vidal, C. Hrelescu, and T. A. Klar, “Gold nanostars for random lasing enhancement,” *Optics Express*, vol. 23, no. 12. p. 15152, 2015, doi: 10.1364/oe.23.015152.

[20] S. Brojabasi, T. Muthukumaran, J. M. Laskar, and J. Philip, “The effect of suspended Fe3O4 nanoparticle size on magneto-optical properties of ferrofluids,” *Opt. Commun.*, vol. 336, pp. 278–285, 2015, doi: 10.1016/j.optcom.2014.09.065.

[21] L. Ye *et al.*, “Random lasing action in magnetic nanoparticles doped dye

solutions," *Opt. Commun.*, vol. 340, pp. 151–154, 2015.

[22] W. Z. W. Ismail, E. M. Goldys, and J. M. Dawes, "Fluorescence resonance energy transfer (FRET) in random dye lasers," in *Conference on Lasers and Electro-Optics/Pacific Rim*, 2015, p. 26P_20.

[23] L. Long *et al.*, "Localized surface plasmon resonance improved lasing performance of Ag nanoparticles/organic dye random laser," *J. Alloys Compd.*, vol. 693, pp. 876–881, 2017, doi: 10.1016/j.jallcom.2016.09.246.

[24] J. M. Dawes, W. Z. W. Ismail, E. M. Goldys, and D. W. Coutts, "Enhancing the performance of random lasers: Effects of localised surface plasmons and resonance energy transfer," in *2016 4th International Conference on Photonics, Optics and Laser Technology (PHOTOPTICS)*, 2016, pp. 1–4.

[25] S. Ning, Z. Wu, N. Zhang, L. Ding, X. Hou, and F. Zhang, "Plasmonically enhanced lasing by different size silver nanoparticles-silver film hybrid structure," *Org. Electron.*, vol. 50, pp. 403–410, 2017, doi: 10.1016/j.orgel.2017.08.018.

[26] C. Y. Tsai *et al.*, "Magnetically Controllable Random Lasers," *Adv. Mater. Technol.*, vol. 2, no. 12, 2017, doi: 10.1002/admt.201700170.

[27] J. Yin, G. Feng, S. Zhou, H. Zhang, S. Wang, and H. Zhang, "The effect of the size of Au nanorods on random laser action in a disordered media of ethylene glycol doped with Rh6G dye," *Nanophotonics VI*, vol. 9884, no. April 2016, p. 988426, 2016, doi: 10.1117/12.2225583.

[28] A. L. Moura, R. Barbosa-Silva, C. T. Dominguez, É. Pecoraro, A. S. L. Gomes, and C. B. De Araújo, "Single bead near-infrared random laser based on silica-gel infiltrated with Rhodamine 640," *J. Appl. Phys.*, vol. 123, no. 13, 2018, doi: 10.1063/1.5024934.

[29] W. Z. W. Ismail, W. M. W. A. Kamil, and J. M. Dawes, "Enhancement of Random Laser Properties on Solid Polymer Films by Increasing Scattering Effect," *J. Russ. Laser Res.*, vol. 40, no. 4, pp. 364–369, 2019, doi: 10.1007/s10946-019-09812-5.

[30] Z. Ren, N. Zheng, K. Ge, G. Zhang, and S. Li, "Investigation of the LSPR on a wavelength-tunable random laser," *Physica Scripta*, vol. 94, no. 10. 2019, doi:

10.1088/1402-4896/ab07df.

[31] H. T. Dai *et al.*, “Magnetically tunable random lasing from polymer dispersed liquid crystal doped ferromagnetic nanoparticles in capillary,” *AIP Adv.*, vol. 9, no. 11, 2019, doi: 10.1063/1.5120438.

[32] V. S. Gummaluri, R. Gayathri, C. Vijayan, and V. M. Murukeshan, “Gold nano-urchins for plasmonic enhancement of random lasing in a dye-doped polymer,” *J. Opt. (United Kingdom)*, vol. 22, no. 6, 2020, doi: 10.1088/2040-8986/ab896b.

[33] C. Peng and L. Deng, “Random lasing based on plasmonic enhancement from dye-doped capillary tubes with Ag-TiO2 composite nanostructure,” *Photonics Nanostructures - Fundam. Appl.*, vol. 42, no. August, p. 100843, 2020, doi: 10.1016/j.photonics.2020.100843.

[34] R. A. Ejbarah, J. M. Jassim, S. F. Haddawi, and S. M. Hamidi, “Transition from incoherent to coherent random lasing by adjusting silver nanowires,” *Appl. Phys. A Mater. Sci. Process.*, vol. 127, no. 6, 2021, doi: 10.1007/s00339-021-04634-2.

[35] R. A. Ejbarah, J. M. Jassim, H. Yazdanfar, and S. M. Hamidi, “Random laser action in the visible region by dye-based sliver nano-hexagonal colloid media,” *Phys. Scr.*, vol. 96, no. 11, p. 115505, 2021.

[36] W. Z. W. Ismail, D. Liu, S. Clement, D. W. Coutts, E. M. Goldys, and J. M. Dawes, “Spectral and coherence signatures of threshold in random lasers,” *J. Opt. (United Kingdom)*, vol. 16, no. 10, 2014, doi: 10.1088/2040-8978/16/10/105008.

[37] G. Van Soest, F. J. Poelwijk, R. Sprik, and A. Lagendijk, “Dynamics of a random laser above threshold,” *Phys. Rev. Lett.*, vol. 86, no. 8, pp. 1522–1525, 2001, doi: 10.1103/PhysRevLett.86.1522.

[38] L. Ye, Y. Feng, C. Lu, G. Hu, and Y. Cui, “Coherent random lasing from liquid waveguide gain layer containing silica nanoparticles,” *Laser Phys. Lett.*, vol. 13, no. 10, 2016, doi: 10.1088/1612-2011/13/10/105002.

[39] Z. Wang *et al.*, “Controlling Random Lasing with Three-Dimensional Plasmonic Nanorod Metamaterials,” *Nano Letters*, vol. 16, no. 4. pp. 2471–2477, 2016, doi: 10.1021/acs.nanolett.6b00034.

[40] D. S. Wiersma, “The physics and applications of random lasers,” *Nat. Phys.*, vol. 4, no. 5, pp. 359–367, 2008.

[41] C.-R. Lee, S.-H. Lin, C.-H. Guo, S.-H. Chang, T.-S. Mo, and S.-C. Chu, “All-optically controllable random laser based on a dye-doped polymer-dispersed liquid crystal with nano-sized droplets,” *Opt. Express*, vol. 18, no. 3, p. 2406, 2010, doi: 10.1364/oe.18.002406.

[42] H. Zhang, G. Feng, J. Y. Yi, J. Mu, K. Yao, and S. Zhou, “Coherent random laser based on liquid waveguide gain channels,” *J. Mod. Opt.*, vol. 62, no. 10, pp. 865–868, 2015, doi: 10.1080/09500340.2015.1009953.

[43] G. D. Dice and A. Y. Elezzabi, “Random lasing from a nanoparticle-based metal-dielectric-dye medium,” *J. Opt. A Pure Appl. Opt.*, vol. 9, no. 2, pp. 186–193, 2007, doi: 10.1088/1464-4258/9/2/012.

[44] Y. J. Lee *et al.*, “Flexible random lasers with tunable lasing emissions,” *Nanoscale*, vol. 10, no. 22, pp. 10403–10411, 2018, doi: 10.1039/c8nr00229k.

[45] M. A. T. Khan, “Spatial coherence measurement of random laser.” 2016.

[46] R. Tang, “RANDOM LASER IN DISORDERED SOLUTIONS,” no. December. 2017.

[47] M. Pang, X. Bao, L. Chen, Z. Qin, Y. Lu, and P. Lu, “Frequency stabilized coherent Brillouin random fiber laser: theory and experiments,” *Opt. Express*, vol. 21, no. 22, p. 27155, 2013, doi: 10.1364/oe.21.027155.

[48] D. Wiersma, “Laser physics: The smallest random laser,” *Nature*, vol. 406, pp. 132–133, 2000.

[49] Y. Nastishin and T. H. Dudok, “Optically pumped mirror less lasing. A review. part I. random lasing,” *Ukr. J. Phys. Opt.*, vol. 14, no. 3, pp. 146–170, 2013, doi: 10.3116/16091833/14/3/146/2013.

[50] A. Ghasempour Ardakani, A. R. Bahrampour, S. M. Mahdavi, and M. Golshani Gharyeh Ali, “Numerical study of random lasing in three dimensional amplifying disordered media,” *Opt. Commun.*, vol. 285, no. 6, pp. 1314–1322, 2012, doi: 10.1016/j.optcom.2011.10.018.

[51] X. WU, “Study of Lasing in Random and Periodic Systems.” 2007.

[52] L. Li and L. Deng, “Low threshold and coherent random lasing from dye-doped cholesteric liquid crystals using oriented cells,” *Laser Phys.*, vol. 23, no. 8, 2013, doi: 10.1088/1054-660X/23/8/085001.

[53] R. C. Polson, M. E. Raikh, and Z. V. Vardeny, “Random Lasing from Weakly Scattering Media: Universality in the Emission Spectra from Pi-Conjugated Polymer Films,” no. September 2013, 2001.

[54] H. Cao, Y. Ling, J. Y. Xu, C. Q. Cao, and P. Kumar, “Photon statistics of random lasers with resonant feedback,” *Physical Review Letters*, vol. 86, no. 20. pp. 4524–4527, 2001, doi: 10.1103/PhysRevLett.86.4524.

[55] A. K. Tiwari, “Coherent random lasing in a disordered array of amplifying microresonators.” 2018.

[56] R. G. S. El-Dardiry, A. P. Mosk, O. L. Muskens, and A. Lagendijk, “Experimental studies on the mode structure of random lasers,” *Phys. Rev. A - At. Mol. Opt. Phys.*, vol. 81, no. 4, pp. 1–8, 2010, doi: 10.1103/PhysRevA.81.043830.

[57] R. M. Ziff, G. E. Uhlenbeck, and M. Kac, “The ideal Bose-Einstein gas, revisited,” *Phys. Rep.*, vol. 32, no. 4, pp. 169–248, 1977, doi: 10.1016/0370-1573(77)90052-7.

[58] L. Florescu and S. John, “Photon statistics and coherence in light emission from a random laser,” *Phys. Rev. Lett.*, vol. 93, no. 1, pp. 013602–1, 2004, doi: 10.1103/PhysRevLett.93.013602.

[59] G. D. Dice, S. Mujumdar, and A. Y. Elezzabi, “Plasmonically enhanced diffusive and subdiffusive metal nanoparticle-dye random laser,” *Applied Physics Letters*, vol. 86, no. 13. pp. 1–3, 2005, doi: 10.1063/1.1894590.

[60] H. Cao, J. Y. Xu, S. H. Chang, and S. T. Ho, “Transition from amplified spontaneous emission to laser action in strongly scattering media,” *Phys. Rev. E - Stat. Physics, Plasmas, Fluids, Relat. Interdiscip. Top.*, vol. 61, no. 2, pp. 1985–1989, 2000, doi: 10.1103/PhysRevE.61.1985.

[61] A. Tulek and Z. V. Vardeny, “Studies of random laser action in π-conjugated polymers,” *J. Opt. A Pure Appl. Opt.*, vol. 12, no. 2, 2010, doi: 10.1088/2040-8978/12/2/024008.

[62] X. Zhao, Z. Wu, S. Ning, S. Liang, D. Wang, and X. Hou, “Random lasing from granular surface of waveguide with blends of PS and PMMA,” *Opt. Express*, vol. 19, no. 17, p. 16126, 2011, doi: 10.1364/oe.19.016126.

[63] L. Sznitko, J. Mysliwiec, and A. Miniewicz, “The role of polymers in random lasing,” *J. Polym. Sci. Part B Polym. Phys.*, vol. 53, no. 14, pp. 951–974, 2015, doi: 10.1002/polb.23731.

[64] D. Wiersma, “Light in strongly scattering and amplifying random media,” *Thesis*, no. november, p. 59, 1995.

[65] P. W. Anderson, “Absence of diffusion in certain random lattices,” *Phys. Rev.*, vol. 109, no. 5, pp. 1492–1505, 1958, doi: 10.1103/PhysRev.109.1492.

[66] F. Luan, B. Gu, A. S. L. Gomes, K. T. Yong, S. Wen, and P. N. Prasad, “Lasing in nanocomposite random media,” *Nano Today*, vol. 10, no. 2, pp. 168–192, 2015, doi: 10.1016/j.nantod.2015.02.006.

[67] Z. Shang, M. Yang, and L. Deng, “Low–threshold and high intensity random lasing enhanced by MnCl2,” *Materials (Basel).*, vol. 9, no. 9, p. 725, 2016.

[68] H. Cao, “Lasing in random media,” *Waves in random media*, vol. 13, no. 3, p. R1, 2003.

[69] M. Li *et al.*, “Ultralow-threshold multiphoton-pumped lasing from colloidal nanoplatelets in solution,” *Nat. Commun.*, vol. 6, no. 1, pp. 1–8, 2015.

[70] R. K. Thareja and A. Mitra, “Random laser action in ZnO,” *Appl. Phys. B*, vol. 71, no. 2, pp. 181–184, 2000.

[71] J. Yi *et al.*, “Behaviors of the Rh6G random laser comprising solvents and scatterers with different refractive indices,” *Opt. Commun.*, vol. 285, no. 24, pp. 5276–5282, 2012.

[72] W. Z. W. Ismail, T. P. Vo, E. M. Goldys, and J. M. Dawes, “Plasmonic enhancement of Rhodamine dye random lasers,” *Laser Phys.*, vol. 25, no. 8, 2015, doi: 10.1088/1054-660X/25/8/085001.

[73] N. A. I. M. Kamil *et al.*, “Principles and characteristics of random lasers and their applications in medical, bioimaging and biosensing,” *AIP Conf. Proc.*, vol. 2203, no. January, 2020, doi: 10.1063/1.5142109.

[74] J. Xia *et al.*, “The transition from incoherent to coherent random laser in defect waveguide based on organic/inorganic hybrid laser dye,” *Nanophotonics*, vol. 7, no. 7, pp. 1341–1350, 2018, doi: 10.1515/nanoph-2018-0034.

[75] H. Cao, “Random Lasers with Coherent Feedback,” *Optical Properties of Nanostructured Random Media*. pp. 303–330, 2007, doi: 10.1007/3-540-44948-5_14.

[76] Z. Hu *et al.*, “Coherent random fiber laser based on nanoparticles scattering in the extremely weakly scattering regime,” *Phys. Rev. Lett.*, vol. 109, no. 25, pp. 2–6, 2012, doi: 10.1103/PhysRevLett.109.253901.

[77] J. Azkargorta, I. Iparraguirre, J. Fernández, R. Balda, S. García-Revilla, and M. Barredo-Zurriarrain, “ Random laser properties of Nd 3+ crystal powders ,” *Opt. Express*, vol. 26, no. 9, p. 11787, 2018, doi: 10.1364/oe.26.011787.

[78] A. Consoli and C. López, “Decoupling gain and feedback in coherent random lasers: Experiments and simulations,” *Sci. Rep.*, vol. 5, pp. 1–10, 2015, doi: 10.1038/srep16848.

[79] A. Sarkar, B. N. S. Bhaktha, and J. Andreasen, “Replica Symmetry Breaking in a Weakly Scattering Optofluidic Random Laser,” *Sci. Rep.*, vol. 10, no. 1, pp. 1–12, 2020, doi: 10.1038/s41598-020-59575-2.

[80] H. Cao, “Random lasers: development, features and applications,” *Opt. Photonics News*, vol. 16, no. 1, pp. 24–29, 2005.

[81] Q. Song *et al.*, “Detection of nanoscale structural changes in bone using random lasers,” *Biomed. Opt. Express*, vol. 1, no. 5, pp. 1401–1407, 2010.

[82] M. S. Dawood, E. G. Khalil, and H. H. Saleh, “Detection of tumor mass based on laser scanning imaging,” *Al-Nahrain J. Eng. Sci.*, vol. 20, no. 1, pp. 176–182, 2017.

[83] Q. Song *et al.*, “Random lasing in bone tissue,” *Opt. Lett.*, vol. 35, no. 9, pp. 1425–1427, 2010.

[84] W. Z. W. Ismail, G. Liu, K. Zhang, E. M. Goldys, and J. M. Dawes, “Dopamine sensing and measurement using threshold and spectral measurements in random

lasers," *Opt. Express*, vol. 24, no. 2, pp. A85–A91, 2016.

[85] R. C. Polson and Z. V Vardeny, "Cancerous tissue mapping from random lasing emission spectra," *J. Opt.*, vol. 12, no. 2, p. 24010, 2010.

[86] N. Sharma, G. Bhatt, and P. Kothiyal, "Gold nanoparticles synthesis, properties, and forthcoming applications-a review," *Indian J. Pharm. Biol. Res.*, vol. 3, no. 2, p. 13, 2015.

[87] C. Etrich, S. Fahr, M. K. Hedayati, F. Faupel, M. Elbahri, and C. Rockstuhl, "Effective optical properties of plasmonic nanocomposites," *Materials (Basel).*, vol. 7, no. 2, pp. 727–741, 2014.

[88] P. Zijlstra, M. Orrit, and A. F. Koenderink, "Metal nanoparticles for microscopy and spectroscopy," in *Nanoparticles*, Springer, 2014, pp. 53–98.

[89] A. Di Giuseppe, *Metrology and Physical Constants*, vol. 185. IOS Press, 2013.

[90] M. A. Mahmoud, M. Chamanzar, A. Adibi, and M. A. El-Sayed, "Effect of the dielectric constant of the surrounding medium and the substrate on the surface plasmon resonance spectrum and sensitivity factors of highly symmetric systems: silver nanocubes," *J. Am. Chem. Soc.*, vol. 134, no. 14, pp. 6434–6442, 2012.

[91] F.-Y. Kong, J.-W. Zhang, R.-F. Li, Z.-X. Wang, W.-J. Wang, and W. Wang, "Unique roles of gold nanoparticles in drug delivery, targeting and imaging applications," *Molecules*, vol. 22, no. 9, p. 1445, 2017.

[92] H. Chen, L. Shao, Q. Li, and J. Wang, "Gold nanorods and their plasmonic properties," *Chem. Soc. Rev.*, vol. 42, no. 7, pp. 2679–2724, 2013.

[93] M. A. M. Duque, R. N. Tiozon, and R. C. N. Espana, "Chitosan from Portunus Pelagicus in the Synthesis of Reduced Gold Nanoparticle as Potential Carrier for the Delivery of Erythropoietin," *bioRxiv*, p. 44875, 2016.

[94] A. A. Ashkarran, S. Estakhri, M. R. H. Nezhad, and S. Eshghi, "Controlling the geometry of silver nanostructures for biological applications," *Phys. Procedia*, vol. 40, pp. 76–83, 2013, doi: 10.1016/j.phpro.2012.12.011.

[95] X. K. Meng, S. C. Tang, and S. Vongehr, "A Review on Diverse Silver Nanostructures," *J. Mater. Sci. Technol.*, vol. 26, no. 6, pp. 487–522, 2010, doi: 10.1016/S1005-0302(10)60078-3.

[96] B. Wiley and Y. Sun, “Synthesis of Silver Nanostructures with Controlled Shapes and Properties,” vol. 40, no. 10, pp. 1067–1076, 2007.

[97] X. Huang and M. A. El-Sayed, “Gold nanoparticles: Optical properties and implementations in cancer diagnosis and photothermal therapy,” *J. Adv. Res.*, vol. 1, no. 1, pp. 13–28, 2010, doi: 10.1016/j.jare.2010.02.002.

[98] S. W. Verbruggen, M. Keulemans, J. A. Martens, and S. Lenaerts, “Predicting the surface plasmon resonance wavelength of gold-silver alloy nanoparticles,” *J. Phys. Chem. C*, vol. 117, no. 37, pp. 19142–19145, 2013, doi: 10.1021/jp4070856.

[99] K. Wongwailikhit and S. Horwongsakul, “The preparation of iron (III) oxide nanoparticles using W/O microemulsion,” *Mater. Lett.*, vol. 65, no. 17–18, pp. 2820–2822, 2011.

[100] S. Laurent *et al.*, “Magnetic iron oxide nanoparticles: synthesis, stabilization, vectorization, physicochemical characterizations, and biological applications,” *Chem. Rev.*, vol. 108, no. 6, pp. 2064–2110, 2008.

[101] A. M. Abu-Dief and S. M. Abdel-Fatah, “Development and functionalization of magnetic nanoparticles as powerful and green catalysts for organic synthesis,” *Beni-Suef Univ. J. Basic Appl. Sci.*, vol. 7, no. 1, pp. 55–67, 2018.

[102] A. Ali *et al.*, “Review on recent progress in magnetic nanoparticles: Synthesis, characterization, and diverse applications,” *Front. Chem.*, vol. 9, p. 629054, 2021.

[103] V. A. J. Silva, P. L. Andrade, M. P. C. Silva, A. D. Bustamante, L. De Los Santos Valladares, and J. Albino Aguiar, “Synthesis and characterization of Fe3O4 nanoparticles coated with fucan polysaccharides,” *J. Magn. Magn. Mater.*, vol. 343, pp. 138–143, 2013, doi: 10.1016/j.jmmm.2013.04.062.

[104] S. Kasani, K. Curtin, and N. Wu, “A review of 2D and 3D plasmonic nanostructure array patterns: fabrication, light management and sensing applications,” *Nanophotonics*, vol. 8, no. 12, pp. 2065–2089, 2019.

[105] H. Yu, Y. Peng, Y. Yang, and Z.-Y. Li, “Plasmon-enhanced light–matter interactions and applications,” *npj Comput. Mater.*, vol. 5, no. 1, pp. 1–14, 2019.

[106] J. Liu *et al.*, “Recent advances of plasmonic nanoparticles and their applications,” *Materials (Basel).*, vol. 11, no. 10, p. 1833, 2018.

[107] H. C. Ishikawa-Ankerhold, R. Ankerhold, and G. P. C. Drummen, “Advanced fluorescence microscopy techniques—Frap, Flip, Flap, Fret and flim,” *Molecules*, vol. 17, no. 4, pp. 4047–4132, 2012.

[108] M. A. Phillips, M. L. Gran, and N. A. Peppas, “Targeted nanodelivery of drugs and diagnostics,” *Nano Today*, vol. 5, no. 2, pp. 143–159, 2010.

[109] G. Feng, G.-Q. Zhang, and D. Ding, “Design of superior phototheranostic agents guided by Jablonski diagrams,” *Chem. Soc. Rev.*, vol. 49, no. 22, pp. 8179–8234, 2020.

[110] M. Planck, “On the law of distribution of energy in the normal spectrum,” *Ann. Phys.*, vol. 4, no. 553, p. 1, 1901.

[111] M. Kasha, “Characterization of electronic transitions in complex molecules,” *Discuss. Faraday Soc.*, vol. 9, pp. 14–19, 1950.

[112] L. Ma, F. Yang, and J. Zheng, “Application of fluorescence resonance energy transfer in protein studies,” *J. Mol. Struct.*, vol. 1077, pp. 87–100, 2014.

[113] R. B. Sekar and A. Periasamy, “Fluorescence resonance energy transfer (FRET) microscopy imaging of live cell protein localizations,” *J. Cell Biol.*, vol. 160, no. 5, p. 629, 2003.

[114] Q. R. Ali, “Energy Transfer Calculations Based on Fluorescence Spectra of Acriflavine and Rhodamine B Laser Dyes,” *Iraqi J. Appl. Phys.*, vol. 16, no. 3, 2020.

[115] L. Bene, T. Ungvári, R. Fedor, and L. Damjanovich, “Single-laser polarization FRET (polFRET) on the cell surface,” *Biochim. Biophys. Acta (BBA)-Molecular Cell Res.*, vol. 1843, no. 12, pp. 3047–3064, 2014.

[116] Q. R. Ali, “Photobleaching Spectroscopic Studies and Lifetime Measurements of Fluorescent Organic Dyes,” *a thesis, Univ. Baghdad, Coll. Sci.*, 2013.

[117] A. Jalihal *et al.*, “Understanding of Förster Resonance Energy Transfer (FRET) in Ionic Materials,” *Sustain. Chem.*, vol. 2, no. 4, pp. 564–575, 2021.

[118] R. M. Clegg, “Fluorescence resonance energy transfer,” *Fluoresc. imaging Spectrosc. Microsc.*, vol. 137, pp. 179–251, 1996.

[119] X. Shi *et al.*, “Random lasing with a high quality factor over the whole visible range based on cascade energy transfer,” *Adv. Opt. Mater.*, vol. 2, no. 1, pp. 88–93, 2014.

[120] U. Noomnarm and R. M. Clegg, “Fluorescence lifetimes: fundamentals and interpretations,” *Photosynth. Res.*, vol. 101, no. 2, pp. 181–194, 2009.

[121] G. A. Kumar and N. V Unnikrishnan, “Energy transfer and optical gain studies of FDS: Rh B dye mixture investigated under cw laser excitation,” *J. Photochem. Photobiol. A Chem.*, vol. 144, no. 2–3, pp. 107–117, 2001.

[122] P. G. Wu and L. Brand, “Resonance energy transfer: methods and applications,” *Anal. Biochem.*, vol. 218, no. 1, pp. 1–13, 1994.

[123] P. L. Hariani, M. Faizal, R. Ridwan, M. Marsi, and D. Setiabudidaya, “Synthesis and properties of Fe3O4 nanoparticles by co-precipitation method to removal procion dye,” *Int. J. Environ. Sci. Dev.*, vol. 4, no. 3, pp. 336–340, 2013.

[124] V. Amendola and M. Meneghetti, “What controls the composition and the structure of nanomaterials generated by laser ablation in liquid solution?,” *Phys. Chem. Chem. Phys.*, vol. 15, no. 9, pp. 3027–3046, 2013.

[125] Q. X. Liu, C. X. Wang, W. Zhang, and G. W. Wang, “Immiscible silver–nickel alloying nanorods growth upon pulsed-laser induced liquid/solid interfacial reaction,” *Chem. Phys. Lett.*, vol. 382, no. 1–2, pp. 1–5, 2003.

[126] V. Amendola and M. Meneghetti, “Laser ablation synthesis in solution and size manipulation of noble metal nanoparticles,” *Phys. Chem. Chem. Phys.*, vol. 11, no. 20, pp. 3805–3821, 2009.

[127] G.-J. Lee, S.-I. Shin, Y.-C. Kim, and S.-G. Oh, “Preparation of silver nanorods through the control of temperature and pH of reaction medium,” *Mater. Chem. Phys.*, vol. 84, no. 2–3, pp. 197–204, 2004.

[128] Y. J. Lee, E. Y. Ahn, and Y. Park, “Shape-dependent cytotoxicity and cellular uptake of gold nanoparticles synthesized using green tea extract,” *Nanoscale Res. Lett.*, vol. 14, pp. 1–14, 2019, doi: 10.1186/s11671-019-2967-1.

[129] M. Koperuncholan, “Bioreduction of chloroauric acid (HAuCl4) for the synthesis of gold nanoparticles (GNPs): A special empathies of pharmacological activity,” *Int. J. Phytopharm*, vol. 5, no. 4, pp. 72–80, 2015.

[130] D. Jing, L. Sun, J. Jin, M. Thangamuthu, and J. Tang, “Magneto-optical transmission in magnetic nanoparticle suspensions for different optical applications: A review,” *J. Phys. D. Appl. Phys.*, vol. 54, no. 1, pp. 1–28, 2021, doi: 10.1088/1361-6463/abb8fd.

[131] G. . Humood.N, “Study of the Effect of Concentration on the Absorption Spectrum of Copper-Phthalocyanine Dye (CuPc),” *Australian Journal of Basic and Applied Sciences*. pp. 407–412, 2015.

[132] F. Pahang, P. Parvin, H. Ghafoori-Fard, A. Bavali, and A. Moafi, “Fluorescence properties of methylene blue molecules coupled with metal oxide nanoparticles,” *OSA Contin.*, vol. 3, no. 3, pp. 688–697, 2020.

[133] M. F. Al-Kadhemy, I. F. Alsharuee, and A. A. D. Al-Zuky, “Analysis of the effect of the concentration of rhodamine B in ethanol on the fluorescence spectrum using the ‘Gauss Mod’ function,” *Journal of Physical Science*, vol. 22, no. 2. pp. 77–86, 2011.

[134] M. Chung and C. Fu, “Optical Transmittance and Dynamic Properties of Ferrofluids (Fe3O4) Under DC-Biased Magnetic Fields,” vol. 47, no. 10, pp. 3170–3172, 2011.

[135] R. A. Ejbarah, J. M. Jassim, and S. M. Hamidi, “Random laser action under picosecond laser pumping,” *Opt. Quantum Electron.*, vol. 52, no. 10, pp. 1–8, 2020.

[136] P. D. Shima, J. Philip, and B. Raj, “Magnetically controllable nanofluid with tunable thermal conductivity and viscosity,” *Appl. Phys. Lett.*, vol. 95, no. 13, pp. 16–19, 2009, doi: 10.1063/1.3238551.

[137] H. Zhang, G. Feng, H. Zhang, C. Yang, J. Yin, and S. Zhou, “Random laser based on Rhodamine 6G (Rh6G) doped poly(methyl methacrylate) (PMMA) films coating on ZnO nanorods synthesized by hydrothermal oxidation,” *Results Phys.*, vol. 7, pp. 2968–2972, 2017, doi: 10.1016/j.rinp.2017.07.072.

[138] Y. Bai, C. Gao, and Y. Yin, “Fully alloyed Ag/Au nanorods with tunable surface

plasmon resonance and high chemical stability," *Nanoscale*, vol. 9, no. 39, pp. 14875–14880, 2017.

[139] S. Kedia and S. Sinha, "Random laser emission at dual wavelengths in a donor-acceptor dye mixture solution," *Results Phys.*, vol. 7, pp. 697–704, 2017, doi: 10.1016/j.rinp.2017.01.028.

[140] B. T. Chiad, F. J. Kadhim, Z. S. Sadik, D. K. Mahdy, M. A. Hameed, and E. A. Abdullah, "Energy Transfer of Rhodamine110-Oxazine1 Mixtures Encapsulated in Glass Like Silica Xerogel Matrices," *J. Mater. Sci. Eng. A*, vol. 3, no. 4A, p. 249, 2013.

[141] K. G. Nair, D. Jayaseelan, and P. Biji, "Direct-writing of circuit interconnects on cellulose paper using ultra-long, silver nanowires based conducting ink," *RSC Advances*, vol. 5, no. 93. pp. 76092–76100, 2015, doi: 10.1039/c5ra10837c.

[142] N. Cuando-Espitia, J. Hernández-Cordero, C. García-Segundo, and R. Quispe-Siccha, "Effects of scatterer size and concentration on the spectral features of dye-based random lasers," *Optics InfoBase Conference Papers*. 2011, doi: 10.1364/iprsn.2011.imd5.

[143] A. R. Shafiqa, A. Abdul Aziz, and B. Mehrdel, "Nanoparticle Optical Properties: Size Dependence of a Single Gold Spherical Nanoparticle," *J. Phys. Conf. Ser.*, vol. 1083, no. 1, 2018, doi: 10.1088/1742-6596/1083/1/012040.

[144] H. Cao and J. Y. Xu, "Transition from amplified spontaneous emission to laser action in strongly scattering media," vol. 61, no. 2, pp. 1985–1989, 2000.

الخلاصة:

تهدف هذه الدراسة إلى إعداد وسائط انبعاث ليزر عشوائية ضمن نطاق أطوال موجية من Vis إلى NIR. يتكون الوسط النشط لليزر العشوائي الذي تم تحضيره لإنتاج مثل هذه الأطوال الموجية من صبغة ليزر مذابة في مذيب وجسيمات نانوية مناسبة. تم استخدام صبغات الليزر في هذا النظام (Rhodamine 640، Methylene blue MB و LDS 821) في الميثانول كمذيب. الجسيمات النانوية التي تم استخدامها كمراكز تشتت هي (أكسيد الحديد المغناطيسي Fe_3O_4 ، أسلاك الفضة النانوية AgNWR و قضبان الذهب النانوية AuNRs). تم تحضير الجسيمات النانوية بأنواعها وأشكالها المختلفة باستخدام الطرق الكيميائية. تمت دراسة خصائص الامتصاص والوميض الطيفي للأصباغ المذابة في الميثانول بتركيزات مختلفة. كما تمت دراسة تحضير وسائط الليزر العشوائية المكونة من الأصباغ مع إضافة الجسيمات النانوية بتراكيز مختلفة من الصبغة والجسيمات النانوية. وجد أن تركيز الأصباغ ونوع الجسيمات النانوية ذات الشكل المحدد لهما تأثير كبير على أطياف الأصباغ عن طريق زيادة الامتصاص وطيف الانبعاث مع اعتبارات محددة. أيضًا ، كانت الأطوال الموجية تتحول إلى أطوال موجية أطول (التحول الأحمر) وإلى أطوال موجية أقصر (التحول الأزرق) تتناسب مع تركيز كل من الصبغة والجسيمات النانوية. تمت دراسة تأثير الخصائص الديناميكية للموائع النانوية المغناطيسية المشتتة (Fe_3O_4) بتركيزات مختلفة على شعاع الليزر الغاوسي الذي يمرعبرها. أظهرت النتائج أن كلاً من حجم المجال المغناطيسي الخارجي وزمن الاستجابة لهما تأثير واضح على إعادة انتشار وتوزيع الجسيمات النانوية (NPs) ، مكونين طبقة من السلاسل ذات الأحجام المختلفة. علاوة على ذلك ، فإن التحكم في طول الانتثار يعني المسار الحر حيث تتغير قيمته من (30 - 160) ميكرومتر. تم اختبار إمكانية استخدام مجال مغناطيسي خارجي على خليط (وسط نشط إلى ليزر عشوائي) من رودامين 640 مع جزيئات Fe_3O_4 النانوية في الميثانول على معاملات إخراج الليزر العشوائية. أظهرت النتائج إمكانية التحكم في الانبعاث لأطوال موجية أطول (انزياح أحمر) حتى (6) نانومتر وعرض نطاق طيفي أقل من (15) نانومتر عن طريق تغيير طاقة العتبة لتصل إلى أقل من (3.5) ملي جول وبتطبيق المجال المغناطيسي الخارجي بين (0-125) كاوس. تم أيضًا حساب عوامل نقل الطاقة لمزيج من صبغتين ، رودامين - 640 كمانح ، والميثيلين الأزرق كمستقبل ، المذابتين في الميثانول ، وتضمنت مسافة النقل الحرجة ، ونصف تركيز الخمد ، وكفاءة النقل. وجد أن كفاءة التحويل تصل إلى 85٪ عند تركيز الصبغة (الميثيلين الأزرق = 1×10^{-3} مولاري). تمت دراسة إضافة أسلاك الفضة النانوية إلى خليط الصبغتين من أجل تحضير وسط فعال لليزر العشوائي ، تم إنتاج طولين موجيين (600 و 700) نانومتر من هذا الليزر.

أما بالنسبة لليزر العشوائي بوسط مكون من خليط من صبغة LDS 821 مذابة في ميثانول مع إضافة تركيز معين من قضبان الذهب النانوية بقطرين مختلفين (6.3 و 7.3) نانومتر متساوية بالأطوال. أظهرت النتائج تغيرًا سريعًا من الليزر غير المتماسك إلى المتماسك ، حيث يظهر النظام خصائص مميزة من خلال عدة قمم منفصلة تظهر في طيف الانبعاث بعدد يصل إلى (10) وعرض نطاق طيفي أقل من (1 نانومتر) . يحدث هذا بسبب تأثير كل من رنين البلازمون وقطر القضبان الذهبية. تم استخدام المجهر الإلكتروني الماسح للانبعاثات الميدانية (FESEM) والفحص المجهري الإلكتروني (TEM) وحيود الأشعة السينية (XRD) لدراسة الخصائص المورفولوجية والهيكلية للجسيمات النانوية.

جمهورية العراق
وزارة التعليم العالي والبحث العلمي
جامعة بابل
كلية العلوم للبنات

انبعاث الليزر العشوائي بأطوال موجية (مرئية – تحت الحمراء ألقريبة) في وسائط نشطة مختلفة

أطروحة
مقدمة الى قسم فيزياء الليزر في كلية العلوم للبنات- جامعة بابل
كجزء من متطلبات نيل درجة الدكتوراه في فيزياء الليزر وتطبيقاته

من قبل

محمد صلاح رحومي السماك

(بكالوريوس فيزياء – جامعة بابل 2009 م)
(ماجستير فيزياء – جامعة بابل 2018 م)

بإشراف
الاستاذ الدكتور

جاسم محمد جاسم

1444 هـ

2023 م

Publications

Journal articles

1- Al-Samak, M. S., and J. M. Jassim. "Determination of scattering mean free path in magnetic nanoparticle suspensions." *Optical and Quantum Electronics* 54.12 (2022): 1-11., DOI: 10.1007/s11082-022-04108-6

2- Al-Samak, M. S., and J. M. Jassim. "Dye-Doped Fe3O4 Nanoparticles for Magnetically Controlling Random Laser Parameters at Visible Wavelengths: Literature Review and Experiment." *Indonesian Journal of Science and Technology* 7.3: 497-510, DOI:10.17509/ijost.v7i3.51453

Under publication

3- Al-Samak, M.S., and J.M. Jassim. Multi-wavelength emission Coherent random laser based resonance energy transfer.

4- Al-Samak, M.S., and J.M. Jassim. Seedless synthesis and characterization of gold nanorods with different aspect ratios.